Molecular Design of Silk Fibroin for Functional Scaffolds

Yusuke KAMBE

2013

Contents

Chapter 1
Introduction of This Study

This study has addressed the research and development of functional silk fibroin scaffolds for articular cartilage tissue engineering. Transgenic silkworm technology was used to design silk fibroin molecules in order to append new functions to fibroin scaffold, and we evaluated biomechanical and biochemical characteristics of chondrogenic cells grown on the scaffold. This study has been conducted with various visions, methodologies, and materials, whose important keywords and concepts are reviewed in Sections 1.1–1.6. At the end of this chapter (Section 1.7), the background and purpose of this study are described.

1.1. Tissue engineering/regenerative medicine

Tissue engineering/regenerative medicine is “an interdisciplinary field that applies the principles and methods of engineering and the life science toward the development of biological substitutes that restore, maintain, or improve tissue function” [1], and its goal is to create living, functional tissues to repair or replace tissues or organ function lost due to age, disease, damage, or congenital defects [2]. According to Langer and Vacanti [1], three general strategies had been adopted for the creation of new tissue as of 1993: isolated cells or cell substitutes, tissue-inducing substances, and cells placed on or within matrices. In that report, they reviewed studies which had conducted the replacement of ectodermal (nervous system, cornea, and skin), endodermal (liver,

pancreas, and tubular structures), and mesodermal-derived tissue (cartilage, bone, and muscle). Some of these studies including clinical trials were worked out by adopting two or more of the three strategies. Eight years after the report, Fuchs et al. [3] presented three concepts emerging in the field of tissue engineering: dynamic *in vitro* culture systems (bioreactors), microfabrication technology to create vascularized tissues and organs, and an appropriate multipotent, undifferentiated stem cell. These concepts were important to guide the formation of tissue with certain structural and functional characteristics, to fabricate larger tissues and organs, and to ensure needed cells prior to transplantation, respectively. The last concept of the three has been being achieved by the appearance of induced pluripotent stem (iPS) cells from adult human fibroblasts [4]. The iPS cells have a potential to differentiate into various types of cells and can be ensured without ethical issues unlike human embryonic stem (ES) cells [5]. Once safety issue is overcome, human iPS cells should be applicable in regenerative medicine [4]. However, regardless of this Nobel Prize-winning discovery, there are still many issues to be resolved to achieve the extensive clinical application of regenerative medicine. This is because cell source is only one factor in tissue engineering. To accomplish the ultimate goal of functional neoorganogenesis for human use, the close, interdisciplinary collaboration of surgeons, engineers, chemists, and biologists is required [3].

1.2. Articular cartilage

Articular cartilage is a connective tissue that covers the surfaces of epiphysis in diarthrodial joints (Fig. 1.1) and has a layered structure (Fig. 1.2). In a frequently-loaded environment *in vivo*, it plays mechanical functions: shock absorption and lubrication. Histologically it is classified as a hyaline cartilage and consists of specialized cells called chondrocytes and extracellular matrices (ECMs) which are produced by the cells. Most of the tissue is composed of the ECMs, and there are no blood vessels, no lymph channels, and no nervous systems.

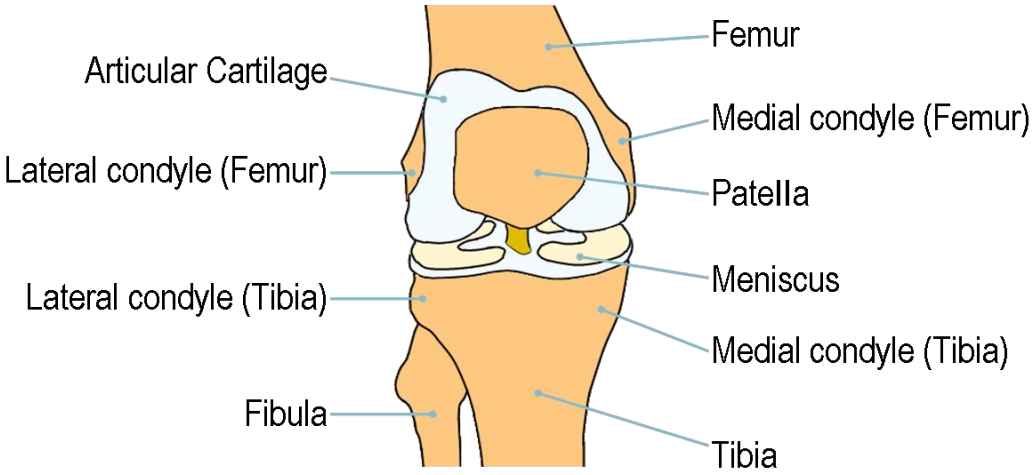

Fig. 1.1. A schematic drawing of human knee articulation [6].

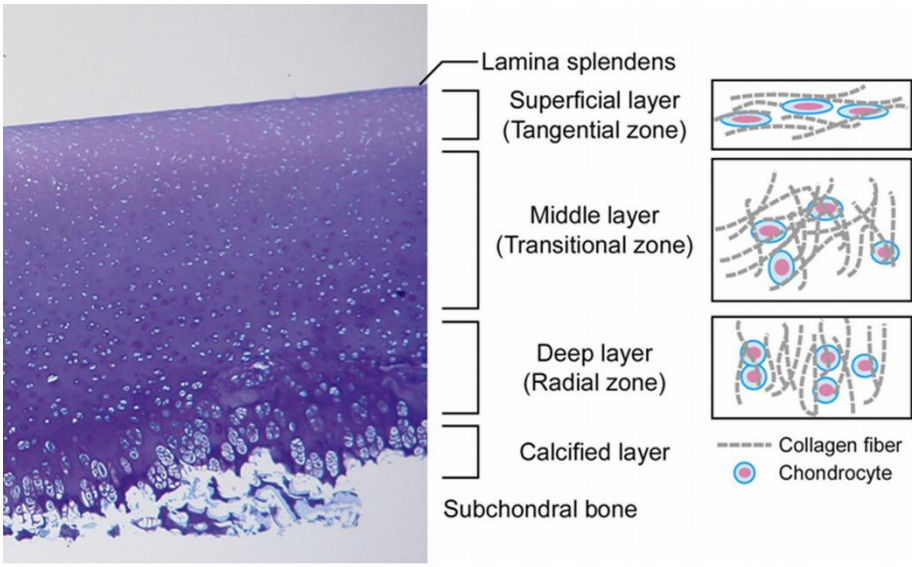

Fig. 1.2. Statified structure of articular cartilage tissue. The photograph represents a cross-section of porcine articular cartilage stained by Toluidine blue [6].

1.2.1. Chondrocytes and their extracellular matrix

Chondrocytes are highly-differentiated mesenchymal cells and have an anchorage dependency. Interactions between chondrocytes and substrates thus play an important role in various activities of the cells, such as survival, proliferation, and differentiation.

When two-dimensionally cultured as e.g., on a culture dish, chondrocytes proliferate well but tend to lose their chondrocgenic phenotype to dedifferentiate into fibroblast-like cells [7-9]. On the other hand, when embedded in three-dimensional gels such as collagen, the cells can maintain their phenotype and synthesize cartilage-specific matrices [10-11] but their proliferation ability tends to be suppressed [13]. Hence, chondrocytes change their phenotype to produce different matrices, depending on their surrounding environment. For example, chondrocytes in intact cartilage synthesize collagen type II, but dedifferentiated and calcified chondrocytes produce collagens type I and type X, respectively.

Cartilage ECM is mainly composed of water (60–80% wet weight), collagens (10–20% wet weight), and proteoglycans (10–15% wet weight) [14]. There are several types of collagens in the ECM, such as type I, II, V, VI, IX, X, XI, and XIV. Proteoglycan is a glycoprotein and consists of several subunits of glycosaminoglycans (GAGs) which bind to a core protein. GAGs are classified into chondroitin sulfate, dermatan sulfate, keratan sulfate, and hyaluronan. Most of the proteoglycans in cartilage tissue are chondroitin sulfate proteoglycan, which are called aggrecan.

1.2.2. Treatment methods for articular cartilage

Articular cartilage has no blood vessels, no lymph channels, and no nervous systems in physiological condition. Additionally, chondrocytes, which account for 5% wet weight in cartilage tissue, lose their ability of proliferation with aging. Due to these characteristics, the self-reparation of the tissue is especially slow [15,16].

Bone-marrow stimulation technique, which consists of multiple perforations, abrasions, and micro-fractures, has been clinically practiced as a treatment method for cartilage defects since 1950s [17]. In this treatment, subchondral bone at a cartilage defect is broken to promote cartilage repair from bone marrow-derived cells and cytokines. However, the defect is considered to be repaired with fibrocartilage, which is different form hyaline cartilage.

Mosaicplasty is one of the treatment methods that are expected to repair the defect with hyaline cartilage [18]. Several cylindrical osteochondral plugs from the less weight-bearing area are harvested, and then they are inserted mosaically into drilled tunnels in the defect. However, it is difficult to regenerate the smooth surface like intact cartilage.

Autologous cell implantation, which is a tissue-engineered therapy, has been applied to a clinical practice. Since the first report in 1994 [19], the improvement of the clinical symptom by autologous chondrocyte implantation has been reported. In this method, chondrocytes harvested from a patient are expanded to implant in the cartilage defect of the patient. However, its effectiveness is still controversial, and its application is limited to regional cartilage defects. Therefore, in order to apply the treatment to a widespread defect, it is necessary to get a large amount of cells with chondrogenic phenotype.

Artificial joint replacement is generally conducted as a treatment for the wide range of cartilage defects. Accordingly, this treatment can ease pain, maintaining the bearing property and lubricity of the joint. However, in some cases reimplantation is required depending on the postoperative course.

1.3. Cell–material adhesion

After cell suspension is seeded onto a material, following phenomena are considered to occur [20]: (i) water and saline contact to the material and (ii) proteins in the solution absorb onto the surface of the material. Then, (iii) cells bind to the proteins absorbed on the material. Finally, (iv) the cells attach and spread on the surface (Fig. 1.3). The phenomena (i) and (ii) can be described from physicochemical perspectives, while the phenomena (iii) and (iv) can be mentioned from biological perspectives.

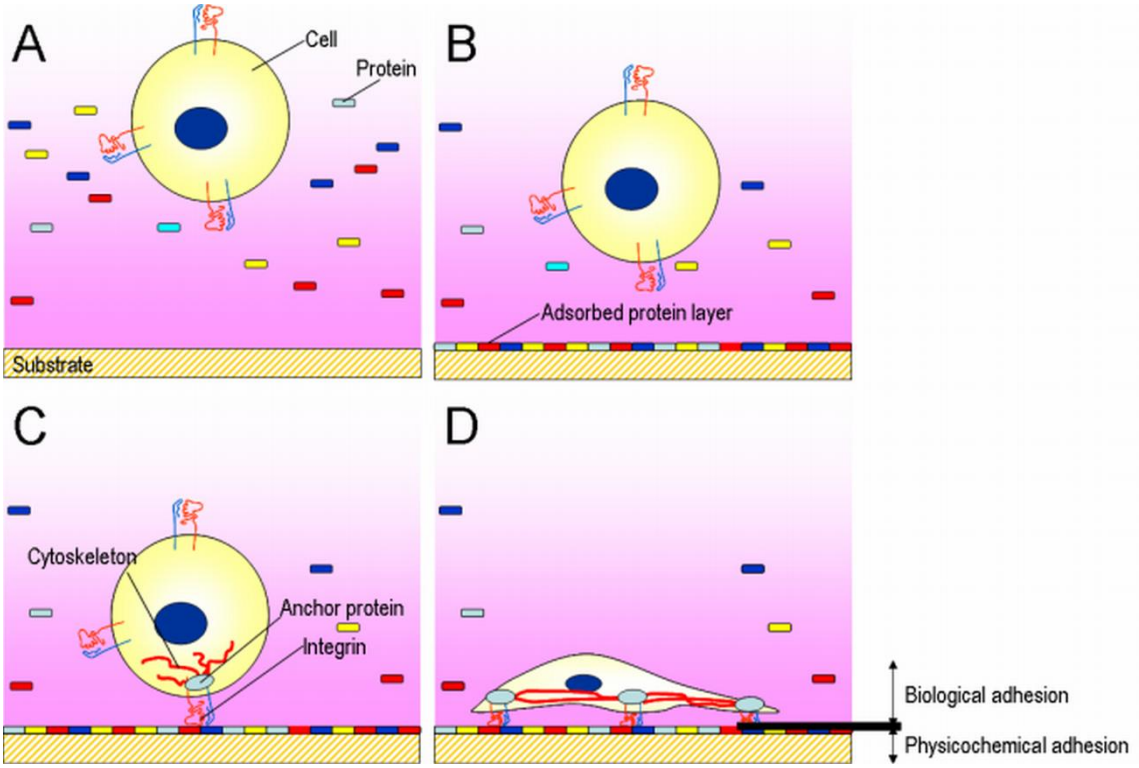

Fig. 1.3. Process of cell–material adhesion *in vitro*. Water and saline contact to the material (A), and then proteins in the solution absorb onto the surface of the material (B). Cells bind to the proteins absorbed on the material (C), attach, and spread (D).

1.3.1. Cell adhesion from physicochemical perspectives

Cells in suspension fall to absorbed protein layer on the surface of a material by gravity. Cell membrane and the material surface then physicochemically interact with each other (e.g., hydrophobic and electrostatic interactions) via absorbed protein layer. The physicochemical surface properties of the material thus play an important role in cell adhesiveness.

A number of proteins have both hydrophobic and hydrophilic interfacial activities due to their hydrophobic and hydrophilic portions. To negate a large interfacial free energy between surface and aqueous solution, proteins absorb on to a hydrophobic surface. In contrast, little proteins absorb onto a hydrophilic surface because of the low surface free

energy. Therefore, the wettability of a material affects protein absorption and hydrophobic interactions between cell membrane and the absorbed protein layer, suggesting that it is involved in cell adhesion. There have been a lot of reports about the relationship between the wettability and cell-adhesive activity of a material. Accordingly, cells adhere effectively to surfaces that have moderate wettability with water contact angles of 40–70°, but are not likely to adhere to extremely hydrophilic and hydrophobic surfaces [21-25].

With respect to surface charge, electrostatic interactions via an electric double layer are considered to have small influences in physiological salt concentrations [26], which can be led by the Derjaguin-Landau-Verwey-Overbeek theory. Namely, cell–surface distance that minimizes the interaction potential between the cell membrane and material surface is small enough to neglect electrostatic repulsions. The distance is 6.3–6.7 nm, while the length of the extracellular part of a transmembrane cell-adhesive molecule is apx. 20 nm. On the other hand, the surface charge affects the amount of absorbed proteins [27], and it is reported that cells well adhere to the surface with positive or negative charge [21,22,24,26].

Hydrogen bond and static repulsive force are also considered to affect cell adhesiveness directly and/or via absorbed protein layer [28,29].

1.3.2. Cell adhesion from biological perspectives

Following to interactions between cell membrane and absorbed protein layer, cell-adhesive proteins in the layer interact specifically with transmembrane cell-adhesive molecules such as integrins. Below is the cell adhesion which can be described from the biological perspectives.

Fibronectin is one of the main cell-adhesive proteins. The protein consists of two subunits (apx. 250 kDa each), which are linked by a disulfide bond to form a dimer, and each subunit chain is composed of type I, II, and III modules. These modules aggregate to form function domains which bind to integrins, collagens, heparins, and fibrins [30].

There are domains celled ED-A, ED-B, and IIICS, whose expression is regulated by alternative splicing. Their expressions thus result in the isoforms of the molecule.

Pierschbacher and Rouslahti [31] found that a peptide Arg-Gly-Asp-Ser (RGDS) is the domain that is responsible for the cell-adhesive activity of the fibronectin. Because the activity can be maintained when the serine is altered by other amino acid, the minimum unit is RGD. This sequence is necessary for the cell-adhesive activity of fibronetin, but is not a sufficient condition. To bind to cells, the peptides appeared to form a structure where they can be recognized by receptors on cellular surface [31,32].

Integrins are transmembrane cell-adhesive proteins and function as receptors for cell-adhesive molecules in ECM. The molecule consists of a α chain (apx. 120–180 kDa) and a β chain (apx. 90–110 kDa), which are noncovalently linked to form a heterodimer. 19 types of α subunits and 8 types of β subunits are identified currently [33], and ligand specificities derive from the combination of them. Integrin α5β1 recognizes an RGD sequence in fibronectin, vitronectin, and fibrin [34,35]. Both α and β chains a single-pass transmembrane protein, and more than 90 percent of the molecule is extracellular domains, which bind to ligand in ECM, while intercellular domains

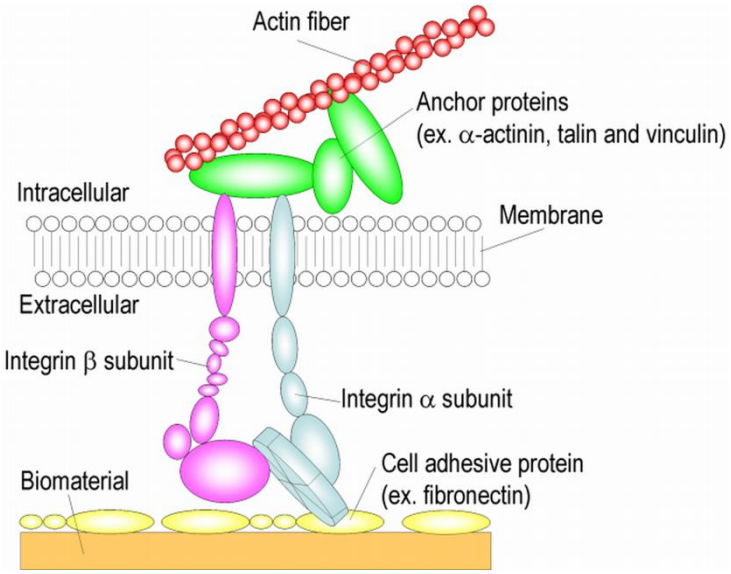

Fig. 1.4. Schematic drawing of the cell–substrate adhesion mediated by integrins.

connect to cytoskeleton, mediated by anchor proteins such as talin, vinculin, and α-actinin (Fig. 1.4). Reportedly, cell–substrate adhesion via integrins activates almost the same pathway as signals originated from cell growth factors. Integrins not only mechanically bind a cell with substrates but also transfer information about the surroundings of the cell into intracellular skeletal systems and signaling cascades. Thus, they play an essential role in cellular adhesion, spreading, migration, survival, proliferation, and differentiation.

1.4. Mechanical properties and mechanical environment of cells

Some types of cells are exposed to a mechanically-loaded environment *in vivo*. For example, hemodynamic fluid shear stress acts on vascular endothelial cells, and complex compression shear stress is loaded on articular chondrocytes. Cells can recognize these mechanical stresses and change their behaviors, which thus has motivated researchers to elucidate the mechanism itself and to use mechanical stimuli for the effective tissue regeneration.

1.4.1. Cellular mechanical properties

Mechanical properties of cells are related to various cell behaviors such as cellular shape, migration, growth, apoptosis, and differentiation. The properties have been evaluated through a variety of techniques. Although information that can be obtained by mechanical tests varies from method to method, cytoskeletal structure is one of the major factors to affect the cellular mechanical properties. Typically, treatment with cytochalasin D, which disrupt actin filaments, dramatically weakens cellular mechanical properties [36,37]. Strength to detach a cell from a substrate has also been quantified, which is defined as ‘cell adhesive force’. Besides the cytoskeleton, cell adhesive constructions appear to affect the cell adhesive force [38-43]. For example, Yamamoto

et al. [38] measured the adhesive force of single murine fibroblasts L929 and showed that the force is dependent on scaffold materials, explaining the number of bindings (e.g., cytoskeleton–integrin, integrin–ligand, ligand–ligand, and ligand–material surface) might determine the force. Although cellular mechanical properties have been measured in numerous studies, what the properties represent and the precise mechanism remain unclear.

1.4.2. Mechanical stimulation of cells

Mechanical stimuli for cells can promote their tissue regeneration and/or function organization. In particular, mechanical stimulation of cells in osteocartilaginous tissues have been studied a lot. For example, chondrocytes cultured stimulated by an appropriate relative tribological movement generated more lubricative tissues than those statically cultured [44]. Furthermore, an ultrasound stimulus has already been clinically applied to fracture treatment due to its healing effects on fresh fractures and nonunions. These physical stimuli are considered to be converted to intracellular signaling via integrins. However, the effect of mechanical stimulation is still controversial and more needs to be clarified.

1.5. Basic fibroblast growth factor

A growth factor is a naturally-occurring protein which binds to cell surface receptors, and it can stimulate cellular growth, proliferation, and differentiation. Several growth factor families have been identified, and their signaling cascades to stimulate cellular behavior have also been elucidated.

Human basic fibroblast growth factor (bFGF) is a single-chain heparin-binding polypeptide, which is generally composed of 155 amino acids and whose molecular weight is apx. 18 kDa. This growth factor is synthesized by different types of cells and

is a potent mitogen for endothelial cells [45] and for mesodermal- and neuroectodermal-derived cells [46,47]. For chondrogenic cells, it promotes cartilage repair *in vivo* [48,49] and matrix production *in vitro* [50-52] when bFGF is used as an additive to a solution such as culture medium.

bFGF is known as a notoriously unstable protein [53]. It is inactivated by treatments with a variety of solvents such as dilute acid, organic solvents, and solutions of guanidinium chloride [54]. Additionally, the growth factor exhibits an instability when stored at room temperature, exposed to alkaline pH or incubated with caralytic amounts of Cu^{2+} ions [55]. However, the stability of bFGF can increase when it binds to heparin or heparin-analogue compounds [56-58].

Human bFGF has four cysteines, and the oxidation of cysteines 78 and 96 (numbering refers to the 155-amino acid form of human bFGF) results in the formation of intermolecular disulphide bonds and multimerization, which cause the inactivation of the growth factor [59-62]. This theory can be explained by reports showing that the replacement of cysteines 78 and 96 by serines using site-directed mutagenesis techniques avoided the multimerization and increased the stability of human bFGF [53,55,60,62].

1.6. Silk fibroin

Below is an explanation about *Bombyx mori* silk proteins [63].

1.6.1. Structure of a silk protein

As shown in Fig. 1.5, the fiber from a silkworm cocoon forms a core-clad structure. The core is fibroin protein, which mainly consists of the silk fiber, while the clad is sericin protein. The latter protein is generally removed by a refinement process.

Fibroin protein consists of a heavy chain (H-chain; apx. 360 kDa) and a light chain

(L-chain; apx. 27 kDa), which are linked by a disulfide bond to form a heterodimer [64] (Fig. 1.6). Six sets of the heterodimers are associated with one P25 protein by hydrophobic interaction, and the whole is secreted from the posterior silk gland as a high-molecular-weight elementary unit [65]. In the H-chain molecule, the long,

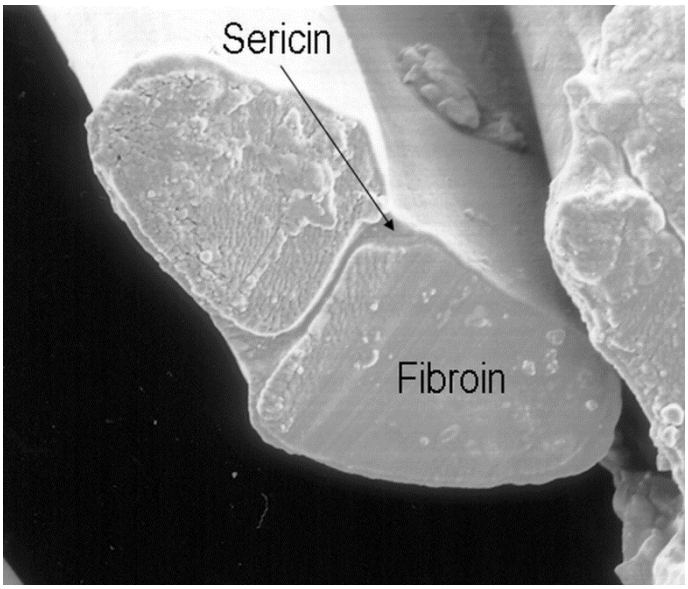

Fig. 1.5.Scanning electron microscopic image of a bave [63].

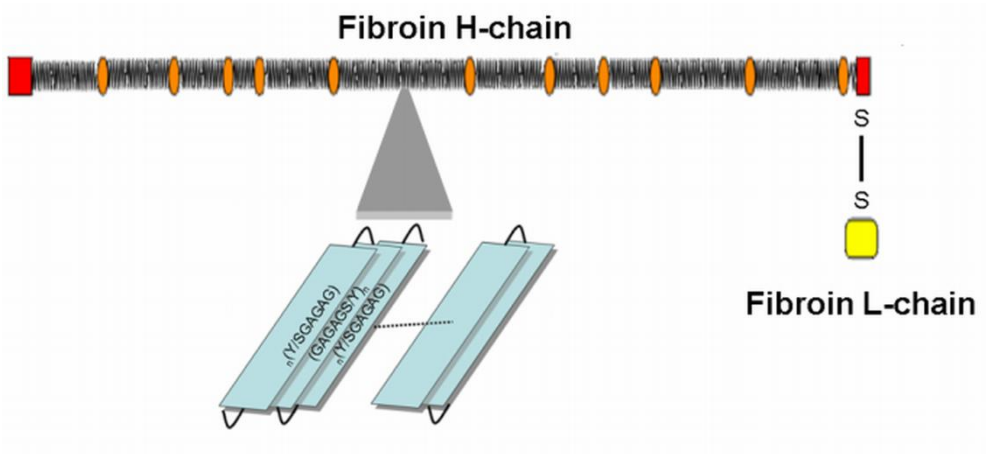

Fig. 1.6. Schematic drawing of a fibroin molecule.

extended, repeated region consists of a hydrophobic β-sheet crystalline region represented as (Gly-Ala-Gly-Ala-Gly-Ser/Tyr)$_n$ ((GAGAGS/Y)$_n$). These regions are linked by hydrophilic noncrystalline regions [66]. The molecular structure of the H-chain is likely to contribute to the mechanical property, moisture-retaining property, and drape of the silk fibers. On the other hand, the L-chain is considered to play a role in fibroin secretion [67], but its relations to the structure and property of the silk fiber have not yet been unclear.

1.6.2. Process to form various materials

To use silk proteins as a biomaterial, it is necessary to process to form various configurations. The fibroin is insoluble in water and most of the organic solvents. However, it is soluble in some particular organic solvents such as a calcium chloride/ethanol-mixed solution and a high concentration of lithium bromide aqueous solution. By dialyzing the fibroin solution against water, fibroin aqueous solution can be obtained, which is a start point to process various materials.

A porous three-dimensional structure is important for use in materials as a scaffold for tissue engineering. Several attempts to form a porous silk fibroin structure have been reported [68], where a repeated freeze-dry process was adopted. However, it was difficult to get high mechanical properties and to control spongy structures. Tamada [69] reported a new process to form fibroin porous three-dimensional structure, which involves freezing and thawing fibroin aqueous solution in the presence of a small amount of an organic solvent. The resultant spongy structure has a high water content requires as well as high mechanical properties. The solvent concentration, fibroin concentration, freezing temperature, and freezing duration affect the sponge formation. This fibroin structure can be autoclaved, and thus can be used as a biomaterial.

1.6.3. Fibroin as a biomaterial

Fibroin has been clinically practiced as a surgical suture. The silk suture has a high clinical usability due to its ease to bind and the stability of its knots [70]. In addition, reportedly, when refined and purified adequately, the silk fiber does not induce inflammatory reactions [63,71-73].

Recently, the number of the studies using fibroin as a scaffold for tissue engineering is increasing. Aoki et al. [13] reported that chondrocytes cultured using a porous silk fibroin sponge can proliferate well and produce more sulfated GAG (sGAG), compared to a collagen gel. Similarly, mesenchymal stem cells grown in a fibroin scaffold synthesized a larger amount of sGAG and showed a higher collagen type II gene expressions than those cultured in a collagen sponge [74].

1.6.4. Transgenic technique for silkworms

A transgenic technique for silkworms has already been established [75], which enables the production of molecularly-designed silk proteins. Once a genetically modified silkworm strain is developed, the modified fibroin can be produced permanently. By using this method, it is possible to develop a fibroin with new functions and mechanical properties (Fig. 1.7). Inoue et al. [76] mentioned several advantages of the application of the transgenic silkworm as a bioreactor to produce recombinant proteins such as that a large amount of a protein can be produced. Moreover, the location of the recombinant protein can be designed, and the protein thus can be immobilized to a particular part of the fibroin molecule. There have been several studies of genetic modification of the H-chain [77], the L-chain [42,76,78-82], or P25 protein [83].

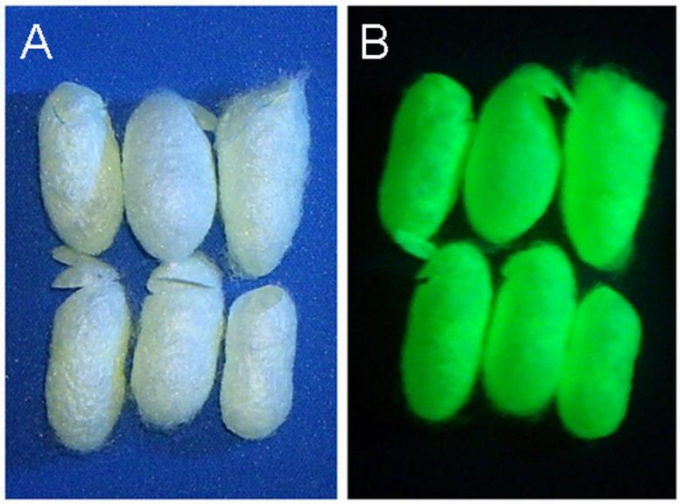

Fig. 1.7. Green fluorescent protein-fused silkworm cocoons under white light (A) and near-ultraviolet light (B).

1.7. Background and purpose of this study

Cartilaginous tissues have an intrinsic lack of regenerative ability and when destroyed, hyaline cartilage tissues never recovered spontaneously [16]. Osteroarthritis (OA) is one of the most common forms of arthritis. As of 2004 the number of patients of OA was estimated to be 24 million in Japan [84]. In addition, according to the National Livelihood Survey in 2010 [85] reported by the Ministry of Health, Labour and Welfare, Japan, arthritis is the number-four cause of being needed long-term care and also the number-one cause of being needed support. Therefore, it is essential to advance therapeutic treatments to improve and maintain the quality of life for people in the aging society like Japan. Various treatments have been used to repair damaged cartilage depending on the size of defects (Fig. 1.8). Cartilage tissue engineering, i.e., cell or tissue transplantation, usually targets the damage with defects whose size is 2–6 cm^2. Just recently, autologous cultured cartilage called JACC® (Japan Tissue Engineering Co., Ltd., Japan) has been approved to sell in Japan by the Japanese government, which is expected to progress the clinical application of cartilage regenerative medicine in Japan.

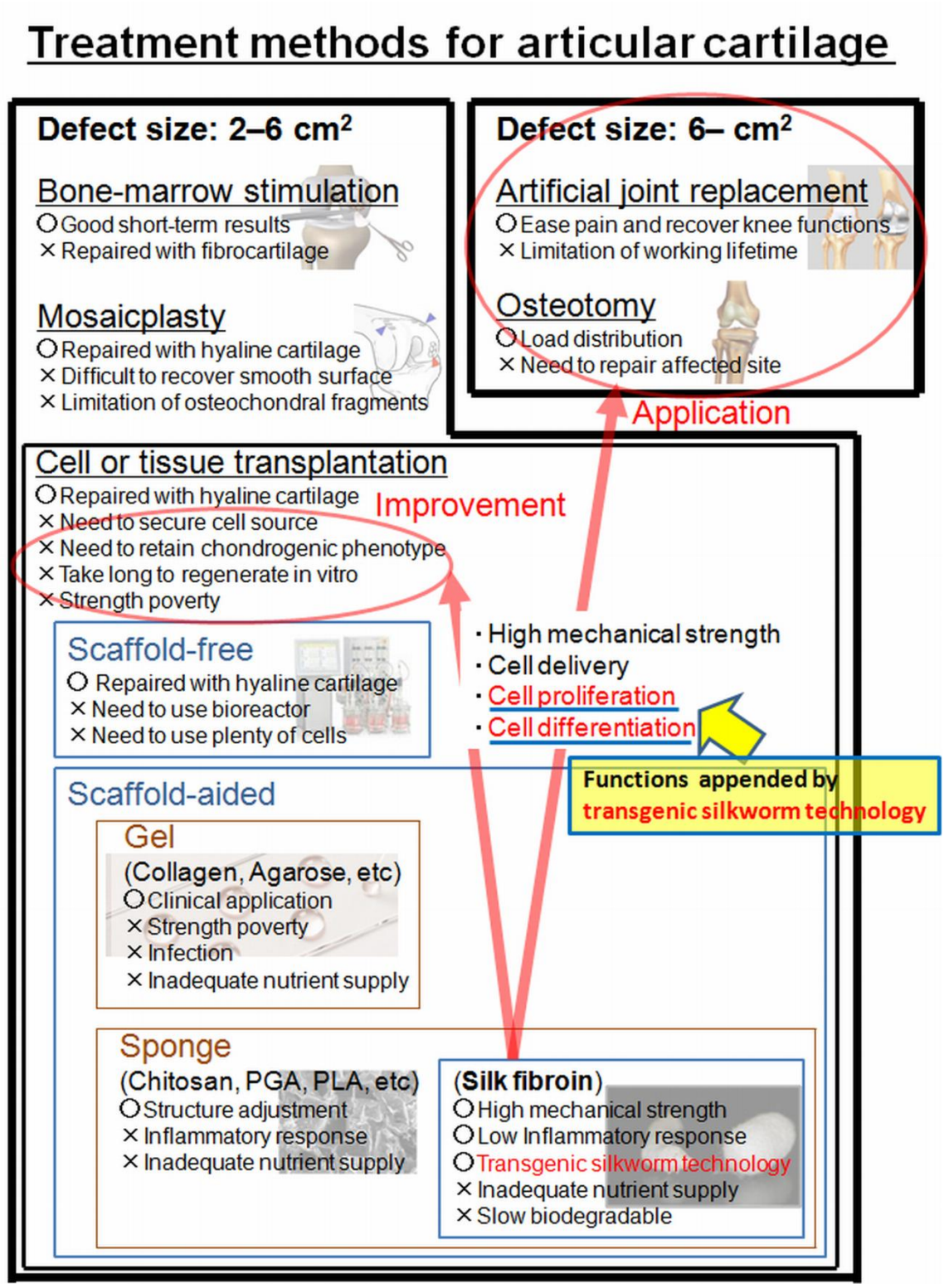

Fig. 1.8. Position of this study in the treatments for articular cartilage. Pictures and graphics in this figure are quoted elsewhere [86-92].

However, there remain a lot of issues to be resolved. Due to the limitation of harvestable chondrocytes, which have poor proliferative potential, the source of chondrogenic cells needs to be secured. Recent advancement in the differentiation induction of iPS cells is likely to achieve the differentiation of murine iPS cells into chondrocyte-like cells [93], but their chondrogenic phenotype is still unclear. Additionally, 3-D structure and mechanical functions of articular cartilage have to be repaired. Scaffold-free approaches to form regenerate cartilage have been studied using cell sheet technology [94] or bioreactors [95], while cellular scaffolds with new functions have been developed by using chemical or physical modifications or post-conjugation techniques. These studies have enabled to prepare regenerated cartilage with adequate mechanical properties and effective chondrogenesis. However, the former approaches require a large number of cells and specific culture devices and the latter ones are accompanied by technical difficulties and high manufacturing costs.

Silk fibroin protein is FDA-approved and has been used in medicine for a wide variety of applications such as surgical suture. Silk fibroin exhibits *in-vitro* and *in-vivo* biocompatibilities [63,71-73], showing the same degree of inflammatory responses as collagen [63]. Besides, fibroin molecules with a molecular weight of 40–120 kDa are reported not to have antigenecities [96]. Although silk fibroin shows relatively slow proteolytic biodegradation [97], which might limit the application range of the fibroin as a biomaterial, it has robust mechanical properties including high mechanical modulus and toughness [98]. The spongy structure of fibroin provides adjustable compressive and tensile moduli superior to collagen sponge [63,69]. Unpublished observations have shown that the silk fibroin spongy scaffold can be sutured to an affected site, covering the whole articular surface of patella in a rabbit model. Therefore, there is a possibility that silk fibroin sponge is used as a scaffold applicable to articular cartilage damage with defects whose size is over 6 cm^2. Furthermore, recent advances in transgenic silkworm technology have made silk fibroin a novel biomaterial, in which recombinant peptides or proteins can be located and combined in accordance with our design. These features of silk fibroin can provide useful clues to resolve issues and to exceed the

technical limits of cartilage tissue engineering as shown in Fig. 1.8.

The final goal of this study is to develop useful, practical scaffolds which enable effective cartilage regeneration (i.e., maintaining and/or improving the proliferative ability and chondrogenic phenotype of cells). To accomplish this goal three purposes have been set: to append promoting effects on cell proliferation to silk fibroin scaffold (Chapter 2); to seek a design index alternative to bioactive macromolecules (Chapter 3); and to add stimulatory effects on chondrogenesis by modulating the cell-adhesive function of silk fibroin scaffold (Chapter 4). The molecular design of silk fibroin by transgenic silkworm technology was applied to append new functions to the fibroin scaffold as shown in Chapters 2 and 4. However, in Chapter 2, a macromolecular growth factor was found to be difficult to exert its biological activity remarkably after fabricated into 3-D porous scaffold. As cells are anchorage-dependent and change their characteristics, such as mechanical and phenotypic properties, via cell–material adhesion, cellular physical properties induced by cell adhesion can be an important factor to design scaffold. Based on this viewpoint, cell adhesive force to scaffold materials was quantified and its relations with chondrogenesis were discussed in Chapters 3 and 4. This study would be expected to provide new, useful orientation in the development of cellular scaffold for tissue engineering.

References

[1] Langer R, Vacanti JP. Tissue engineering. Science 1993;260:920-6.

[2] http://report.nih.gov/nihfactsheets/ViewFactSheet.aspx?csid=62&key=R (in Dec 2012)

[3] Fuchs JR, Nasseri BA, Vacanti JP. Tissue engineering: a 21st century solution to surgical reconstruction. Ann Thorac Surg 2001;72:577-91.

[4] Takahashi K, Tanabe K, Ohnuki M, Narita M, Ichisaka T, Tomoda K, et al. Induction of pluripotent stem cells from adult human fibroblasts by defined factors. Cell 2007;131:861-72.

[5] Evans PM, Kaufman MH. Establishment in culture of pluripotential cells from mouse embryos. Nature 1981;292:154-6.

[6] Yamamoto K. Functional expression and evaluation of tribological performances on living tissue. 2006.

[7] Von der Mark K, Gauss V, Von der Mark H, Müller P. Relationship between cell shape and type of collagen synthesised as chondrocytes lose their cartilage phenotype in culture. Nature 1977;267:531-2.

[8] Benya PD, Shaffer JD. Dedifferentiated chondrocytes reexpress the differentiated collagen phenotype when cultured in agarose gels. Cell 1982;30:215-24.

[9] Brodkin KR, García AJ, Levenston ME. Chondrocyte phenotypes on different extracellular matrix monolayers. Biomaterials 2004;25:5929-38.

[10] Schuman L, Buma P, Versleyen D, de Man B, van der Kraan PM, van den Berg WB, et al. Chondrocyte behaviour within different types of collagen gel in vitro. Biomaterials 1995;16:809–14.

[11] Rahfoth B, Weisser J, Sternkopf F, Aigner T, von der Mark K, Brauer R. Transplantation of allograft chondrocytes embedded in agarose gel into cartilage defects of rabbits. Osteoarth Cart 1998;6:50–65.

[12] Gille J, Meisner U, Ehlers EM, Muller A, Russlies M, Behrens P. Migration pattern, morphology and viability of cells suspended in or sealed with fibrin glue: a

histomorphologic study. Tissue Cell 2005;37:339–48.

[13] Aoki H, Tomita N, Morita Y, Hattori K, Harada Y, Sonobe M, et al. Culture of chondrocytes in fibroin-hydrogel sponge. Biomed Mater Eng 2003;13:309-16.

[14] Woo S, Mow VC, Lai WM, Skalak R, Chien S. Handbook of Bioengineering. The McGraw-Hill Company 1987.

[15] Buckwalter JA, Mankin HJ. Articular cartilage repair and transplantation. Arthritis Rheum 1998;41:1331-42.

[16] Hunter W. Of the structure and diseases of articulating cartilages. Philos Trans 1743;470:514-21.

[17] Pridie KH. A method of resurfacing osteoarthritic knee joints. J Bone Joint Surg Br 1959;41:618-19.

[18] Matsusue Y, Yamamuro T, Hama H. Arthroscopic multiple osteochondral transplantation to the chondral defect in the knee associated with anterior cruciate ligament disruption. Arthroscopy 1993;9:318-21.

[19] Brittberg M, Lindahl A, Nilsson A, Ohlssion C, Isaksson O, Peterson L. Treatment of deep cartilage defects in the knee with autologous chondrocyte transplantation. N Engl J Med 1994;331:889-95.

[20] Iwata H. Biomaterials. Kyoritsu Shuppan Co., Ltd., 2005.

[21] Van Wachem PB, Hogt AH, Beugeling T, Feijen J, Bantjes A, Detmers JP, et al. Adhesion of cultured human endothelial cells onto methacrylate polymers with varying surface wettability and charge. Biomaterials 1987;8:323-8.

[22] Kishida A, Iwata H, Tamada Y, Ikada Y. Cell behaviour on polymer surfaces grafted with non-ionic and ionic monomers. Biomaterials 1991;12:786-92.

[23] Tamada Y, Ikada Y. Cell adhesion to plasma-treated polymer surfaces. Polymer 1993;34:2208-12.

[24] Lee JH, Lee JW, Khang G, Lee HB. Interaction of cells on chargeable functional group gradient surfaces. Biomaterials 1997;19:351-8.

[25] Arima Y, Iwata H. Effect of wettability and surface functional groups on protein adsorption and cell adhesion using well-defined mixed self-assembled monolayers.

Biomaterials 2007;28:3074-82.

[26] Arima Y, Iwata H. Effects of surface functional groups on protein adsorption and subsequent cell adhesion using self-assembled monolayers. J Mater Chem 2007;17:4079-87.

[27] Lestelius M, Liedberg B, Tengvall P. In vitro plasma protein adsorption on ω-functionalized alkanethiolate self-assembled monolayers. Langmuir 1997;13:5900-8.

[28] Ostuni E, Chapman RG, Holmlin RE, Takayama S, Whitesides GM. A survey of structure-property relationships of surface that resist the adsorption of protein. Langmuir 2001;17:5605-20.

[29] Prime KL, Whitesides GM. Adsorption of proteins onto surfaces containing end-attached oligo (ethylene oxide): a model system using self-assembled monolayers. J Am Chem Soc 1993;115:10714-21.

[30] Hynes RO. Fibronectins. Springer-Verlag, 1990.

[31] Pierschbacher MD, Ruoslahti E. Cell attachment activity of fibronectin can be duplicated by small synthetic fragments of the molecule. Nature 1984;309:30-4.

[32] Maeda T, Oyama R, Ichihara-Tanaka K, Kimizuka F, Sekiguchi K. A novel cell adhesive protein engineered by insertion of the Arg-Gly-Asp-Ser tetrapeptide. J Biol Chem 1989;264:15165-8.

[33] Humphries MJ. Integrin structure. Biochem Soc Trans 2000;28:311-39.

[34] Ruoslahti E, Pierschbacher MD. Arg-Gly-Asp: a versatile cell recognition signal. Cell 1986;44:517-8.

[35] Hynes RO. Integrins: versatility, modulation, and signaling in cell adhesion. Cell 1992;69:11-25.

[36] Nagayama K, Nagano Y, Sato M, Matsumoto T. Effect of actin filament distribution on tensile properties of smooth muscle cells obtained from rat thoracic aortas. J Biomech 2006;39:293-301.

[37] Tan SCW, Pan WX, Ma G, Cai N, Leong KW, Liao K. Viscoelastic behaviour of human mesenchymal stem cells. BMC Cell Biol 2008;9:40.

[38] Yamamoto A, Mishima S, Maruyama N, Sumita M. Quantitative evaluation of cell attachment to glass, polystyrene, and fibronectin- or collagen-coated polystyrene by measurement of cell adhesive shear force and cell detachment energy. J Biomedl Mater Res 2000;50:114-24.

[39] Wu CC, Su HW, Lee CC, Tang MJ, Su FC. Quantitative measurement of changes in adhesion force involving focal adhesion kinase during cell attachment, spread, and migration. Biochem Biophys Res Commun 2005;329:256-65.

[40] Yamamoto K, Tomita N, Fukuda Y, Suzuki S, Igarashi N, Suguro T, et al. Time-dependent changes in adhesive force between chondrocytes and silk fibroin substrate. Biomaterials 2007;28:1838-46.

[41] Cai N, Wong CC, Tan SCW, Chan V, Liao K. Temporal effect of functional blocking of β_1 integrin on cell adhesion strength under serum depletion. Langmuir 2009;25:10939-47.

[42] Kambe Y, Yamamoto K, Kojima K, Tamada Y, Tomita N. Effects of RGDS sequence genetically interfused in the silk fibroin light chain protein on chondrocyte adhesion and cartilage synthesis. Biomaterials 2010;31:7503-11.

[43] Kambe Y, Takeda Y, Yamamoto K, Kojima K, Tamada Y, Tomita N. Effect of RGDS-expressing fibroin dose on initial adhesive force of a single chondrocyte. Biomed Mater Eng 2010;20:309-16.

[44] Yamamoto K, Takaya R, Tamada Y, Tomita N. Effects of tribological loading history on the expression of tribological function of regenerated cartilage. Tribology Online 2008;3:148-52.

[45] Shing Y, Folkman J, Sullivan R, Butterfield C, Murray J, Klagsbrun M. Heparin affinity: purification of a tumor-derived capillary endothelial cell growth factor. Science 1984;223:1296-99.

[46] Gospodarowicz D, Ferrara N, Schweigerer L, Neufeld G. Structural characterization and biological functions of fibroblast growth factor. Endocrine Rev 1987;8:95-114.

[47] Burgess WH, Maciag T. The heparin-binding (fibroblast) growth factor family of

proteins. Ann Rev Biochem 1989;58:575-606.

[48] Cuevas P, Burgos J, Baird A. Basic fibroblast growth factor (FGF) promotes cartilage repair in vivo. Biochem Biophys Res Commun 1988;156:611-8.

[49] Fujimoto E, Ochi M, Kato Y, Mochizuki Y, Sumen Y, IkutaY. Beneficial effect of basic fibroblast growth factor on the repair of full-thickness defects in rabbit articular cartilage. Arch Orthop Trauma Surg 1999;199:139-45.

[50] Schmal H, Zwingmann J, Fehrenbach M, Finkenzeller G, Stark GB, Südkamp NP, et al. bFGF influences human articular chondrocyte differentiation. Cytotherapy 2007;9:184-93.

[51] Khan M, Palmer EA, Archer CW. Fibroblast growth factor-2 induced chondrocyte cluster formation in experimentally wounded articular cartilage is blocked by soluble Jagged-1. Osteoarthritis Cartilage 2010;18:208-19.

[52] Kim JH, Lee MC, Seong SC, Park KH, Lee S. Enhanced proliferation and chondrogenic differentiation of human synovium-derived stem cells expanded with basic fibroblast growth factor. Tissue Eng Part A 2011;17:991-1002.

[53] Estape D, Van den Heuvel J, Rinas U. Susceptibility towards intramolecular disulphide-bond formation affects conformational stability and folding of human basic fibroblast growth factor. Biochem J 1998;335:343-9.

[54] Westall FC, Rubin R, Gospodarowicz D. Brain-derived fibroblast growth factor: a study of its inactivation. Life Sci 1983;33:2425-9.

[55] Caccia P, Nitti G, Cletini O, Pucci P, Ruoppolo M, Bertolero F, et al. Stabilization of recombinant human basic fibroblast growth factor by chemical modifications of cysteine residues. Eur J Biochem 1992;204:649-55.

[56] Gospodarowicz D, Cheng J. Heparin protects basic and acidic FGF from inactivation. J Cell Physiol 1986;128:475-84.

[57] Vemuri S, Beylin I, Sluzky V, Stratton P, Eberlein G, Wang YJ. Characterization, stability, and formulations of basic fibroblast growth factor. J Pharm Pharmacol 1994;46:484-6.

[58] Tardieu M, Bourin MC, Desgranges P, Barbier P, Barritault D, Caruelle JP.

Mesoglycan and sulodexide act as stabilizers and protectors of fibroblast growth factors (FGFs). Growth Factors 1994;11:291-300.

[59] Thompson SA, Fiddes JC. Chemical characterization of the cysteines of basic fibroblast growth factor. Ann N Y Acad Sci 1991;638:78-88.

[60] Fox GM, Schiffer SG, Rohde MF, Tsai LB, Banks AR, Arakawa T. Production, biological activity, and structure of recombinant basic fibroblast growth factor and an analog with cysteine replaced by serine. J Biol Chem 1988;263:18452-8.

[61] Iwane M, Kurosawa T, Sasada R, Seno M, Nakagawa T, Igarashi K. Expression of cDNA encoding human basic fibroblast growth factor in E. coli. Biochem Biophys Res Commun 1987;146:470-7.

[62] Seno M, Sasada R, Iwane M, Sudo K, Kurokawa T, Ito K et al. Stabilizing basic fibroblast growth factor using protein engineering. Biochem Biophys Res Commun 1988;151:701-8.

[63] Tamada Y. Prospect of biomaterial study from insects. J Jpn Soc Biomater 2008;26:412-8.

[64] Tanaka K, Kajiyama N, Ishikura K, Waga S, Kikuchi A, Ohtomo K, et al. Determination of the site of disulfide linkage between heavy and light chains of silk fibroin produced by *Bombyx mori*. Biochim Biophys Acta 1999;1432:92-103.

[65] Inoue S, Tanaka K, Arisaka F, Kimura S, Ohtomo K, Mizuno S. Silk fibroin of *Bombyx mori* is secreted, assembling a high molecular mass elementary unit consisting of H-chain, L-chain, and P25, with a 6:6:1 molar ratio. J Biol Chem 2000;275:40517-28.

[66] Mita K, Ichimura S, James TC. Highly repetitive structure and its organization of the silk fibroin gene. J Mol Evol 1994;38:583-92.

[67] Mori K, Tanaka K, Kikuchi Y, Waga M, Waga S, Mizuno S. Production of a chimeric fibroin light-chain polypeptide in a fibroin secretion-deficient nalled pupa mutant of the silkworm *Bombyx mori*. J Mol Biol 1995;251:217-28.

[68] Nazarov R, Jin HJ, Kaplan DL. Porous 3-D scaffolds from regenerated silk fibroin. Biomacromolecules 2004;5:718-26.

[69] Tamada Y. New process to form a silk fibroin porous 3-D structure. Biomacromolecules 2005;6:3100-6.

[70] Kadono K, Tamai S, Tomita N, Tmihata K. Handling characteristics of suture materials. Jpn J Biomech 1999;20:261-5.

[71] Altman GH, Diaz F, Jakuba C, Calabro T, Horan RL, Chen J, et al. Silk-based biomaterials. Biomaterials 2003;24:401-16.

[72] Panilaitis B, Altman GH, Chen J, Jin HJ, Karageorgiou V, Kaplan DL. Macrophages responses to silk. Biomaterials 2003;24:3079-85.

[73] Meinel L, Hofmann S, Karageorgiou V, Kirker-Head C, Vunjak-Novakovic G, Kaplan DL. The inflammatory responses to silk film in vitro and in vivo. Biomaterials 2005;26:147-55.

[74] Wang Y, Kim UJ, Blasioli DJ, Kim HJ, Kaplan DJ. In vitro cartilage tissue engineering with 3D porous aqueous-derived silk fibroin and mesenchymal stem cells. Biomaterials 2005;26:7082-94.

[75] Tamura T, Thibert C, Royer C, Kanda T, Abraham E, Kamba M, et al. Germline transformation of the silkworm *Bombyx mori* L. using a *piggyBac* transposon-derived vector. Nat Biotechnol 2000;18:81-4.

[76] Inoue S, Kanda T, Imamura M, Quan GX, Kojima K, Tanaka H, et al. A fibroin secretion-deficient silkworm mutant, *Nd-s*^{D}, provides an efficient system for producing recombinant proteins. Insect Biochem Mol Biol 2005;35:51-9.

[77] Kojima K, Kuwana Y, Sezutsu H, Kobayashi I, Uchino K, Tamura T, et al. A new method for the modification of fibroin heavy chain protein in the transgenic silkworm. Biosci Biotechnol Biochem 2007;71:2943-51.

[78] Tomita M, Munetsuna H, Sato T, Adachi T, Hino R, Hayashi M, et al. Transgenic silkworms produced recombinant human type III procollagen in cocoons. Nat Biotechnol 2003;21:52-6.

[79] Adachi T, Tomita M, Shimizu K, Ogawa S, Yoshizato K. Generation of hybrid transgenic silkworms that express *Bombyx mori* prolyl-hydroxylase α-subunits and human collagens in posterior silk glands: production of cocoons that contained

collagens with hydroxylated proline residues. J Biotechnol 2006;126:205-19.

[80] Hino R, Tomita M, Yoshizato K. The generation of germline transgenic silkworms for the production of biologically active recombinant fusion proteins of fibroin and human basic fibroblast growth factor. Biomaterials 2006;27:5715-24.

[81] Yanagisawa S, Zhu Z, Kobayashi I, Uchino K, Tamada Y, Tamura T, et al. Improving cell-adhesive properties of recombinant *Bombyx mori* silk by incorporation of collagen of fibronectin derived peptides produced by transgenic silkworms. Biomacromolecules 2007;8:3487-92.

[82] Sato M, Kojima K, Sakuma C, Murakami M, Aratani E, Takenouchi T, et al. Production of scFv-conjugated affinity silk powder by transgenic silkworm technology. PLoS one 2012;7:e34632.

[83] Royer C, Jalabert A, Da Rocha M, Grenier AM, Mauchamp B, Couble P, et al. Biosynthesis and cocoon-export of a recombinant globular protein in transgenic silkworms. Transgenic Res 2005;14:463-72.

[84] http://www.h.u-tokyo.ac.jp/vcms_lf/center22_rinsyo_undouki_19-21.pdf (in Dec 2012)

[85] http://www.mhlw.go.jp/toukei/saikin/hw/k-tyosa/k-tyosa10/4-2.html (in Dec 2012)

[86] http://aseed.coloplast.com/?bone=1 (in Dec 2012)

[87] http://www.northwaleskneeclinic.co.uk/images/mosaicplasty.jpg (in Dec 2012)

[88] http://www.engin.umich.edu/class/bme456/artjoint/artjoint.htm (in Dec 2012)

[89] http://www.knee-replacement-explained.com/KNEE-OSTEOTOMY.html (in Dec 2012)

[90] http://www.medicalexpo.com/prod/sartorius-group/autoclavable-bioreactors-69922-450990.html (in Dec 2012)

[91] http://help.qgelbio.com/entries/188248-how-can-i-prevent-the-gels-from-sticking-to-the-3d-disc-caster-when-harvesting (in Dec 2012)

[92] Sugiyama K, Okamura A, Kawazoe N, Tateishi T, Satp S, Chen G. Coating of collagen on a poly(L-lactic acid) sponge surface for tissue engineering. Mater Sci Eng C 2012;32:290-5.

[93] Diekman BO, Christoforou N, Willard VP, Sun H, Sanchez-Adams J, Leong KW, et al. Cartilage tissue engineering using differentiated and purified induced pluripotent stem cells. Proc Natl Acad Sci USA 2012. 10.1073/pnas.1210422109.

[94] Kaneshiro N, Sato M, Ishihara M, Mitani G, Sakai H, Mochida J. Bioengineered chondrocyte sheets may be potentially useful for the treatment of partial thickness defects of articular cartilage. Biochem Biophys Res Commun 2006;349:723-310

[95] Furukawa KS, Sato M, Nagai T, Ting S, Mochida J, Ushida T. Scaffold-free cartilage tissue by mechanical stress loading for tissue engineering. Tissue Eng (IN-TEC) 2009.

[96] Zhang YQ, Ma Y, Xia YY, Shen WD, Mao JP, Shirai K. Synthesis of silk fibroin-insulin bioconjugates and their characterization and activities in vivo. J Biomed Mater Res B Appl Biomater 2006;79:275-83.

[97] Horan RL, Antle K, Collette AL, Wang Y, Huang J, Chen J, et al. In vitro degradation of silk fibroin. Biomaterials 2005;26:3385-93.

[98] Perez-Rigueiro J, Elices M, Llorca J, Viney C. Tensile properties of Argiope trifasciata drag line silk obtained from the spider's web. Appl Polym Sci 2001;82:2245-51.

Chapter 2
Development of bFGF-Fused Silk Fibroin, Evaluation of Its Activity, and Application as a Scaffold for Cartilage Regeneration

2.1. Introduction

To achieve the clinical application of regenerative medicine, the development of functional scaffolds has been being addressed. Silk fibroin obtained through degumming *Bombyx mori* (silkworm) silk was historically used as a surgical suture, and various processes into cellular scaffolds such as a porous three-dimensional (3-D) structure have been established [1-5]. In fact, silk fibroin has been widely studied as a scaffold material for tissue regeneration such as bone [6-8], cartilage [9-13], and nerve regeneration [14]. Moreover, physical and/or biological characteristics of silk fibroin protein can be altered by chemical modification [15-18] or post-conjugation [6-8,10] with functional factors. However, in the case of these modifications, the immobilization, release, and/or loading efficiency of the functional factors can be controversial along with technical difficulties and/or high manufacturing.

The establishment and progress of transgenic silkworm technology [19] have enabled the production of silk fibroin proteins fused with recombinant proteins. Some of these modified fibroins could maintain or recover new functions derived from the recombinant protein even after a process into a material [13,20-23]. Yanagisawa et al. [22] and we developed Arg-Gly-Asp (RGD)-fused silk fibroin and showed that more

cells attached to the cast film of the fibroin than that of wild-type fibroin. We also manufactured a spongy structure of the RGD-fused fibroin as a scaffold for chondrocytes and demonstrated the cells on the RGD-fused fibroin sponge effectively formed the cartilage tissue [13]. Sato et al. [23] produced single-chain variable fragment (scFv)-conjugated silk fibroin and showed the powder of the fibroin retained an affinity to Wiskott-Aldrich syndrome protein, which is the target molecule of the scFv. Basic fibroblast growth factor (bFGF)-fused silk fibroin was developed by Hino et al. [21]. They conducted refolding of the bFGF-fused fibroin and showed the modified fibroin immobilized on a culture dish enhanced the growth of human umbilical vein endothelial cells (HUVECs). These studies suggest that the silk fibroin fused with a functional protein can be used as a biomaterial for scaffold-based tissue regeneration, and we actually demonstrated that more cartilage-like tissues were synthesized in/on the RGD-fused fibroin spongy scaffold than in/on the wild-type fibroin sponge. However, in the case of the RGD-fused fibroin only eight amino-acid residues ($(RGDS)_2$) are fused with the fibroin protein, and it remains unclear whether a genetically-modified fibroin fused with a macromolecular recombinant protein displays the function of the recombinant protein even after fabricated into a 3-D scaffold.

In the present study, we have aimed to develop a silk fibroin scaffold with cell-growth function for cartilage regeneration by using a transgenic silkworm strain that produces silk fibroin protein fused with bFGF. This growth factor is reported to promote cartilage repair *in vivo* [24,25] and chondrogenesis *in vitro* [26-28], showing enhancement effects on the viability and/or matrix production of chondrogenic cells. In the bFGF-fesed fibroin molecule, bFGF is designed to be linked to the fibroin light chain (L-chain) protein through a linker with a collaganase-cleavage site. This cleavage site is composed of amino acids, Pro-Leu-Gly-Ile-Ala-Gly (PLGIAG), which is cleaved between the Gly and Ile by a collagenase: matrix metarlloproteinase 1 (MMP1) [29]. Thus, our strategy is that bFGF fused with the fibroin scaffold is to be released along with cartilage metabolism. Using Western blot analysis, we confirmed that bFGF was fused with the fibroin L-chain and could be released from the L-chain by a collagenase

treatment. Then, cell-proliferative activity of the bFGF-fused fibroin was investigated at various stages in a process to form a silk fibroin spongy structure. Finally, we evaluated the usefulness of the bFGF-fused fibroin sponge as a scaffold for cartilage tissue engineering.

2.2. Materials and methods

2.2.1. Construction of a vector carrying cDNA encoding bFGF-fused fibroin L-chain

Two oligonucleotides (bFGF_col2link-5Bg2: 5'-GAGATCTCCACTAGGAATAGCAGGAATG-3'; and bFGF_col2link-3: 5'-GATGCTCCCGGCTGCCATTCCTGCTATTC-3') were mixed, and an oligonucleotide cassette (5'-GAGATCTCCACTAGGAATAGCAGGAATGGCAGCCGGGAGCATC-3') was obtained by polymerase chain reaction (PCR)-amplification. On the other hand, cDNA encoding 155-amino acid residue-long human bFGF (accession number, J04513) was amplified by PCR from a cloned cDNA encoding human bFGF provided elsewhere using two oligonucleotides (bFGF_ORF-5: 5'-ATGGCAGCCGGGAGCATCACC-3'; and bFGF_ORF-3SalI: 5'-GGTCGACTCAGCTCTTAGCAGAC-3'). The two resultant oligonucleotide cassettes were annealed, and cDNA encoding a bFGF with a collagenase cleavage site, PLGIAG, was obtained by PCR using bFGF-col2link-5Bg2 and bFGF_ORF-3SalI. This amplified fragment was treated with *Bgl*II and *Sal*I and cloned between *Bam*HI and *Sal*I sites of pLC-vec. The resultant plasmid was designated pLC-col2bFGF. To obtain a transfer plasmid, the expression cassette in pLC-col2bFGF was digested with *Fse*I and *Asc*I, and, finally, the resulting fragment was cloned between the *Fse*I and blunt-ended *Asc*I sites of pBac(3×P3-DsRed2afm)E1 [20]. This transfer plasmid was designated pBac(3×P3-DsRed2afm)E1_pLC-col2bFGF, whose structure is shown in Fig. 2.1.

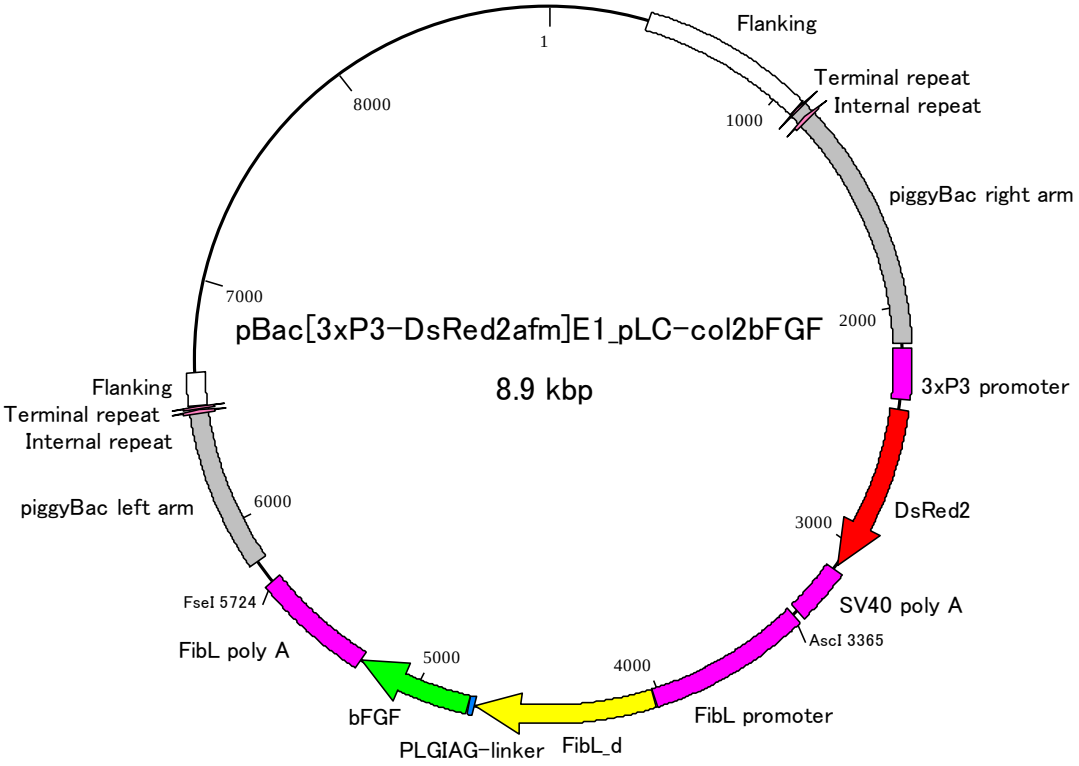

Fig. 2.1. Structure of the pBac(3×P3-DsRed2afm)E1_ pLC-col2bFGF vector.

2.2.2. Generation of transgenic silkworms

Silkworm transgenesis was performed as described by Tamura et al. [19] with minor modifications. Briefly, the plasmid pBac(3×P3-DsRed2afm)E1_pLC-col2bFGF was injected into silkworm eggs along with a helper plasmid pHA3PIG coding for *piggyBac* transposase [19] at 3–6 h post-oviposition. Hatched larvae (G0) were reared and permitted to mate with each other. The resultant embryos (G1) were screened by using a fluorescent microscope (MZ16 FA; Leica Microsystems, Germany) for transgenic individuals with DsRed2 expression 6–7 days after oviposition. The transgenic silkworms were reared together and sib-mated for at least three generations, with sequential screening by the strong excitation of DsRed2 fluorescence in the adult eye. The resulting strain was designated NK34, which carries the transgene coding for the fibroin L-chain fused with collagenase-cleavage site and human bFGF at the carboxyl-

terminus.

2.2.3. SDS-PAGE and Western blotting

Cocoon shells of wild-type or NK34 silkworms were diced into apx. 1 mm^2. They were suspended in an 8 M urea aqueous solution with 5% 2-mercaptoethanol (2ME) and incubated at 80°C for 15 min with some stirrings, followed by washing with distilled water prewormed at 80°C. This urea refinement procedure was repeated twice to roughly remove sericin proteins. The rest silk proteins were dissolved in 9.0 M LiBr aqueous solution by stirring at room temperature (RT) for 1 h. After centrifugation, the supernatant was dialyzed against phosphate buffered saline (PBS, pH 7.4; Wako Pure Chemical Industries Ltd., Japan) by using the EasySep (molecular weight cut off (MWCO), 14,000; Tomy Seiko Co., Ltd., Japan) in accordance with the manufactures instructions. Then the protein concentration was determined by the absorbance at 280-nm ultraviolet light and adjusted to 20 mg/3 ml with PBS, where different concentrations of collagenase (Collagenase L; Nitta Gelatin Inc., Japan) were added (final concentration, 4 mg/ml silk protein and 0, 0.4, 4, and 40 μg/ml collagenase). After incubation at 37°C for 24 h, the resultant solutions were mixed with the equal volume of the Laemmli Sample Buffer (Bio-Rad Laboratories Inc., USA) containing 5% 2ME and incubated at 60°C for 20 min. 15 or 5 μl of the solution was applied to sodium dodecyl sulfate-polyacrylamide gel electrophoresis (SDS-PAGE).

SDS-PAGE was performed on a Mini-PROTEAN TGX gel (Any kD™; Bio-Rad Laboratories Inc.). Commercial recombinant human bFGF (rhbFGF; Wako Pure Chemical Industries Ltd.) was also applied on the gel as a positive control. Separated proteins were visualized by staining a gel with EzStain AQua (Atto Corp., Japan) containing Coomassie brilliant blue (CBB). For immunoblotting, separated proteins on another gel were transferred onto a polyvinylidene fluoride (PVDF) membrane (Immun-Blot® PVDF Membrane for Protein Blotting; Bio-Rad Laboratories Inc.) by using Trans-Blot® SD Semi-Dry Transfer Cell (Bio-Rad Laboratories Inc.) and

subjected to Western blot assay with Chemi-Lumi One Super (Nacalai Tesque Inc., Japan) according to the manufacturer's instructions. Signals were detected with an LAS-3000 mini compact chemiluminescence system (Fujifilm Corp., Japan). Rabbit anti-human bFGF polyclonal antibody (ab10420; Abcam plc., UK) and horseradish peroxidase-conjugated goat anti-rabbit IgG polyclonal antibody (ab6721; Abcam plc.) were used as the primary and the secondary antibodies, respectively.

2.2.4. Sample preparation

Processes to prepare samples for evaluation of the biological activity of the bFGF-fused fibroin are shown in Fig. 2.2. These details are described below.

2.2.4.1. Silk fibroin extracted from PSG

Posterior silkglands (PSGs) was extracted from *Bombyx mori* wild-type C515 or NK34 silkworms and immersed in solution A composed of 1.7 mM Na_2HPO_4, 16.7 mM KH_2PO_4, 150 mM NaCl, 1 mM KCl, and 3 mM $CaCl_2$ to extract fibroin proteins. The solution was filtered through a paper membrane with 9.5-μm pores (#5B; Kiriyama glass Co., Japan) and centrifuged at 9,100×g for 30 min at 4°C to remove impurities. The fibroin solutions were sterilized by filtering through a polyethersulfone (PES) membrane with 0.22-μm pores (Millipore Corp., USA). This procedure was designated Process I, which is shown in Fig. 2.2.

2.2.4.2. Silk proteins extracted from cocoons

Cocoons of wild-type or NK34 silkworms were diced into apx. 5 mm square, dissolved in a 9.0 M LiBr aqueous solution at RT for 6–10 h with stirring. Then, the solution was dialyzed in water at 4°C using a cellulose dialysis membrane (Spectra/Por 1; MWCO, 6–8000; Spectrum Laboratories Inc., USA) for 3 days, changing the water every 10–14 h. The resultant silk protein aqueous solution was sterilized by 0.22-μm

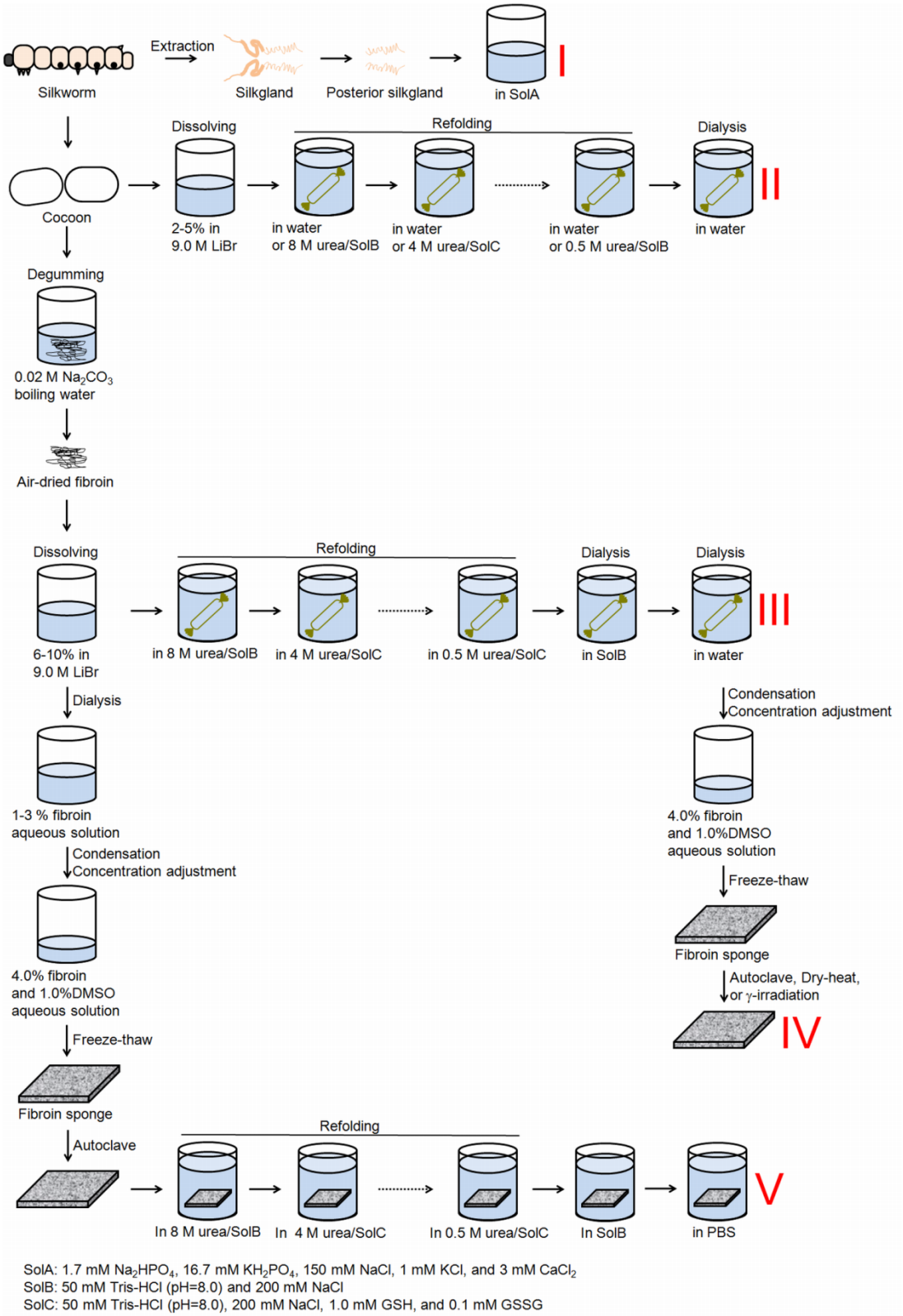

Fig. 2.2. Flowchart of a process to form a silk fibroin sponge and the evaluation points of the cell-proliferative activity of the bFGF-fused fibroin (I–V).

filtering. Separately, in order to refold the bFGF fused with the fibroin L-chain, silk proteins dissolved in 9.0 M LiBr were was subjected to a refolding process with the serial dilution of urea and/or the glutathione redox system according to Hino et al. [21]. As a negative control, wild-type silk fibroin was also subjected to the refolding process. Silk proteins in 9.0 M LiBr were dialyzed against 8 M urea in solution B composed of 50 mM Tris-HCl (pH 8.0) and 200 mM NaCl at 4°C for 10–14 h. The dialysate was replaced with 4 M urea in solution C composed of 1.0 mM reduced glutathione (GSH), 0.1 mM oxidized glutathione (GSSG), 50 mM Tris-HCl (pH 8.0), and 200 mM NaCl, and the solution was incubated at 4°C for 10–14 h. Such serial dilution of urea was repeated until the concentration of urea became 0.5 M. Finally, the silk protein solution was dialyzed against water three times at 4°C for 10–14 h each, following to the dialysis against solution B. The resultant silk protein aqueous solution was sterilized by 0.22-μm filtering. These procedures were designated Process II.

2.2.4.3. Degummed silk fibroin

Cocoons of wild-type or NK34 silkworms were chopped into apx. 5 mm squire and boiled for 30 min in a 0.02 M Na_2CO_3 aqueous solution. They were then washed with boiled water to remove sericin proteins. The degummed silk fibroin was dried in air at 50°C overnight and dissolved in a 9.0 M LiBr aqueous solution at RT for 6–10 h with stirring. Then, the solution was dialyzed against 8 M urea/solution B at 4°C for 10–14 h with a cellulose dialysis membrane (Spectra/Por 1; MWCO, 6–8000). Serial urea dilution with the glutathione redox system was conducted similarly to Item 2.2.4.2. The solution was finally dialyzed against water and sterilized by 0.22-μm filtering. This procedure was designated Process III.

4.2.4.4. Fibroin sponges made from the refolded fibroin aqueous solution

The fibroin aqueous solution prepared from Process III in the dialysis membrane was

concentrated by standing in a dehydrator at RT. Insoluble portions were removed by centrifugation at 20,000 rpm for 30 min at 4°C, and its concentration was determined by a bicinchoninic acid (BCA) assay with fibroin protein standards. Dimethyl sulfoxide (DMSO) was added gradually, with stirring, to the fibroin aqueous solution at the determined volume depending on the final concentration of the fibroin (4.0% (wt/vol)) and DMSO (1.0%). The mixed solution was frozen at –20°C for 17 h and thawed at RT to yield a sponge-like structure. The fibroin sponges were washed by immersion in water to remove DMSO. Then the fibroin sponges were sterilized by autoclaving, dry-heating, or γ-irradiation: Sponges were immersed in PBS and autoclaved at 121°C and 2 hPa for 20 min; wet sponges were frozen at –80°C, dried using Freeze Dryer (FDU-1100; Tokyo Rikakikai Co., Ltd., Japan), and incubated at 180°C for 30 min; and wet sponges were freeze-dried as above and irradiated at RT with 25 kGy from a ^{60}Co. This procedure was designated Process IV.

2.2.4.5. Fibroin sponges with the refolding treatment

Degummed wild-type or bFGF-fused fibroin fibers were prepared as described in Item 2.2.4.3 and dissolved in 9.0 M LiBr. Then, the solution was dialyzed in water using a cellulose dialysis membrane (Spectra/Por 1; MWCO, 6–8000) for 3 days, changing the water every 10–14 h. The fibroin aqueous solution was used to prepared fibroin sponge as described in Item 4.2.4.4. The fibroin sponges were autoclaved in PBS and then incubated at 4°C for 10–14 h in 8 M urea/solution B. Half of the urea solution was replaced with a buffer containing 2.0 mM GSH, 0.2 mM GSSG, 50 mM Tris-HCl (pH 8.0), and 200 mM NaCl (final concentration, 4 M urea, 1.0 mM GSH, 0.1 mM GSSG, 50 mM Tris-HCl (pH 8.0), and 200 mM NaCl). After the incubation at 4°C for 10–14 h, half of the solution was changed with solution C. Such serial dilution of urea was repeated until the concentration of urea became 0.5 M. The sponges were finally incubated in PBS followed by the incubation in the solution B. All the buffer solutions were filtered through the PES membrane with 0.22-μm pores. This procedure was

designated Process V.

2.2.5. Structure and elasticity of the fibroin sponge

Scanning electron microscopy (SEM) and compression test were used to evaluate the effect of the genetic modification on the topology and mechanical properties of fibroin sponges, respectively. Three different samples were used for these experiments (n =3).

For the structure observation, the wild-type and bFGF-fused fibroin sponges with/without the refolding prepared through Process V were roughly dehydrated by placing on gauze. Following this, the dried fibroin sponges were imaged by a scanning electron microscope (TM-1000; Hitachi Ltd., Japan).

The sponges with/without the refolding were use for a mechanical test. By using the EZ test (Shimadzu Corp., Japan) with a 10-N load cell and an 8-mm-diameter load plate, the compressive modulus was determined at an initial 0.1–0.2 strain of 1.5-mm thickness samples. The head speed was 5.0 mm/min. This test was performed at RT.

2.2.6. Evaluation of cell-proliferative activity of bFGF-fused silk fibroin

The activity of bFGF fused with the L-chain was evaluated in a various phase of the process to form a fibroin sponge as shown in Fig. 2.2: posterior silkgland (PSG) (Process I), cocoons (Process II), fibroin solution (Process III), and fibroin sponge (Processes IV and V).

2.2.6.1. WST-1 assay

A WST-1 assay was conducted to evaluate the activity of the bFGF-fused fibroin solutions prepared from Processes I, II, and III. The concentration of the solutions was determined by a BCA assay with fibroin protein standards. The murine fibroblast line NIH3T3 provided by RIKEN BRC through the National Bio-Resource Project of MEXT, Japan were seeded onto wells of 96-well tissue culture plate (Asahi Glass Co.,

Ltd., Japan) at a concentration of 2.0×10^3 cells/well and cultured with Eagle's MEM (Nissui Parmaceutical Co., Ltd., Japan) supplemented with 10% fetal bovine serum (FBS; Gibco Invitrogen Co., USA), 10 ng/ml kanamycin (Gibco Invitrogen Co.) for antibiotics, 0.2% sodium bicarbonate (Gibco Invitrogen Co.), and 2 mM L-glutamin (Gibco Invitrogen Co.) at 37°C in a humidified atmosphere of 95% air and 5% CO_2. After incubation for 24 h, the medium was replaced with Eagle's MEM containing 1% FBS, 10 ng/ml kanamycin, 0.2% sodium bicarbonate, 2 mM L-glutamin, 10 μg/ml heparin, and different amounts of silk proteins or fibroin, and the cells were cultured for 48 h. Instead of silk proteins or fibroin, rhbFGF was added to the 1% FBS medium as a positive control. Then, the cells were incubated with WST-1 reagent (Roche Diagnostics, Germany) for 2 h, followed by the absorbance measurement at 450 nm using a plate reader (VersaMax^{TM}; Molecular Device LLC, USA). The absorbance at 650 nm was used as a reference. The number of measurements in the wild-type, bFGF-fused, and rhbFGF groups was n = 4, 4, and 3, respectively.

2.2.6.2. LDH assay

A lactate dehydrogenase (LDH) assay [30] was conducted to measure the activity of bFGF-fused fibroin fibers and sponges prepared from Processes IV and V. NIH3T3 cells were seeded onto the fibroin sponge scaffold at a concentration of 1.0×10^4 and 2.0×10^4 cells/scaffold (diameter, 6 and 8 mm, respectively; thickness, 1.5 mm) and cultured with the Eagle's MEM supplemented with 1% FBS, 10 ng/ml kanamycin, 0.2% sodium bicarbonate, 2 mM L-glutamin, and 10 μg/ml heparin. Cell density in the fibroin sponges was quantified by the LDH assay after culturing for 1, 3, and 5 days or 3, 7, and 10 days. Samples were incubated in 0.5% Triton X-100 (9690T; Research Organics, Inc., USA) in PBS solution at 4°C to dissolve the cells, and the LDH activity of the solution was measured using the kinetics of NADH-consuming reactions at 340 nm absorbance. The cell number was calculated using the LDH activity with calibration. The medium was changed every 2 days. The number of measurements in each group

was n = 3.

2.2.7. Chondrogenesis in/on the fibroin sponge

Chondrocytes were prepared as described previously [9]. Briefly, articular cartilage tissues were aseptically harvested from the proximal humerus, distal femur and proximal tibia of 4-week-old Japanese white rabbits (Oriental Bio Service Co., Ltd., Japan). Chondrocytes were isolated via enzymatic digestion. After obtaining a single-cell suspension, the cells were cultured to 80% confluence on a T-flask (Asahi Glass Co., Ltd., Japan) with Dulbecco's modified Eagle's Medium (DMEM) (Nacalai Tesque Inc.) containing 10% FBS (Nacalai Tesque Inc.) and 1% antibiotic mixture (10,000 units/ml penicillin, 10,000 μg/ml streptomycin, and 25 μg/ml amphotericin B) (Nacalai Tesque Inc.) at 37°C in a humidified atmosphere of 95% air and 5% CO_2 for 5 to 7 days. The medium was changed every 2 or 3 days.

After expansion in culture, chondrocytes were removed from the flask by mixing with 0.25% trypsin-EDTA (Nacalai Tesque Inc., Japan) and washed twice with PBS. Then the chondrocytes were seeded onto the fibroin sponge scaffold prepared from Process V (diameter, 6 mm; thickness, 1.5 mm) at a concentration of 1.0×10^5 cells/scaffold, they were cultured with Dulbecco's modified Eagle's Medium (DMEM) (Nacalai Tesque Inc.) containing 2% FBS and 10 ng/ml kanamycin at 37°C in a humidified atmosphere of 95% air and 5% CO_2 for 1, 3, and 5 days. Half of the medium was changed every 2 days.

All the animal experiments followed the Regulation on Animal Experimentation at Kyoto University, and were approved by the Animal Research Committee at Kyoto University.

The number of chondrocytes in the fibroin sponge was determined by the LDH assay as described in Item 4.2.5.3. On the other hand, the amount of sulfated glycosaminoglycan (sGAG) content in the samples was assayed using the 1,9-dimethylmethylene blue (DMMB) method [31]. As described previously [32], each

chondrocyte-fibroin construct was digested with 1.5 ml of 24 mg/ml papain solution in PBS at 60°C for 1 h. The sample solution was mixed with a DMMB solution, and the absorbance at 530 nm was measured by the plate reader. The amount of sGAG in each sample was calculated using a standard curve calibrated by using a solution of chondroitin sulfate C sodium salt (Nacalai Tesque, Inc.). The number of measurements in each group was n = 3.

2.2.8. Statistical analysis

Two-way ANOVA was used to analyze effects of the type of fibroins and the refolding treatment on the mechanical properties of fibroin sponges, effects of the type of fibroins and the fibroin concentration on cell-proliferative activity, and effects of the type of fibroins and culture period on cell number and on sGAG production, followed by Tukey test for post hoc comparisons. A value of $p < 0.05$ was considered significant.

2.3. Results

2.3.1. SDS-PAGE and Western blotting

Proteins extracted from silk fibers of wild-type and NK34 silkworms were reacted with different concentrations of collagenase, separated by SDS-PAGE, and immunoblotted with anti-bFGF antibodies (Fig. 2.3). On CBB-stained gels, no band was detected at the position corresponding to the predicted size (MW, apx. 45 kDa) of bFGF-fused fibroin L-chain (A). However, as shown in Fig. 2.3B, such bands were clearly observed on Western blot for the silk fibers of the NK34 silkworms but not for those of the wild-type silkworms. Additionally, another band was detected on the lanes of the collagenase-treated NK34 groups. The band was at the position of monomer bFGF (MW, apx. 18 kDa), which was confirmed by the comparison to the positive control.

2.3.2. Structures and elasticity of fibroin sponges

Figure 2.4 shows the representative scanning electron micrographs for the wild-type and bFGF-fused fibroin sponges with/without the refolding treatment. The samples were prepared via Process V. All of the sponges appeared to be similar in their morphology, possessing similar pore size, pore structure, and pore size distribution.

Compressive elastic modulus of the wild-type and bFGF-fused fibroin sponges after

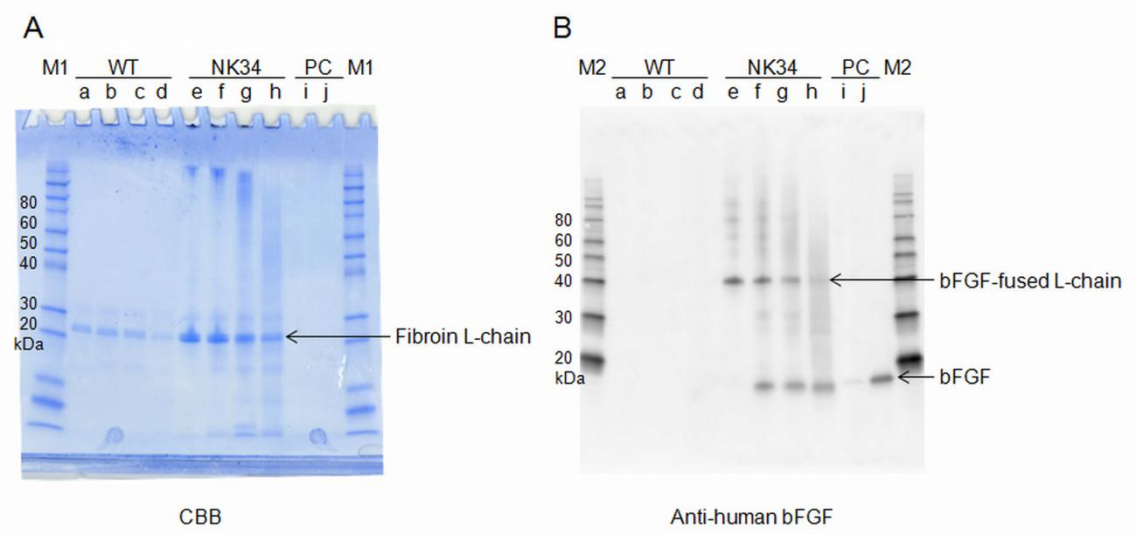

Fig. 2.3. SDS-PAGE (A) and Western blotting (B) of proteins extracted from the wild-type (WT) and NK34 transgenic silk fibers. 4 mg/ml of the proteins were incubated with 0 (a, e), 0.4 (b, f), 4 (c, g), 40 (d, h) μg/ml of collagenase. 30 or 10 μg of the silk proteins were loaded on each lane of gels for CBB staining or immnoblotting, respectively. 0.2 (i) and 2 (j) μg/ml of commercial rhbFGF solutions were used as the positive control (PC). 15 or 5 μl of the PC solutions were used for CBB staining or Western blotting, respectively. Novex® Sharp Protein Standard (Invitrogen Corp., USA) was used as a marker (M1), while MagicMark™ XP Western Protein Standard (Invitrogen Corp.) was used as another marker (M2). Arabic numerals at the left side of the photographs are molecular weight in kDa.

Process V are summarized in Table 2.1. Although the refolding treatment tended to decrease the mechanical property of the fibroin sponges, two-way ANOVA showed that both factors (type of fibroin and with/without the refolding) did not affect the elastic modulus of the sponges.

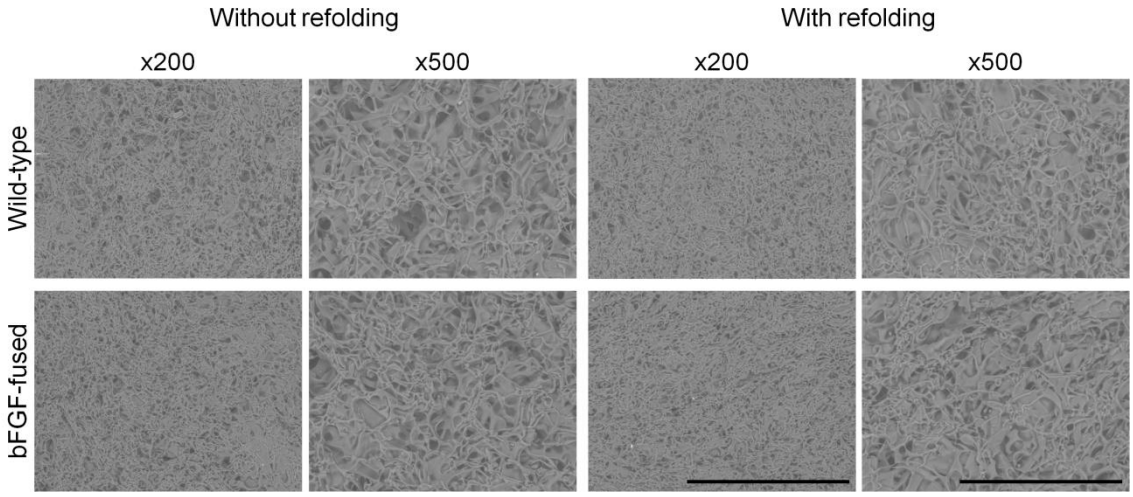

Fig. 2.4. Scanning electron micrographs of wild-type and bFGF-fused fibroin sponges with/without the refolding treatment. Scale bar = 500 and 200 μm for 200- and 500-fold magnifications, respectively.

Table 2.1. Compressive elastic modulus of each type of fibroin sponges with or without the refolding treatment.

Fibroin sponges	Without refolding [kPa]	With refolding [kPa]
Wild-type	10.5 ± 1.4	9.4 ± 0.4
bFGF-fused	10.7 ± 0.3	9.5 ± 0.6

Data is shown in the form: mean ± SD. Three different samples in each group were used to determine the compressive elastic modulus of the each group. No significant differences were detected by two-way ANOVA-test.

2.3.3. Cell-proliferative activity

2.3.3.1. Silk fibroin extracted from PSG (Process I)

The dose-dependent changes in the absorbance reflecting cell number is shown in Fig. 2.5. As the concentration of rhbFGF increased, the absorbance also increased, indicating that the proliferation of the NIH3T3 cells was stimulated by the growth factor. In comparison to the wild-type group, the bFGF-fused group demonstrated significantly higher absorbance at the concentration of 200 μg/ml.

2.3.3.2. Silk proteins extracted from cocoons (Process II)

Figure 2.6 shows the cell-proliferative activity of silk proteins from cocoons with (B)

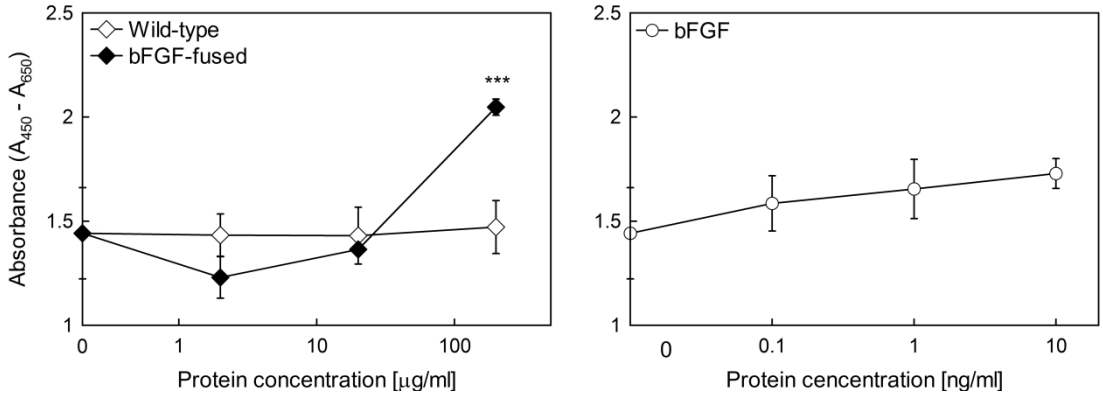

Fig. 2.5. Dose-dependent changes in cell-proliferative activity of wild-type and bFGF-fused fibroin solutions extracted from PSG of wild-type and NK34 silkworms, respectively. Commercial rhbFGF solutions were used as the positive control. Data is shown in the form: mean ± SD. Asterisks indicate significant differences between the wild-type and bFGF-fused groups (***: $p < 0.001$; Tukey test following to two-way ANOVA).

or without (A) the refolding treatment with the glutathione redox system. Without the refolding treatment, there were no statistical differences in cell numbers between the wild-type and bFGF-fused groups as shown in Fig. 2.6A. Meanwhile, with the refolding treatment, the absorbance of the bFGF-fused group was statistically higher than that of the wild-type group at 100 μg/ml.

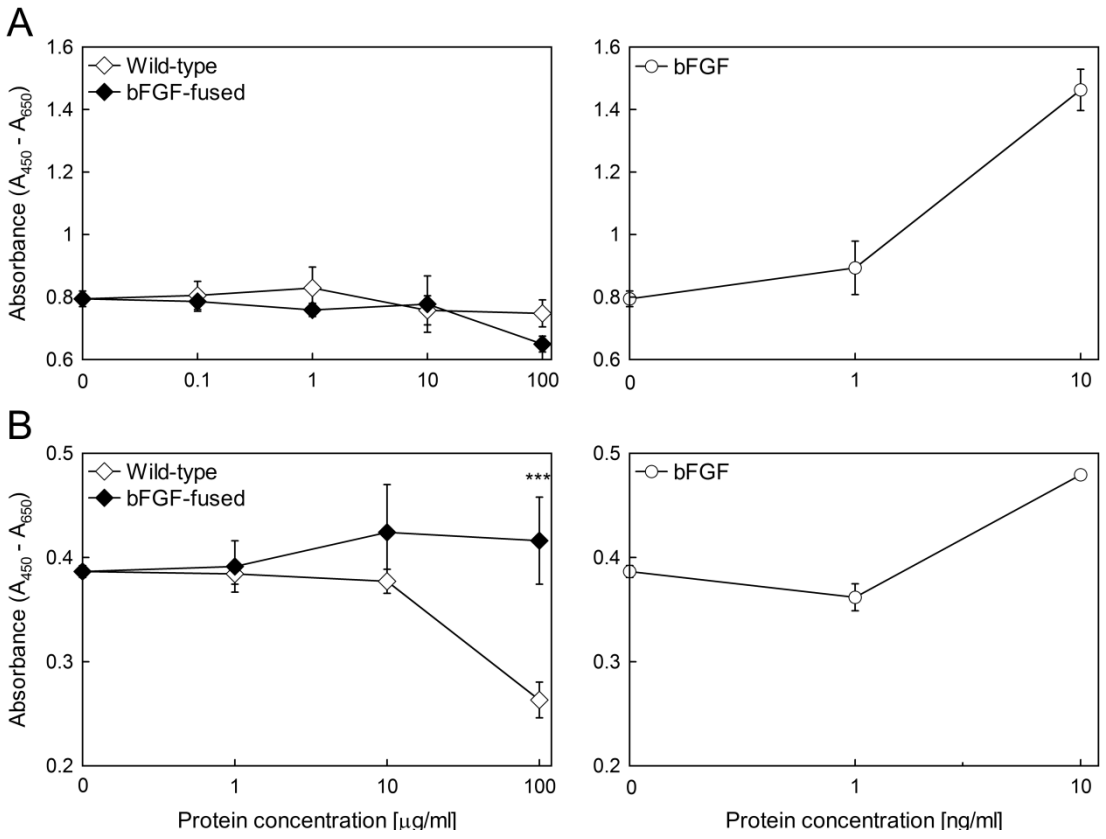

Fig. 2.6. Dose-dependent changes in cell-proliferative activity of silk protein solutions prepared from cocoons of wild-type and NK34 silkworms, including wild-type and bFGF-fused fibroin proteins, respectively. The solutions were treated with (B) or without (A) the refolding with glutathione system. Commercial rhbFGF solutions were used as the positive control. Data is shown in the form: mean ± SD. Asterisks indicate significant differences between the wild-type and bFGF-fused groups (***: $p < 0.001$; Tukey test following to two-way ANOVA).

2.3.3.3. Aqueous solution of refolded silk fibroin (Process III)

Figure 2.7 shows the cell-proliferative activity of the refolded silk fibroin in aqueous solution. Two-way ANOVA demonstrated that the type of fibroin affected the growth ($p < 0.001$), and post-hoc Tukey comparison showed that the cell-proliferative activity of the bFGF-fused group was significantly higher than that of the wild-type group.

2.3.4.4. Sterilized fibroin sponges made from the refolded fibroin aqueous solution (Process IV)

The time-dependent changes in the number of NIH3T3 cells seeded onto the wild-type and bFGF-fused fibroin sponges sterilized by autoclaving, dry-heating, or γ-irradiation are shown in Fig. 2.8. 1.0×10^4 cells were seeded onto a fibroin sponge scaffold (diameter, 6 mm; thickness, 1.5 mm). Regardless of sterilization methods, there were no statistical differences between the wild-type and bFGF-fused groups.

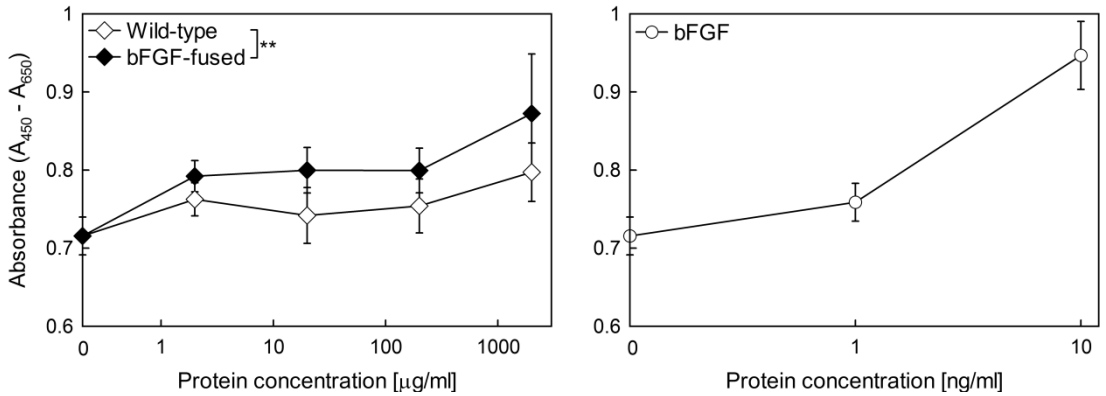

Fig. 2.7. Dose-dependent changes in cell-proliferative activity of degummed wild-type and bFGF-fused fibroin solutions with the refolding process. Commercial rhbFGF solutions were used as the positive control. Data is shown in the form: mean ± SD. Asterisks indicate significant differences between the wild-type and bFGF-fused groups (**: $p < 0.001$; Tukey test following to two-way ANOVA).

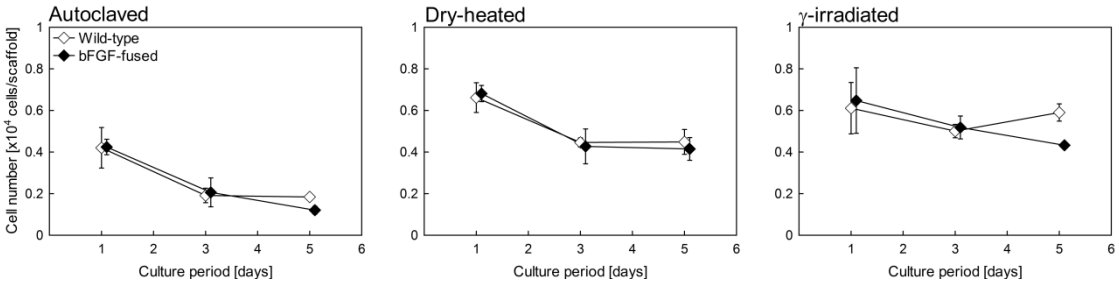

Fig. 2.8. Time-dependent changes in the number of NIH3T3 cells grown in/on wild-type and bFGF-fused fibroin sponges sterilized by autoclaving, dry-heating, or γ-irradiation. Data is shown in the form: mean ± SD. No significant differences were detected according to two-way ANOVA.

4.3.4.5. Fibroin sponges with the refolding treatment (Process V)

The number of NIH3T3 cells grown in/on the fibroin sponges as a function of culture time is shown in Fig. 2.9. 2.0×10^4 cells were seeded onto a fibroin sponge scaffold (diameter, 8 mm; thickness, 1.5 mm). The wild-type group showed few time-dependent changes in the cell number, while the cells grown on the bFGF-fused fibroin sponge proliferated with culture time. However, there were no significant differences between the groups.

2.3.4. Chondrogenesis in fibroin sponges

The time-dependent changes in the number of chondrocytes and the amount of sGAG in the fibroin sponge scaffolds are shown in Figs. 2.10A and 2.10B, respectively. Two-way ANOVA exhibited that there were no statistically significant differences between the wild-type and bFGF-fused groups in both the cell number and sGAG production. Both groups similarly showed a decrease in cell number with culture period. On the other hand, only the bFGF-fused group demonstrated a time-dependent increase in sGAG production.

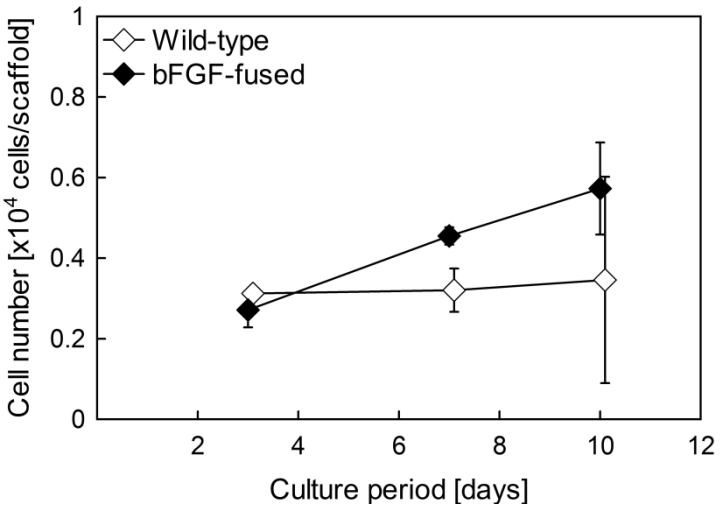

Fig. 2.9. Time-dependent changes in the number of NIH3T3 cells grown in/on wild-type and bFGF-fused fibroin sponges with the refolding treatment. Data is shown in the form: mean ± SD. No significant differences were detected according to two-way ANOVA.

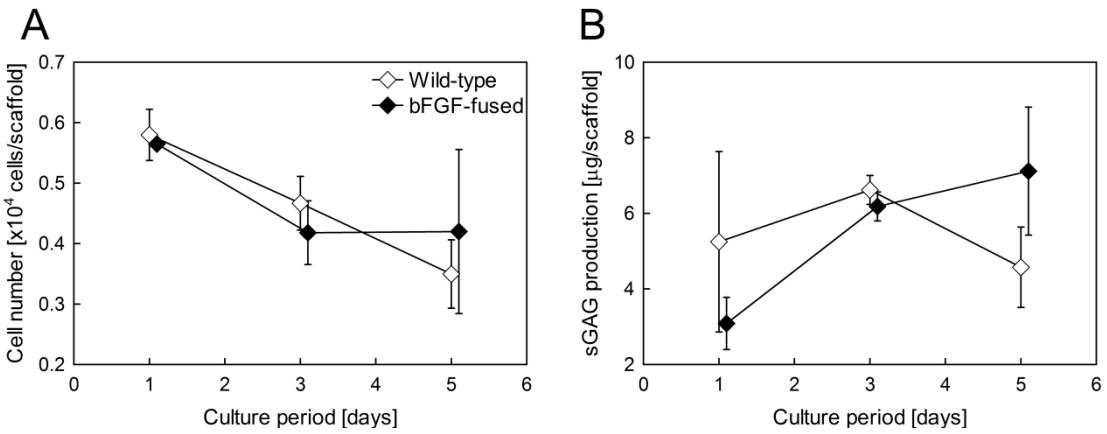

Fig.2.10. Time-dependent changes in the number chondrocytes (A) and the amount of sGAG (B) in/on wild-type and bFGF-fused fibroin sponges with the refolding treatment. Data is shown in the form: mean ± SD. No significant differences were detected according to two-way ANOVA.

2.4. Discussion

By using transgenic silkworm technology, here we designed and developed bFGF-fused silk fibroin in order to use it as a scaffold material for chondrogenic cells. Fibroin protein consists of a heavy chain (H-chain; MW, apx. 360 kDa) and an L-chain (MW, apx. 27 kDa), which are linked by a disulfide bond to form a heterodimer [33]. The modified fibroin molecule in this study was designed to have a bFGF at the carboxyl terminal of the L-chain. Additionally, 6 amino-acid residues PLGIAG, which is a collagenase-cleavage site [29], are introduced between the L-chain and the bFGF so that the growth factor can be released from fibroin molecule by collagenase. Western blot assay as shown in Fig. 2.3 demonstrated that fibroin proteins extracted from cocoons of NK34 silkworms had bFGF-positive molecules, whose MW was about 42 kDa. As the MW of bFGF is apx. 18 kDa, a bFGF was successfully fused with the L-chain by transgenic silkworm technology (L-chain 27 kDa + bFGF 18 kDa = 45 kDa). Furthermore, the Western blot assay presented this bFGF could be released from the L-chain by a collagenase treatment. These results suggest that we successfully generated the transgenic silkworms which produced the bFGF-fused fibroin in accordance with our design.

bFGF is an unstable protein; it is inactivated when stored at RT [34] and treated with a variety of solvents, including dilute acid, organic solvents and solutions of guanidinium chloride [35]. Therefore, bFGF fused with fibroin L-chain would be denatured through the process to form a 3-D spongy structure of the fibroin, including degumming, solubilization, dialysis, condensation, freezing with DMSO, and sterilization. As can be seen in Fig. 2.5, bFGF-fused fibroin extracted from PSG stimulated the proliferation of NIH3T3 cells, suggesting that the bFGF fused with the L-chain secreted from PSG retains its biological activity. Meanwhile, Fig. 2.6A shows that the bFGF-fused fibroin in silk proteins extracted from cocoons had no effects on cell proliferation. Since the spinning of silk fibers accompanies conformational changes in silk proteins and exposure to alkaline pH inactivates bFGF [34], spinning and/or

dissolution in 9.0 M LiBr aqueous solution whose pH is 9.56 ± 0.2 [36] could cause the denaturation of the bFGF fused with the L-chain. However, the inactivated bFGF was reactivated by a refolding process with a glutathione redox system as shown in Fig. 2.6B, which also recovered the cell-proliferative activity of the degummed bFGF-fused fibroin as can be seen in Fig.2.7. Hino et al. [21] reported that the refolding with the glutathione redox system restored the biological activity of another type of bFGF-fused fibroin (r(FL/bFGF)nF) which was degummed with trypsin and solubilized in a solution containing $CaCl_2$, ethanol, and water. Although they referred treatments with alkali and urea at high temperatures were considered to irreversibly decompose the bFGF-fused fibroin, our results suggest that the activity of the bFGF-fused fibroin can be restored by the refolding process even after degummed in a boiling 0.02 M Na_2CO_3 aqueous solution and dissolved in a 9.0 M LiBr aqueous solution.

These results suggest that the biologically-active bFGF-fused fibroin aqueous solution has been prepared successfully, but the solution has to be processed into various forms, including film, gel, powder, and sponge to utilize the rbFGF-fued fibroin as an effective biomaterial. Hino et al. [21] have already fabricated r(FL/bFGF)nF film which can stimulates the proliferative activity of HUVECs. However, scaffold with a 3-D spongy structure and with optimal mechanical properties is also required in the field of tissue-engineering, including articular cartilage regeneration. Although fibroin sponges were formed from the refolded bFGF-fused fibroin aqueous solution, they did not have growth-promoting effects on NIH3T3 cells as shown in Fig. 2.8, indicating that the fabrication processes, such as condensation, freeze-thaw with DMSO, and/or sterilization (autoclaving, dry-heating, or γ-irradiation), destroyed the refolded conformation of the bFGF fused with the L-chain. Then the bFGF-fused fibroin sponge was treated with the refolding process, following to the sterilization by autoclaving. As reducing agent such as GSH can cleave disulfide bonds, it is concerned that the L-chain, including the bFGF-fused one, was lost from a fibroin sponge in the refolding process with the glutathione redox system. However, according to a SDS-PAGE analysis of fibroin sponges, the band of L-chain proteins was detected even after the refolding

treatment (data not shown here). Taking this result into account, bFGF-fused L-chains could remain in a fibroin sponge after the refolding treatment. Additionally, as shown in Fig. 2.4 and Table 2.1, no remarkable differences in the topology and mechanical properties were observed between the wild-type and bFGF-fused fibroin sponges with or without the refolding treatment. Therefore, although no significant differences between the groups were detected, we inferred that the refolded bFGF fused with the L-chain in fibroin sponge might have some kinds of effects on the different time-dependent changes in cell number and sGAG production between the wild-type and bFGF-fused groups as shown in Figs. 2.9 and 2.10B, respectively.

Taken together, the results of this study suggest that the bFGF-fused fibroin was developed by using transgenic silkworm technology, which also enabled the release of the bFGF by a collagenase digestion as we designed. Although the process to form a 3-D spongy structure of the fibroin and its sterilization denatured the bFGF and lost its biological activity, the refolding process with the glutathione redox system might recover the bFGF activity in fibroin spongy scaffold. However, bFGF is reported to have more dramatic effects on fibroblasts and chondrocytes [21,37] than our results have shown. Thus it is necessary to develop techniques to retain the biological activity of macromolecules fused with fibroin. One of the solutions is to increase the transgenic efficiency of fibroin protein. The efficiency of the bFGF-fused fibroin was not quantified in this study, but the band of the bFGF fused with the L-chain could not be observed by the CBB staining of the gel. Besides, Hino et al. [21] reported that the concentration (% weight) of r(FL/bFGF) in the proteins of the fibroin layers was 0.04%. We hope recent studies aiming at the improvement of transgenic efficiency [38] can resolve the issues. Another possibility is to conduct the refold process of the bFGF-fused fibroin sponge sterilized by dry-heating or γ-irradiation. Unpublished observations have shown that the crystalline structure in a fibroin sponge is less affected by dry-heating compared to autoclaving, and it is expected the environment of the bFGF fused with the L-chain in a dry condition can be different from that in a wet condition.

2.5. Conclusions

The results of the present study have demonstrated that transgenic silkworm technology enables to develop bFGF-fused fibroin, and the growth factor can be released from the fibroin by a collagenase digestion. A process to form a 3-D porous structure of the bFGF-fused fibroin inactivated the cell-proliferative activity of the bFGF, but there is a possibility that a refolding treatment with the phase-manner urea dilution and glutathione redox system restores the activity; the bFGF-fused fibroin degummed in a boiling 0.02 M Na_2CO_3 and dissolved in 9.0 M LiBr was reactivated by the refolding, while the bFGF-fused fibroin sponge sterilized by autoclaving was difficult to refold. Further studies are required for a practical use of the genetically-modified fibroin fused with a macromolecular recombinant protein.

References

[1] Li M, Zhang C, Lu S, Wu Z, Yan H. Study on porous silk fibroin materials: 3. Influence of repeated freeze-thawing on the structure and properties of porous silk fibroin materials. Polym Adv Technol 2002;13:605-10.

[2] Nazarov R, Jin HJ, Kaplan DL. Porous 3-D scaffolds from regenerated silk fibroin. Biomacromolecules 2004;5:718-26.

[3] Tamada Y. New process to form a silk fibroin porous 3-D structure. Biomacromolecules 2005;6:3100-6.

[4] Byette F, Bouchard F, Pellerin C, Paquin J, Marcotte I, Mateescu MA. Cell-culture compatible silk fibroin scaffolds concomitantly patterned by freezing conditions and salt concentration. Polym Bull 2011;67:159-75.

[5] Wray LS, Rnjak-Kovacina J, Mandal BB, Schmidt DF, Gil ES, Kaplan DL. A silk-based scaffold platform with tunable architecture for engineering critically-sized tissue constructs. Biomaterials 2012;33:9214-24.

[6] Sofia S, McCarthy MB, Gronowicz G, Kaplan DL. Functionalized silk-based biomaterials for bone formation. J Biomed Mater Res 2001;54:139-48.

[7] Meinel L, Karageorgiou V, Hofmann S, Fajardo R, Snyder B, Li C, et al. Engineering bone-like tissue *in vitro* using human bone marrow stem cells and silk scaffolds. J Biomed Mater Res A 2004;71:25-34.

[8] Karageorgiou V, Meinel L, Hofmann S, Malhotra A, Volloch V, Kaplan DL. Bone morphogenetic protein-2 decorated silk fibroin films induce osteogenic differenciation of human bone marrow stromal cells. J Biomed Mater Res A 2004;71:528-37.

[9] Aoki H, Tomita N, Morita Y, Hattori K, Harada Y, Sonobe M, et al. Culture of chondrocytes in fibroin-hydrogel sponge. Biomed Mater Eng 2003;13:309-16.

[10] Meinel L, Hofmann S, Karageorgiou V, Zichner L, Langer R, Kaplan D, et al. Engineering cartilage-like tissue using human mesenchymal stem cells and silk protein scaffolds. Biotechnol Bioeng 2004;88:379-91.

[11] Wang Y, Kim UJ, Blasioli DJ, Kim HJ, Kaplan DJ. In vitro cartilage tissue engineering with 3D porous aqueous-derived silk fibroin and mesenchymal stem cells. Biomaterials 2005;26:7082-94.

[12] Hofmann S, Knecht S, Langer R, Kaplan DL, Vunjak-Novakovic G, Merkle HP et al. Cartilage-like tissue engineering using silk scaffolds and mesenchymal stem cells. Tissue Eng 2006;12:2729-39.

[13] Kambe Y, Yamamoto K, Kojima K, Tamada Y, Tomita N. Effects of RGDS sequence genetically interfused in the silk fibroin light chain protein on chondrocyte adhesion and cartilage synthesis. Biomaterials 2010;31:7503-11.

[14] Yang Y, Ding F, Wu J, Hu W, Liu W, Lie J, et al. Development and evaluation of silk fibroin-based nerve grafts used for peripheral nerve regeneration. Biomaterials 2007;28:5526-35.

[15] Gotoh Y, Tsukada M, Minoura N, Imai Y. Synthesis of poly(ethyleneglycol)silk fibroin conjugates and surface interaction between L929 cells and the conjugates. Biomaterials 1997;18:267-71.

[16] Tamada Y. Sulfation of silk fibroin by chlorosulfonic acid and the anticoagulant activity. Biomaterials 2004;25:377-83.

[17] Murphy AR, John PS, Kaplan DL. Modification of silk fibroin using diazonium coupling chemistry and the effects on hMSC proliferation and differentiation. Biomaterials 2008;29:2829-38.

[18] Gotoh Y, Ishizuka Y, Matsuura T, Niimi S. Spheroid formation and expression of liver-specific functions of human hepatocellular carcinoma-derived FLC-4 cells cultured in lactose-silk fibroin conjugate sponges. Biomacromolecules 2011;12:1532-9.

[19] Tamura T, Thibert C, Royer C, Kanda T, Abraham E, Kamba M, et al. Germline transformation of the silkworm *Bombyx mori* L. using a *piggyBac* transposon-derived vector. Nat Biotechnol 2000;18:81-4.

[20] Inoue S, Kanda T, Imamura M, Quan GX, Kojima K, Tanaka H, et al. A fibroin secretion-deficient silkworm mutant, *Nd-s*^{D}, provides an efficient system for

producing recombinant proteins. Insect Biochem Mol Biol 2005;35:51-9.

[21] Hino R, Tomita M, Yoshizato K. The generation of germline transgenic silkworms for the production of biologically active recombinant fusion proteins of fibroin and human basic fibroblast growth factor. Biomaterials 2006;27:5715-24.

[22] Yanagisawa S, Zhu Z, Kobayashi I, Uchino K, Tamada Y, Tamura T, et al. Improving cell-adhesive properties of recombinant *Bombyx mori* silk by incorporation of collagen of fibronectin derived peptides produced by transgenic silkworms. Biomacromolecules 2007;8:3487-92.

[23] Sato M, Kojima K, Sakuma C, Murakami M, Aratani E, Takenouchi T, et al. Production of scFv-conjugated affinity silk powder by transgenic silkworm technology. PLoS one 2012;7:e34632.

[24] Cuevas P, Burgos J, Baird A. Basic fibroblast growth factor (FGF) promotes cartilage repair in vivo. Biochem Biophys Res Commun 1988;156:611-8.

[25] Fujimoto E, Ochi M, Kato Y, Mochizuki Y, Sumen Y, IkutaY. Beneficial effect of basic fibroblast growth factor on the repair of full-thickness defects in rabbit articular cartilage. Arch Orthop Trauma Surg 1999;199:139-45.

[26] Schmal H, Zwingmann J, Fehrenbach M, Finkenzeller G, Stark GB, Südkamp NP, et al. bFGF influences human articular chondrocyte differentiation. Cytotherapy 2007;9:184-93.

[27] Khan M, Palmer EA, Archer CW. Fibroblast growth factor-2 induced chondrocyte cluster formation in experimentally wounded articular cartilage is blocked by soluble Jagged-1. Osteoarthritis Cartilage 2010;18:208-19.

[28] Kim JH, Lee MC, Seong SC, Park KH, Lee S. Enhanced proliferation and chondrogenic differentiation of human synovium-derived stem cells expanded with basic fibroblast growth factor. Tissue Eng Part A 2011;17:991-1002.

[29] Tweten RK. Development of a novel, proteinase-activated toxin targeting tumor neovascularization. DTIC Online 1998; ADB249654.

[30] Tamada Y, Kulik EA, Ikeda Y. Simple method for platelet counting. Biomaterials 1995;16: 259-61.

[31] Farndale RW, Buttle DJ, Barrett AJ. Improved quantification and discrimination of sulphated glycosaminoglycans by use of dimethylmethylen blue. Biochem Biophys Acta 1986;883:173-7.

[32] Yamamoto K, Takaya R, Tamada Y, Tomita N. Effects of tribological loading history on the expression of tribological function of regenerated cartilage. Tribology Online 2008;3:148-52.

[33] Tanaka K, Kajiyama N, Ishikura K, Waga S, Kikuchi A, Ohtomo K, et al. Determination of the site of disulfide linkage between heavy and light chains of silk fibroin produced by *Bombyx mori*. Biochim Biophys Acta 1999;1432:92-103.

[34] Caccia P, Nitti G, Cletini O, Pucci P, Ruoppolo M, Bertolero F, et al. Stabilization of recombinant human basic fibroblast growth factor by chemical modifications of cysteine residues. Eur J Biochem 1992;204:649-55.

[35] Westall FC, Rubin R, Gospodarowicz D. Brain-derived fibroblast growth factor: a study of its inactivation. Life Sci 1983;33:2425-9.

[36] Murakami M, Tamada Y, Kojima K. Dissolving whole cocoon silk proteins by using a pH-adjusted buffered LiBr solution (in Japanese). J Silk Sci Tech Jpn 2012;20:80-94.

[37] Tan H, Gong Y, Lao L, Mao Z, Gao C. Gelatin/chitosan/hyaluronan ternary complex scaffold containing basic fibroblast growth factor for cartilage tissue engineering. J Mater Sci 2007;18:1961-8.

[38] Tomita M. Transgenic silkworms that weave recombinant proteins into silk cocoons. Biotechnol Lett 2011;33:645-54.

Chapter 3
Adhesive Force Behavior of Single ATDC5 Cells in Chondrogenic Culture

3.1. Introduction

Responding to the results of Chapter 2 that biologically-active macromolecules are difficult to exert their activity remarkably after fabricated into 3-D porous scaffold, here we have tried seeking another design index alternative to bioactive proteins. Mechanical properties of single cells are important for various cell activities, such as survival, migration, and signal transduction. Their relations to cell differentiation have also been investigated [1-4]. Darling et al. [2], with an atomic force microscopy (AFM), measured elastic and viscoelastic properties of differentiated human mesenchymal stem cells (MSCs) such as chondrocytes, osteoblasts, and adipocytes, and showed that, in spread morphology, the three types of cells exhibited significantly different mechanical characteristics. Using a micropipette aspiration technique for single cells in suspension, Yu et al. [3] demonstrated that human MSCs undergoing osteogenesis had higher Young's modulus than control MSCs. These results confirmed that cellular mechanical characteristics are involved in cell differentiation. Past studies also measured mechanical properties of cells during their differentiation [1,3] or dedifferentiation [4] process, however changes of the property in the process were neither statistically analyzed nor adequately discussed; instead the characteristic at a time point in the process was compared with that of a control group. It is thus still unclear whether

mechanical properties of cells are meaningful enough to characterize cellular differentiative stages.

Articular chondrocytes, a mesenchymal lineage, function in frequently-loaded circumstances *in vivo*, and their mechanical environment strongly affect the activity of the cells even *in vitro*. For example, the maintenance of chondrogenic phenotype of chondrocytes was influenced by the elasticity of a scaffold [5]. Moreover, adherent morphologies of chondrocytes are well known to be related to their differentiation phenotype. Chondrocytes which adhere and spread well on a substrate tend to exhibit fibroblast-like shape and express more cartilage-nonspecific extracellular matrices (ECMs) like collagen type I relative to cartilage-specific ECMs like collagen type II and aggrecan, whereas chondrocytes with spherical morphology are considered to maintain the chondrogenic phenotype [6-8]. Hence mechanical interactions between chondrogenic cells and scaffolds can be involved in their differentiation. Cell–material adhesion has been mechanically evaluated by measuring force to detach cells from a substrate. However, most of these studies showed the dependency of the cell adhesive force on substrate types and/or incubation time [9-16], and few studies have focused on the relationship between mechanical cell adhesiveness and cell differentiation.

The motivation of this study is to clarify changes in mechanical properties of individual cells during chondrogenic differentiation process, focusing on cell adhesion. We used the murine chondrogenic cell line ATDC5, which is illustrative of chondrogenesis in the early stage of endochondral ossification, and the cells differentiate into chondrocytes from undifferentiated mesenchymal cells during *in vitro* culture [17,18]. Biochemical phenotypic changes during differentiation culture with insulin were evaluated by Alcian blue and Alizarin red S stainings and relative messenger RNA (mRNA) expression levels. Mechanical properties of single cells were measured by using a cell detachment test established previously [13,16]. In this test vertical force was applied to individual cells to pull them away from a substrate, and we obtained the adhesive force and stiffness of single ATDC5 cells. Additionally, cell morphology was observed by immunofluorescence staining of F-actin.

3.2. Materials and methods

3.2.1. ATDC5 cells and culture conditions

The murine chondrogenic cell line, ATDC5 (RCB0565), was provided by RIKEN BRC through the National Bio-Resource Project of MEXT, Japan. The cells were seeded onto either a 24-well plate (Asahi Glass Co., Ltd., Japan) or a 6-well plate (Asahi Glass Co., Ltd.) at 1.1×10^4 cells/cm^2 and cultured with DMEM/F12 (a mixture of Dulbecco's modified Eagle's medium and Ham's F12 medium) (Sigma-Aldrich Co., USA) containing 5% heat-inactivated fetal bovine serum (FBS) (Nacalai Tesque Inc., Japan) and 1% antibiotic mixture (10,000 units/ml penicillin, 10 mg/ml streptomycin, and 25 µg/ml amphotericin B) (Nacalai Tesque Inc.) at 37°C in a humidified atmosphere of 95% air and 5% CO_2. This medium, which shall be referred to as the maintenance medium, was changed every 2 days. Once the cells became confluent (on day 4 after seeding), the maintenance medium was replaced with fresh maintenance medium supplemented with 1% ITS mixture (1 mg/ml insulin, 550 µg/ml transferrin, and 670 ng/ml sodium selenite) (Invitrogen Corp., USA) to induce differentiation in chondrocyte-like cells [18]. This medium, which shall be referred to as the differentiation medium, was changed every 2 days.

3.2.2. Alcian blue staining

After incubating for 3, 7, 10, 14, or 17 days, ATDC5 cells grown on a 24-well plate were rinsed twice with phosphate-buffered saline (PBS) (Nacalai Tesque Inc.) and then fixed with 4% paraformaldehyde (PFA) solution for 15 min. The cells were then incubated in 0.1 M HCl for 1 min and stained with 0.1% (wt/vol) Alcian Blue 8GX (Sigma-Aldrich Co.) in 0.1 M HCl for 1 h. Following this, they were incubated in 0.1 M HCl for 5 min and washed five times with ultrapure water. Digital images of the cells were acquired by a phase-contrast microscope (IX-71; Olympus Corp., Japan) and a digital camera (DMC-FX30; Panasonic Corp., Japan). This procedure was performed at

room temperature (RT).

3.2.3. Alizarin red S staining

After 3, 7, 10, 14, or 17 days in culture, ATDC5 cells cultured on a 24-well plate were washed and fixed as described in Item 3.2.1. The cells were stained with 1% Alizarin red S (Wako Pure Chemical Industries Ltd., Japan) for 10 min and rinsed five times with ultrapure water. Digital images of the cells were photographed as described in the previous section. This procedure was performed at RT.

3.2.4. Real-time PCR analysis

ATDC5 cells cultured on a 6-well plate were washed twice with ice-cold PBS after 3, 7, 10, 14, or 17 days in culture. Total RNA was then extracted from the cells using a TriPure Isolation Reagent (Roche Diagnostics, Germany) and a High Pure RNA Tissue Kit (Roche Diagnostics). Complementary DNA (cDNA) was synthesized by reverse-transcription polymerase chain reaction (PCR) using a Transcriptor First Strand cDNA Synthesis Kit (Roche Diagnostics) and a thermal cycler (PC-320, Astec Co., Ltd., Japan). Three different samples were used (n = 3).

Quantitative real-time PCR was performed using a LightCycler® FastStart DNA Master^{PLUS} SYBR Green I (Roche Diagnostics), and SYBR Green PCR amplification and real-time fluorescence detection were performed using the LightCycler® ST300 (Roche Diagnostics). Primers (Sigma-Aldrich Co.) were designed for β-actin, sex determining region Y-box containing gene 9 (Sox9), aggrecan, collagen type II αI chain, and collagen type X αI chain, where β-actin was used as a house-keeping gene. The primer sequences are shown in Table 3.1.

3.2.5. Immunofluorescence staining of F-actin

After culturing for 3, 7, 10, 14, or 17 days on a 24-well plate, ATDC5 cells were

Table 3.1

Primer sequences for real-time PCR analysis.

Gene target	Primer sequence (5' - 3')	GenBank ID	Reference #
β-actin	Sense: AGATGTGGATCAGCAAGC AG Antisense: GCGCAAGTTAGGTTTTGTCA	NM_007393	[19]
Sox9	Sense: ACTTCCGCGACGTGGACATC Antisense: TGTAGGTGACCTGGCCGTG	NM_011448	[20]
Aggrecan	Sense: AGGTCTGTGCCATCTGTGAG Antisense: CCGAGAAATGACACCTGCTA	NM_007424	[19]
Collagen type II αI chain	Sense: GAACAGCATCGCCTACCTGG Antisense: TGTTTCGTGCAGCCATCCT	NM_03116	[21]
Collagen type X αI chain	Sense: CTCCTACCACGTGCATGTGAA Antisense: ACTCCCTGAAGCCTGATCCA	NM_009925	[21]

removed from the plate by mixing with 0.25% trypsin/1 mM EDTA (Nacalai Tesque, Inc.) and washed twice with PBS. The cells were seeded onto a ProNectin® F-coated cover glass plate (diameter, 15 mm; thickness, 0.15 mm) (Matsunami Glass Ind., Ltd., Japan) at 3.1×10^3 cells/cm^2 and incubated with maintenance medium at 37°C in a

humidified atmosphere of 95% air and 5% CO_2 for 6 h. Following this, F-actin and the nuclei of the ATDC5 cells were stained as reported previously [13]. Briefly, after fixing with 4% PFA solution, the cells were permeabilized in 0.1% Triton X-100 (9690T; Research Organics Inc., USA), and then incubated in fresh blocking solution prepared with 1% (wt/vol) bovine serum albumin (Serological Corp., USA). Rhodamine phalloidin (R415; Molecular Probes, USA) and 4',6-diamidino-2-phenylindole (S7113; Millipore Corp., USA) were used to stain F-actin and the nucleus, respectively. Stained cells were observed with an inverted fluorescence microscope (IX-71 and BH2-RFL-T3; Olympus Corp.). This staining procedure was performed at RT.

The ProNectin® F (Sanyo Chemical Industries Ltd., Japan) substrate was prepared according to the manufacturer's instructions. Briefly, a stock solution was diluted to 10 μg/ml in PBS, and a glass plate was soaked in the diluted solution for 5 min at RT. After removing the coating solution, the glass plate was washed twice with PBS.

3.2.6. Evaluation of mechanical properties of single ATDC5 cells

After 3, 7, 10, 14, or 17 days in culture, ATDC5 cells grown on a 24-well plate were trypsinized, rinsed twice with PBS, and seeded onto a ProNectin® F-coated cover glass plate (45 × 1.5 mm; thickness, 30 μm; Young's modulus, 71.4 GPa) (Matsunami Glass Ind., Ltd.) at 3.1×10^3 cells/cm^2 as described in Item 3.2.5. The plate was then incubated with maintenance medium at 37°C in a humidified atmosphere of 95% air and 5% CO_2 for 6 h. After incubation, the cell detachment test was done as described previously [13,16]. Figures 3.1 and 3.2 show the apparatus for the test. The ultra-thin glass plate seeded with ATDC5 cells was fixed to a holder and completely submerged into a chamber filled with a mixture of phenol red-free L-15 medium (Invitrogen Corp.), 5% FBS, and 1% antibiotic mixtures, pre-warmed to 37°C. The plate acted as a cantilever, and a micropipette aspirator was used to capture a single cell adhering to the substrate as shown in Fig. 3.3. The cell was then detached by pulling the micropipette at a constant rate of 5 μm/sec using a motorized single-axis stage (KS101-20HD; Suruga

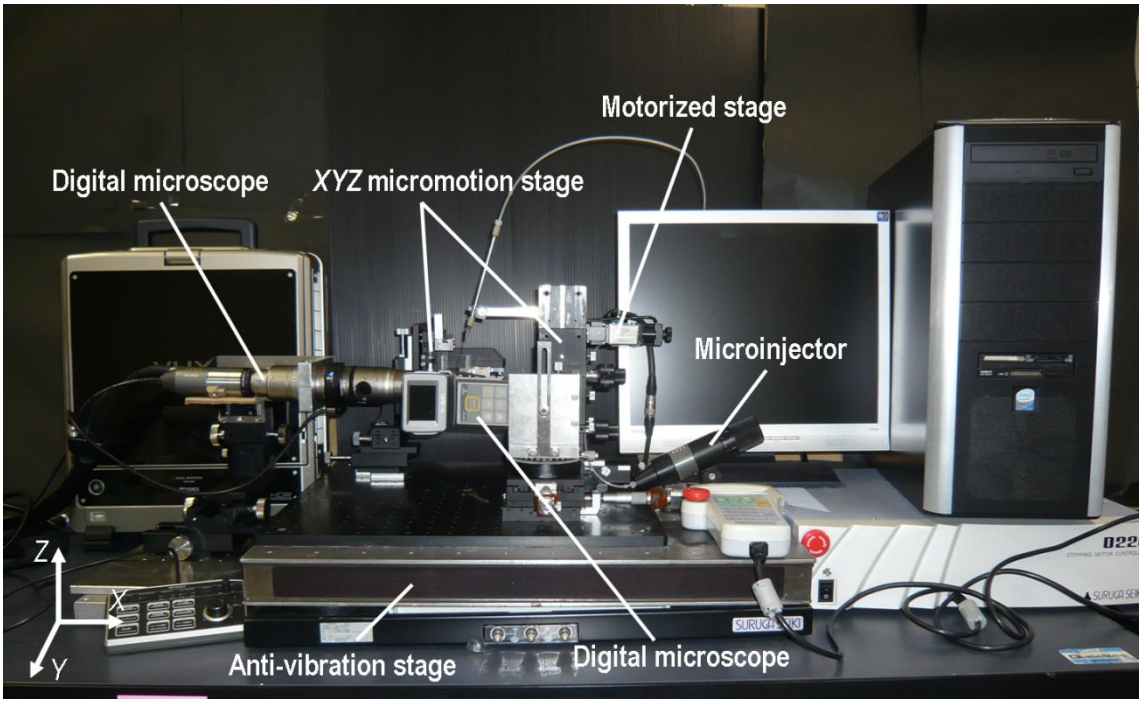

Fig. 3.1. Photograph of the apparatus for the cell detachment test.

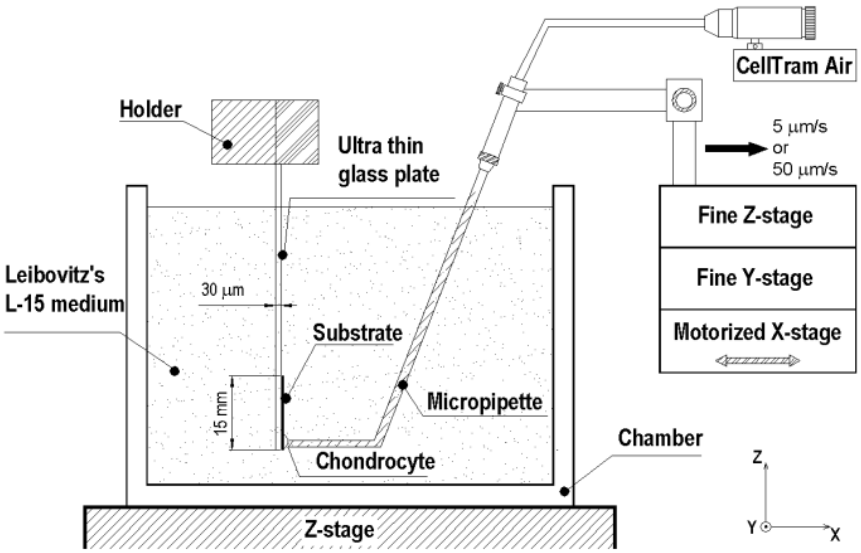

Fig. 3.2. A schematic drawing of an apparatus for measuring the detachment force of a single cell on a substrate. A single chondrocyte was vertically pulled by the micropipette which was able to hold a cell using negative pressure. The detachment process was recorded by the video microscope from the direction of the *Y*-axis in this image [13].

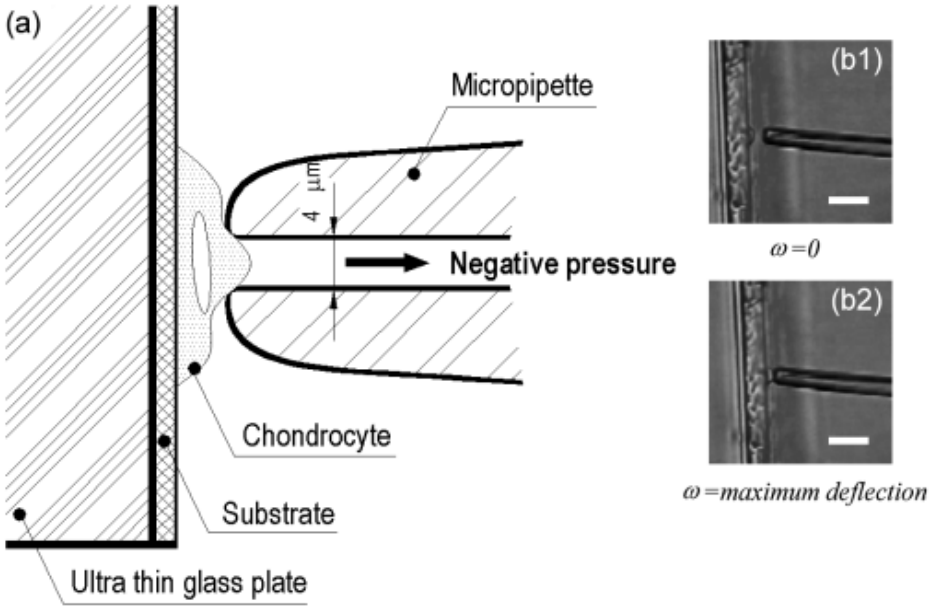

Fig. 3.3. A schematic drawing of holding a chondrocyte using micropipette aspiration (a) and photograph in the process of detaching a chondrocyte on fibroin substrate at 9 h after seeding. (b1) $\omega = 0$, (b2) $\omega =$ *maximum deflection*. Scale bar = 50 μm [13].

Seiki Co., Ltd., Japan). The detachment process was observed through a video microscope (DG-2; Scalar Co., Japan) connected to a time-lapse video capture board able to acquire 29.97 frames per second (GV-MVP/RX3; I-O Data Device Inc., Japan). This measurement was performed at RT. The number of measurements at 3, 7, 10, 14, and 17 days of culture was n = 26, 29, 24, 28, and 22, respectively.

Each digital frame of the detachment animation was analyzed by lab specific image analysis software. Using this software, the 32-bit image was transformed into 8-bit grayscale according to the National Television System Committee coefficients, and digitized with a threshold based on the Otsu method [22]. Then, the position of the ultra-thin glass plate at the cell was determined. By analyzing the digital frames of the detachment process, we obtained a time–deflection curve like the one shown in Fig. 3.4A.

The reaction force of a leaf spring at the cell ($F(t)$) was given by

$$F(t) = 3IEL^{-3}\omega(t), \quad (3.1)$$

where t is the measurement time from when pulling began, I is the moment of inertia of the sectional area of the glass plate, E is the Young's modulus of the glass plate, L is the length from the fixed edge of the leaf spring to the cell, and $\omega(t)$ is the deflection at L at t. Cell adhesive force (F_{ad}) was defined and calculated using the maximum deflection.

The displacement of the micropipette in the tensile direction at the time t ($\Delta x_{pipette}(t)$) was calculated by

$$\Delta x_{pipette}(t) = vt, \quad (3.2)$$

where v was the pulling velocity (5 μm/sec). The elongation of the cell in the detachment process at the time t ($\Delta h(t)$) was given by

$$\Delta h(t) = \Delta x_{pipette}(t) - \omega(t), \quad (3.3)$$

and a cell elongation–force curve, similar to the one shown in Fig. 3.4B, was obtained. The apparent stiffness of the cell (k_{cell}) was defined by fitting a straight line from the origin to the maximum-force point on the curve.

3.2.7. Y27632 treatment to ATDC5 cells

The ATDC5 cells were seeded onto either a 24-well plate or a 6-well plate and cultured with the maintenance medium as described in Item 3.2.1. On day 4 in culture, the maintenance medium was replaced with the differentiation medium supplemented with 10 μM Y27632 (Wako Pure Chemical Industries Ltd.), which is a Rho-associated protein kinase (ROCK) inhibiter. The medium and the inhibitor were changed every 2 days.

On day 7 after seeding, the real-time PCR analysis, immunofluorescence staining of

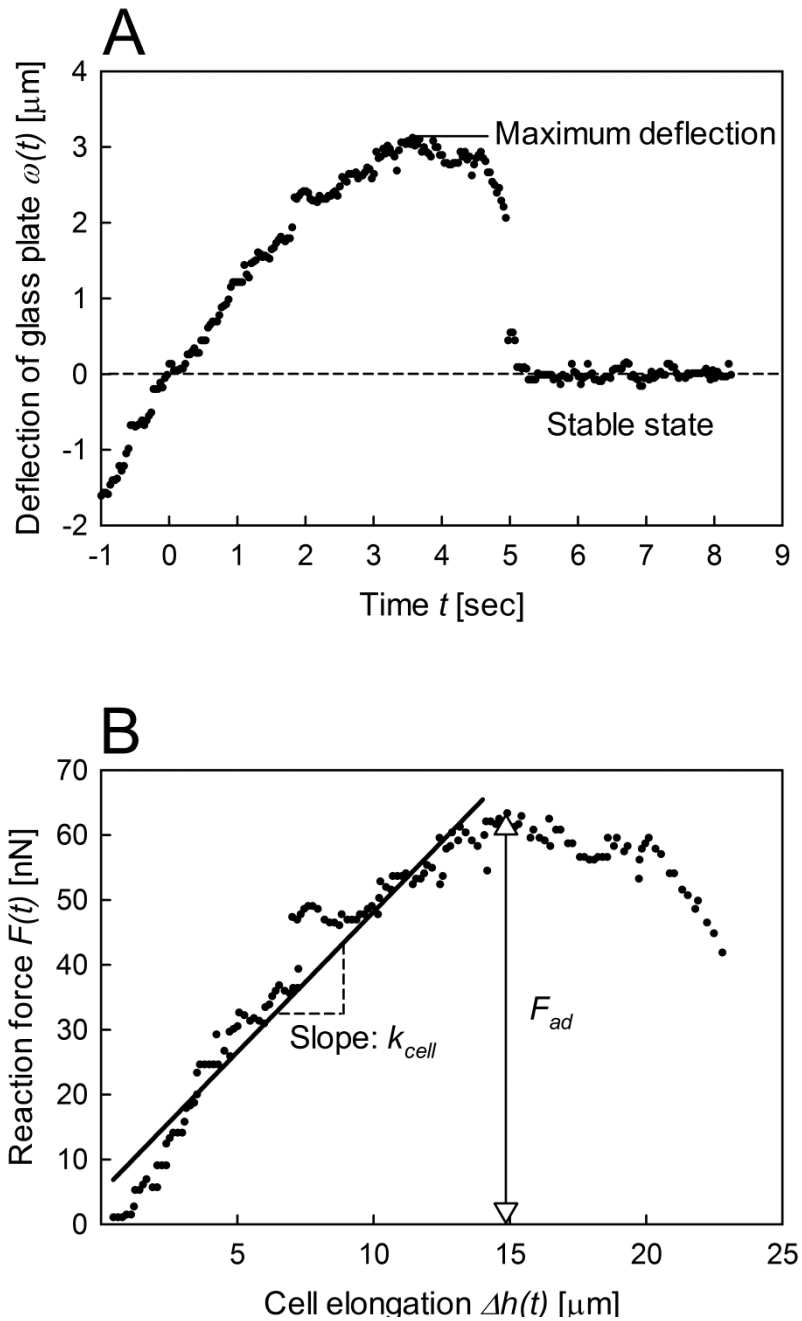

Fig. 3.4. Typical examples of the time–deflection (A) and cell elongation–force (B) curves obtained by analyzing the result of the cell detachment test.

F-acitn, and cell detachment test were conducted as described in Items 3.2.4, 3.2.5, and 3.2.6, respectively. The number of measurements was n = 3 (gene expression levels) and 13 (mechanical properties).

3.2.8. Statistical analysis

Data on the mechanical properties of single cells were not always normally distributed according to the Shapiro-Wilks test and were log-transformed before statistical analysis. Quantitative data on the gene expression level, cell adhesive force, and cell stiffness were analyzed using one-way ANOVA followed by Tukey or Tukey-Kramer post hoc comparisons as appropriate. Effects of the Y27632 treatment on the gene expression levels and mechanical properties were analyzed by two-sided Student's t-test. A value of $p < 0.05$ was considered significant.

3.3. Results

3.3.1. Differentiation of ATDC5 cells in chondrogenic culture

The representative photographs of Alcian blue and Alizarin red S stainings after 3, 7, 10, 14, and 17 days in culture are shown in Fig. 3.5. ATDC5 cells became confluent between 3 and 7 days in culture, and little Alcian blue-positive staining can be observed in this period. However, at 10 days after seeding, Alcian blue-positive areas appeared. These areas gradually expanded and staining intensities increased as culture time advanced. Meanwhile, depositions stained with Alizarin red S began to be observed on day 14, and the dye-affinity became stronger on day 17.

Figure 3.6 shows the changes in mRNA expression levels for Sox9, aggrecan, and collagens type II and type X over the culture period, with all measurements normalized to the expression level at the baseline (3 days). Expression levels of chondrogenic marker genes (Sox9, aggrecan, and collagen type II) exhibited similar time evolutions. They tended to increase with culture time and peaked at 14 days, when the levels were significantly higher than the previous period. Sox9 and aggrecan gene expressions on day 17 were statistically greater than those on days 3, 7, and 10. The gene expression level of collagen type X, which is hypertrophic and calcified chondrocyte-specific

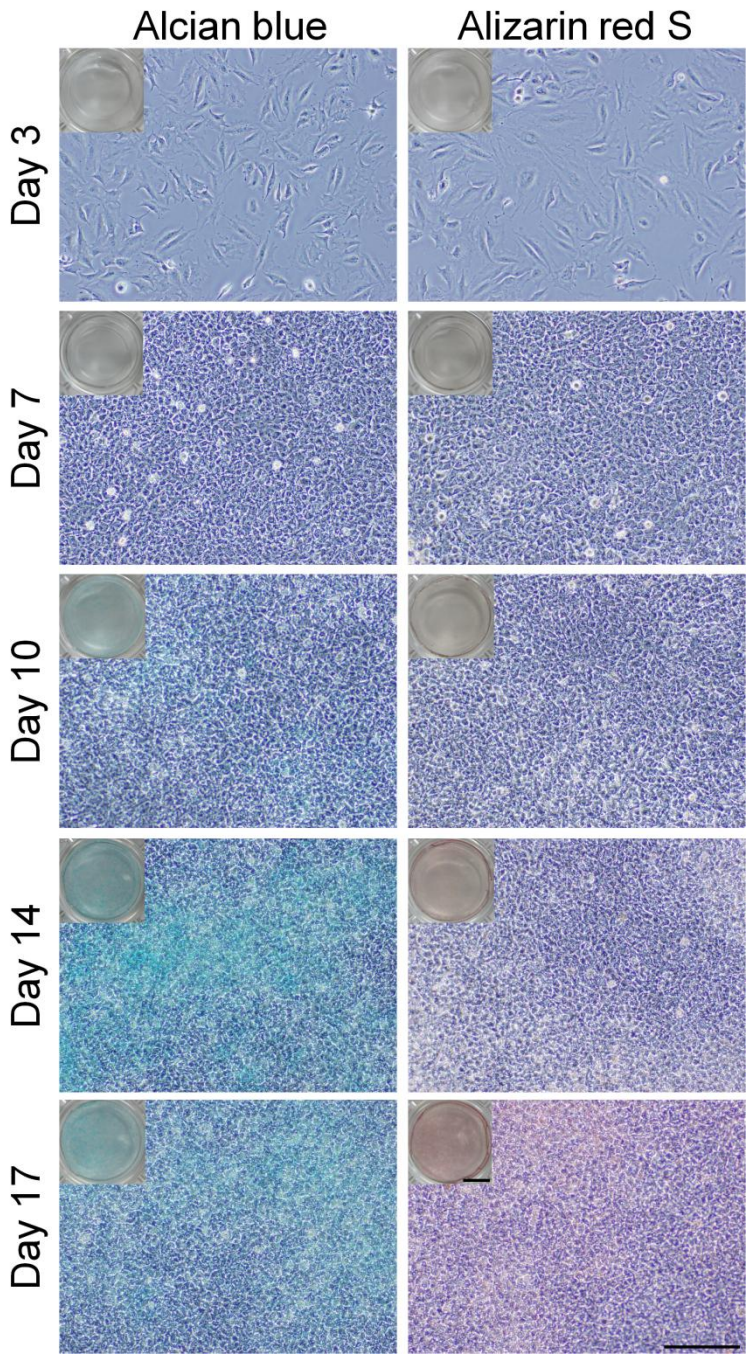

Fig. 3.5. Photographs of Alcian blue- and Arizarin red S-stained ATDC5 cells grown on a 24-well plate at 3, 7, 10, 14, and 17 days in culture. They were taken using a digital camera (upper left part) and a phase-contrast microscope (main part). Scale bar = 5 mm (upper left part) and 200 μm (main part).

[23,24], increased with time in culture. This temporal change was different from those of the other genes in this study. In particular, the collagen type X gene expression on day 17 was significantly higher than the rest time points.

3.3.2. Cell morphology

The representative images of F-actin in ATDC5 cells trypsinized and grown on ProNectin® F for 6 h after culturing for 3, 7, 10, 14, and 17 days are shown in Fig. 3.7.

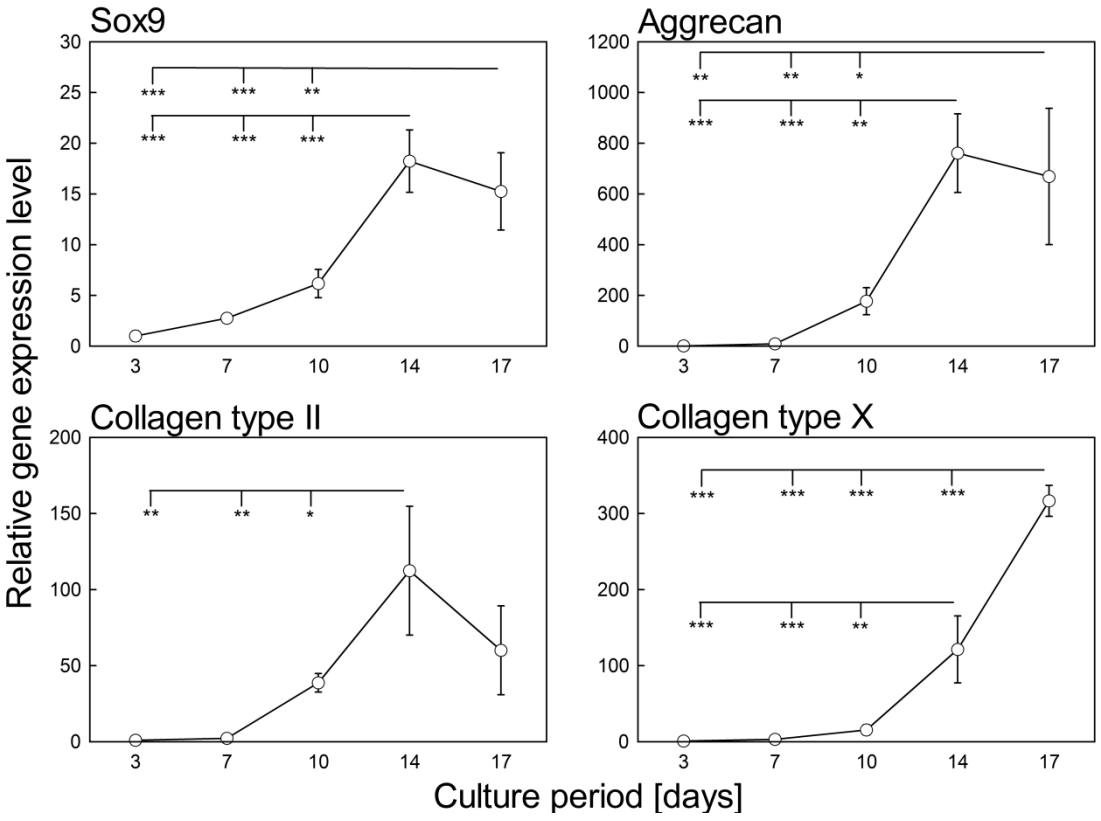

Fig. 3.6. Temporal changes in relative mRNA expression levels of Sox9, aggrecan, and collagens type II and type X in ATDC5 cells cultured on a 6-well plate normalized to the expression level at baseline (3 days). Data is shown in the form: mean ± SD. Asterisks indicate significant differences (*: $p < 0.05$, **: $p < 0.01$, ***: $p < 0.001$; post hoc comparisons, following to one-way ANOVA).

On day 3, the cells mainly exhibited polygonal morphology with a stressed network of bundled actin fibers, which was also observed at 7 and 10 days. This spread morphology, however, tended to be replaced with spherical shape with a cortical shell of F-actin on day 14. These cells had dot-like immature actin fibers inside the shell. At 17 days, the ATDC5 cells typically showed the morphology like day 14, but some of them had spines.

3.3.3. Mechanical properties of single ATDC5 cells

The time-dependent changes in the adhesive force and stiffness of single ATDC5 cells are shown in Fig. 3.8. Both characteristics did not fluctuate during 3 and 10 days in culture, but experienced a negative peak on day 14, when the mechanical properties were statistically lower than those on days 3 and 7. In Fig. 3.8C, the values for the stiffness of each cell were plotted against the adhesive force of the cell to examine their relationships. The correlation coefficient for them was 0.42.

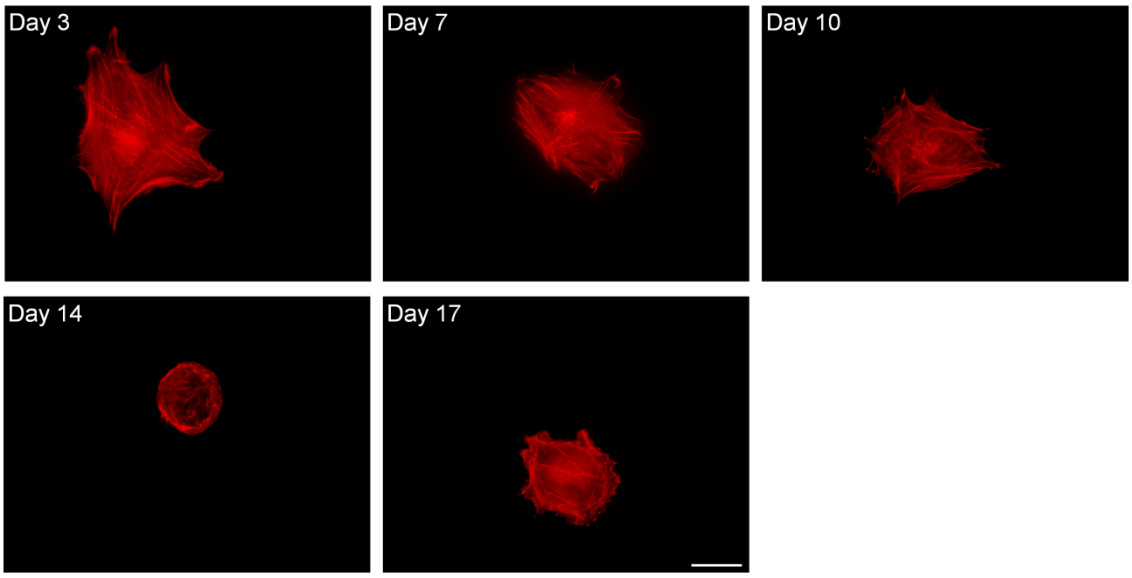

Fig. 3.7. Immunofluorescence staining of F-actin in an ATDC5 cell incubated on a ProNectin® F substrate for 6 h after culturing for 3, 7, 10, 14, and 17 days. Scale bar = 20 μm.

Distributions of the adhesive force at each time point were shown in Fig. 3.9. Vertical axis represents the probability of observations, which is calculated by dividing the number of population in a certain range of the mechanical property by the total number

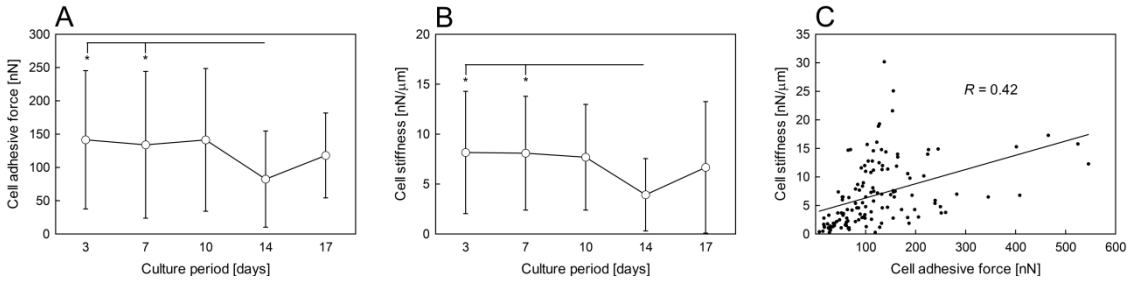

Fig. 3.8. Time-dependent transitions in the adhesive force (A) and stiffness (B) of single ATDC5 cells trypsinized and incubated on ProNectin® F for 6 h after culturing for 3, 7, 10, 14, and 17 days. Data is shown in the form: mean ± SD. Asterisks indicate significant differences (*: $p < 0.05$; post hoc comparisons, following to one-way ANOVA). Stiffness of each ATDC5 cell was represented as a function of cell adhesive force (C). Line fitting was done using liner approximation method. *R*: correlation coefficient. Dot number = 129.

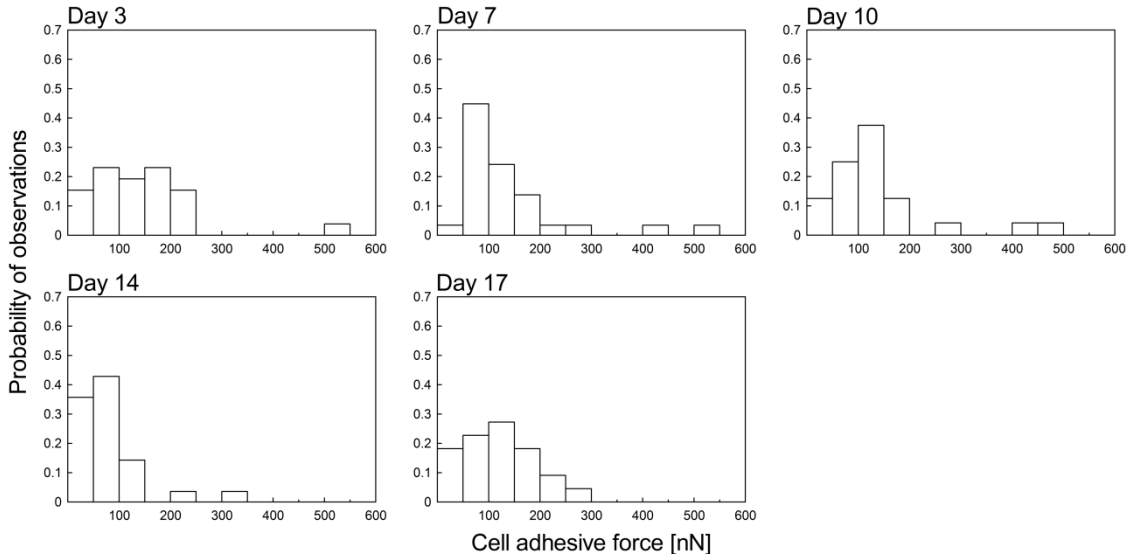

Fig. 3.9. Cell distribution map of the adhesion force on days 3, 7, 10, 14, and 17.

of observations. The ATDC5 cells showed an almost even distribution of the adhesive force ranged from 0 to 250 nN at 3 days. As culture time advanced, the distribution range tended to be narrower, showing a peak around 100 nN. Especially, on day 14, about 80 percent of cells exhibited adhesion force lower than 100 nN. However, the cells at 17 days represented broad distributions of the force like day 3. Similar tendencies were observed in cell distribution maps of the cell stiffness (Fig. 3.10).

3.3.4. Effects of the Y27632 treatment

The representative images of F-actin, gene expressions, and mechanical properties of ATDC5 cells with (Y27632) or without (Control) the Y27632 treatment are shown in Fig. 3.11. On day 7, more defibrinated actin filaments were observed in the cells of the Y27632 group, compared to the Control group. The treatment with Y27632 increased the gene expression levels, showing significant differences in the levels of the chondrogenic marker genes, while both the adhesive force and stiffness of individual ATDC5 cells were remarkably decreased by the treatment.

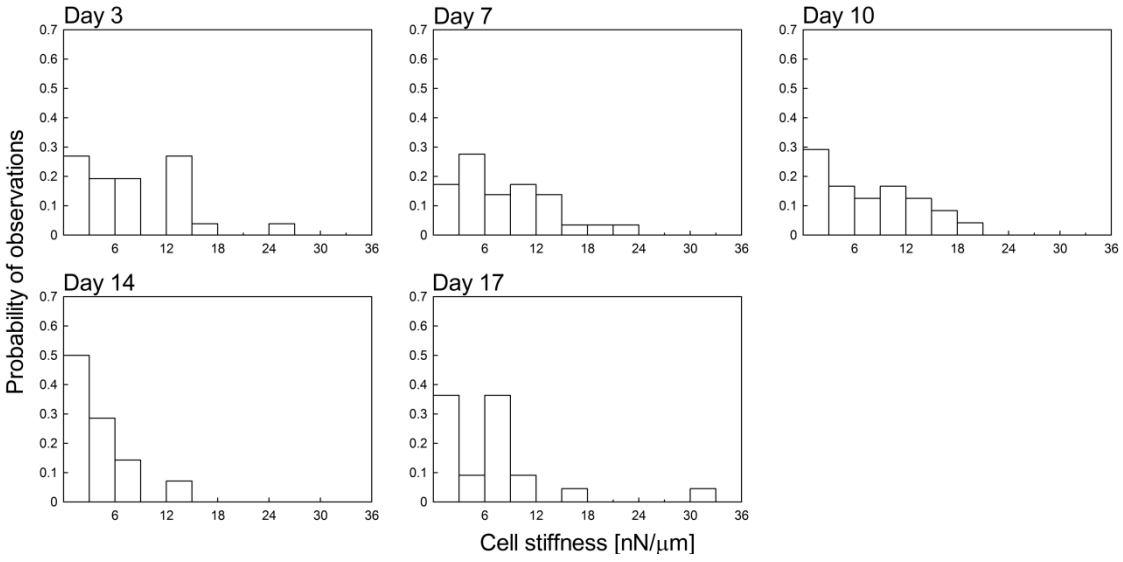

Fig. 3.10. Cell distribution map of the stiffness on days 3, 7, 10, 14, and 17.

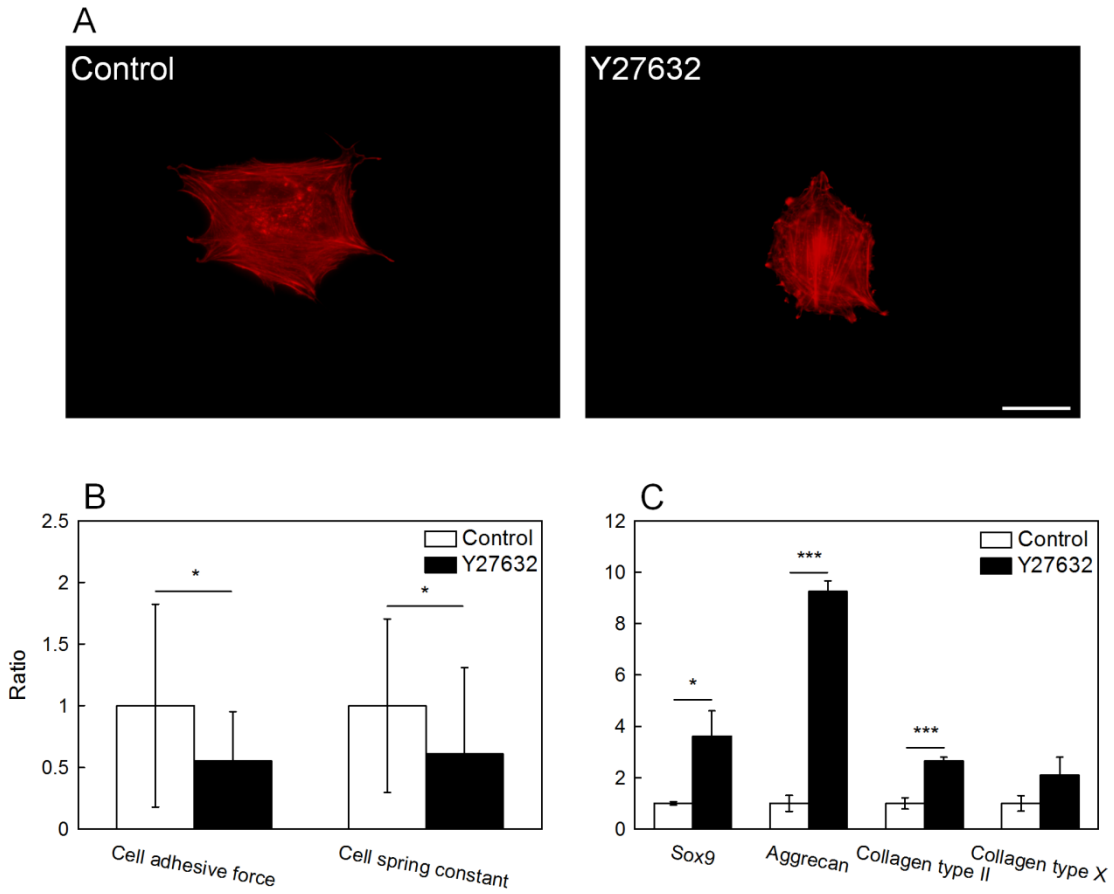

Fig. 3.11. Effects of the treatment with Y27632 on properties of ATDC5 cells. Immunofluorescence staining of F-actin in a cell incubated on a ProNectin® F substrate for 6 h after culturing for 7 days (A). Scale bar = 20 μm. Relative adhesive force and stiffness of single ATDC5 cells trypsinized and incubated on ProNectin® F for 6 h after culturing for 7 days normalized to the value at baseline (Control) (B). Relative gene expression levels of Sox9, aggrecan, and collagens type II and type X in the cells cultured on a 6-well plate for 7 days normalized to the expression level at baseline (Control) (C). Data is shown in the form: mean ± SD. Asterisks indicate significant differences (*: $p < 0.05$, ***: $p < 0.001$; two-sided Student's t-test).

3.4. Discussion

Mechanical properties of cells have been quantified through a variety of techniques. In this study, the adhesive force and stiffness of single ATDC5 cells were measured by detaching the cells vertically from a substrate. Both characteristics showed a similar time evolution, suggesting that they were temporally affected by same factors. One of them can be cellular internal construction since cytoskeletal structures are well known to affect cell stiffness [25,26] and cell adhesive force to a substrate [10,11,13-15]. Our results also showed that the ATDC5 cells typically exhibited a spherical shape with immature actin fibers on day 14, when the mechanical properties were the lowest. More directly, the treatment with a ROCK inhibitor Y27632, which eventually inhibits actin polymerization [27,28], statistically decreased both the adhesive force and the stiffness. However, the two properties of each cell did not have a strong correlation. With respect to the adhesive force, the formation of focal adhesions, derived from bindings between transmembrane cell-adhesive molecules (e.g., integrins) and extracellular ligands (e.g., Arg-Gly-Asp sequences), is reported to have a strong impact [9,12-16]. For example, the blocking of an integrin subunit by its antibody significantly weakened the adhesive force of fibroblasts [14], and the expression of focal adhesion kinase (FAK), which is a member to construct a focal adhesion, strengthened the force [12]. As integrins bind to actin cytoskeleton, mediated by anchor molecules like FAK, cell-adhesive constructions can mutually affect the adhesive force with the cytoskeletal architecture. This might lead the weak correlation of the adhesive force with the stiffness, which appears to mainly include the information about cytoskeletal structures.

Cells in long-term cultures are affected not only by putative differentiation process but also by processes as e.g., contact inhibition. These processes do not necessarily have to influence the differentiation of the ATDC5 cells but can heavily change the actin cytoskeleton and cell adhesion. However, in terms of the chondrogenic differentiation, it has been shown that Sox9 expression and activity are regulated by actin organization [29,30]. Woods et al. [29] reported that the RhoA-induced development of actin stress

fibers suppressed Sox9 gene expression, while the inhibition of RhoA/ROCK signaling by Y27632 led a cortical actin architecture and enhanced Sox9 gene expression. Our results also demonstrated that the vigorous inhibition of actin polymerization by Y27632 both weakened the adhesive force and promoted the chondrogenic gene expressions of the ATDC5 cells on day 7, even when the effects of contact inhibition-induced changes in cellular structures are considered to be comparatively small. Therefore, changes in the constructions of cytoskeleton and cell adhesion can affect both the mechanical properties and differentiation of the ATDC5 cells. This result also suggests the involvement of mechanical cell adhesiveness in chodrogenic differentiation, mediated by the cellular structure.

From these observations, we inferred that the differentiation-dependent changes in the adhesive force of individual ATDC5 cells were evaluated in this study. The photographs of Alcian blue staining exhibited that the ATDC5 cells gradually produced sulfate glycosaminoglycan as the chondrogenic culture advanced. Additionally, quantitative real-time PCR analysis showed that chondrogenic gene expression levels (Sox9, aggrecan, and collagen type II) maintained an upward trend during 3 and 14 days, showing a strong increase from days 10 to 14. However, they tended to decrease between 14 and 17 days in culture. In contrast, hypertrophic and calcific marker gene expression (collagen type X) kept increasing throughout the culture period. These results are consistent with those reported elsewhere [21,30]. Taking these facts into account, it is suggested that the ATDC5 cells mainly differentiated into chondrocytes from anaplastic cells until day 14 and then to hypertrophic and calcified chondrocytes between 14 and 17 days in this study. This suggestion is also supported by the result of Alizarin red S staining because calcium deposition were observed at day 14 and the mineralization progressed to day 17.

Under these differentiation processes, changes in the adhesive force of single ATDC5 cells were examined. Chondrocyte-like cells (day 14) had a significantly lower adhesive force than the cells on the way to the differentiation into chondrcoytes (days 3 and 7). However, the force did not fluctuate between 3 and 10 days in spite of the increasing

tendency of the chondrogenic marker genes in that period. Additionally, no statistical differences in the mechanical characteristic were detected between days 10 and 14, when the gene expressions increased dramatically. On the other hand, focusing on the time evolution of the cell distribution map of the adhesive force, the distribution tended to become narrower and its peak appeared to shift toward lower value as the cells differentiated into chondrocytes from anaplastic mesenchymal cells between days 3 and 14. The force then got to range widely again with the progression of hypertrophy and calcification from 14 to 17 days. These temporal tendencies were also observed in the distribution of the cell stiffness. Thus the cells could have various levels of mechanical properties in undifferentiated and transitional states, whereas they tended to show comparatively-unified degree of the properties when the differentiation process is in a lull. The results shown by Darling et al. [2] may also support this suggestion. Using an AFM, they demonstrated that human MSCs, chondrocytes, and osteoblasts had elasticity distributions similar to the adhesive force distributions of the ATDC5 cells on days 3, 14, and 17, respectively.

The results of this study suggest that, when evaluated as a bulk, the mechanical adhesiveness of single ATDC5 cells do not reflect chondrogenic differentiation process as clearly as cellular biochemical properties such as gene expressions. However, the mechanical characteristics of the cells had large population variations and were not necessarily normally distributed, suggesting that subpopulations of cells with different properties existed as Darling et al. [2] mentioned previously. In fact, individual ATDC5 cells are unequal in chondrogenic culture because their chondrogenic differentiation is performed with the formation of cartilage nodules [17,18]. Therefore, with the recognition that cells have diversity, the mechanical characteristic can be useful to pursue differentiation stages; the phase of chondrogenic differentiation appears to be featured by the range and peak of cell distribution of the adhesive force. Furthermore, these findings can provide the significance of mechanical interactions between individual cells and their surrounding environment in the fields of generation and scaffold-based tissue regeneration, where cell–substrate adhesion plays a role.

3.5. Conclusions

This study has shown that changes in cellular structures such as cytoskeleton affected both adhesive force and chondrogenic gene expressions of ATDC5 cells, suggesting biomechanical and biochemical properties of the cells are interrelated. When estimated as a bulk, the mechanical adhesiveness of single cells did not represent the chondrogenic differentiation stages as clearly as biochemical characteristics. However, cell distribution maps of the adhesion force could change specifically in the differentiation process, showing the position and width of distribution peak is of importance. The findings of this study indicate that the phenotypic information of chondrogenic cells can be represented as cellular mechanical information, and, conversely, cell-adhesive functions of materials is a key factor to develop useful scaffolds for cartilage regeneration.

References

[1] Collinsworth AM, Zhang S, Kraus WE, Truskey GA. Apparent elastic modulus and hysteresis of skeletal muscle cells throughout differentiation. Am J Physiol Cell Physiol 2002;283:C1219-27.

[2] Darling EM, Topel M, Zauscher S, Thomas PV, Guilak F. Viscoelastic properties of human mesenchymally-derived stem cells and primary osteoblasts, chondrocytes, and adipocytes. J Biomech 2008;41:454-64.

[3] Darling EM, Pritchett PE, Evans BA, Superfine R, Zauscher S, Guilak F. Mechanical properties and gene expression of chondrocytes on micropatterned substrates following dedifferentiation in monolayer. Cell Mol Bioeng 2009;2:395-404.

[4] Yu H, Tay CY, Leong WS, Tan SCW, Lio K, Tan LP. Mechanical behavior of human mesenchymal stem cells during adipogenic and osteogenic differentiation. Biochem Biophys Res Commun 2010;393:150-5.

[5] Schuh E, Kramer J, Rohwedel J, Notbohm H, Müller R, Gutsmann T, et al. Effect of matrix elasticity on the maintenance of the chondrogenic phenotype. Tissue Eng Part A 2010;16:1281-90.

[6] Von der Mark K, Gauss V, Von der Mark H, Müller P. Relationship between cell shape and type of collagen synthesised as chondrocytes lose their cartilage phenotype in culture. Nature 1977;267:531-2.

[7] Benya PD, Shaffer JD. Dedifferentiated chondrocytes reexpress the differentiated collagen phenotype when cultured in agarose gels. Cell 1982;30:215-24.

[8] Brodkin KR, García AJ, Levenston ME. Chondrocyte phenotypes on different extracellular matrix monolayers. Biomaterials 2004;25:5929-38.

[9] Yamamoto A, Mishima S, Maruyama N, Sumita M. Quantitative evaluation of cell attachment to glass, polystyrene, and fibronectin- or collagen-coated polystyrene by measurement of cell adhesive shear force and cell detachment energy. J Biomedl Mater Res 2000;50:114-124.

[10] Hoben G, Huang W, Thoma BS, LeBaron RG, Athanasiou KA. Quantification of varying adhesion levels in chondrocytes using the cytodetacher. Ann Biomed Eng 2002;30:703-12.

[11] Huang W, Anvari B, Torres JH, LeBaron RG, Athanasiou KA. Temporal effects of cell adhesion on mechanical characteristics of the single chondrocyte. J Orthop Res 2003;21:88-95.

[12] Wu CC, Su HW, Lee CC, Tang MJ, Su FC. Quantitative measurement of changes in adhesion force involving focal adhesion kinase during cell attachment, spread, and migration. Biochem Biophys Res Commun 2005;329:256-65.

[13] Yamamoto K, Tomita N, Fukuda Y, Suzuki S, Igarashi N, Suguro T, et al. Time-dependent changes in adhesive force between chondrocytes and silk fibroin substrate. Biomaterials 2007;28:1838-46.

[14] Cai N, Wong CC, Tan SCW, Chan V, Liao K. Temporal effect of functional blocking of β_1 integrin on cell adhesion strength under serum depletion. Langmuir 2009;25:10939-47.

[15] Kambe Y, Yamamoto K, Kojima K, Tamada Y, Tomita N. Effects of RGDS sequence genetically interfused in the silk fibroin light chain protein on chondrocyte adhesion and cartilage synthesis. Biomaterials 2010;31:7503-11.

[16] Kambe Y, Takeda Y, Yamamoto K, Kojima K, Tamada Y, Tomita N. Effect of RGDS-expressing fibroin dose on initial adhesive force of a single chondrocyte. Biomed Mater Eng 2010;20:309-316.

[17] Atsumi T, Ikawa Y, Miwa Y, Kimata K. A chondrogenic cell line derived from a differentiating culture of AT805 teratocarcinoma cells. Cell Differ Dev 1990;30:109-16.

[18] Shukunami C, Shigeno C, Atsumi T, Ishizeki K, Suzuki F, Hiraki Y. Chondrogenic differentiation of clonal mouse embryonic cell line ATDC5 in vitro: differentiation-dependent gene expression of parathyroid hormone (PTH)/PTH-related peptide receptor. J Cell Biol 1996;133:457-68.

[19] Zhang X, Ziran N, Goater JJ, Schwarz EM, Puzas JE, Rosier RN, et al. Primary murine limb bud mesenchymal cells in long-term culture complete chondrocyte differentiation: TGF-β delays hypertrophy and PGE2 inhibits terminal differentiation. Bone 2004;34:809-17.

[20] Yoon ST, Kim KS, Li J, Park JS, Akamaru T, Elmer WA, et al. The effect of bone morphogenetic protein-2 on rat intervertebral disc cells in vitro. Spine 2003;28:1773-80.

[21] Challa TD, Rais Y, Ornan EM. Effect of adiponectin on ATDC5 proliferation, differentiation and signal pathways. Mol Cell Endocrinol 2010;323:282-91.

[22] Otsu N. A threshold selection method from gray-level histograms. IEEE Trans Sys Man Cybern B Cybern 1979;9:62-6.

[23] Castagnola P, Dozin B, Moro G, Cancedda R. Changes in the expression of collagen genes show two stages in chondrocyte differentiation in vitro. J Cell Biol 1988;106:461–7.

[24] Gerstenfeld LC, Landis WJ. Gene expression and extracellular matrix ultrastructure of a mineralizing chondrocyte cell culture system. J Cell Biol 1991;104:1435–41.

[25] Nagayama K, Nagano Y, Sato M, Matsumoto T. Effect of actin filament distribution on tensile properties of smooth muscle cells obtained from rat thoracic aortas. J Biomech 2006;39:293-301.

[26] Tan SCW, Pan WX, Ma G, Cai N, Leong KW, Liao K. Viscoelastic behaviour of human mesenchymal stem cells. BMC Cell Biol 2008;9:40.

[27] Hirose M, Ishizaki T, Watanabe N, Uehata M, Kranenburg O, Moolenaar WH, et al. Molecular dissection of the Rho-associated protein kinase (p160ROCK)-regulated neurite remodeling in neuroblastoma N1E-115 cells. J Cell Biol 1998;141:1625-36.

[28] Maekawa M, Ishizaki T, Boku S, Watanabe N, Fujita A, Iwamatsu A, et al. Signaling from Rho to the actin cytoskeleton through protein kinases ROCK and LIM-kinase. Science 1999;285:895-8.

[29] Woods A, Wang G, Beier F. RhoA/ROCK signaling regulates Sox9 expression and actin organization during chondrogenesis. J Biol Chem 2005;280:11626-34.

[30] Kumar D, Lassar AB. The transcriptional activity of Sox9 in chondrocytes is regulated by RhoA signaling and actin polymerization. Mol Cell Biol 2009;29:4262-73.

[31] Newman B, Gigout LI, Sudre L, Grant ME, Wallis GA. Coordinated expression of matrix Gla protein is required during endochondral ossification for chondrocyte survival. J Cell Biol 2001;154:659-66.

Chapter 4
Development of RGDS-Fused Silk Fibroin and Its Effects on Chondrocyte Adhesion and Cartilage Synthesis

4.1. Introduction

A large number of cells with the chondrogenic phenotype are required for clinical cartilage regeneration. However, the cellular supply source is limited when autologous cartilage cells are used for tissue-engineered therapy. To resolve this problem, numerous biomaterials have been developed for tissue regeneration by applying chemical and/or genetic modification technologies, and focusing on modulation of cell adhesive activities [1-9]. Our previous studies have shown that chondrocytes cultured using a porous silk fibroin sponge can proliferate well and synthesize glycosaminoglycan (GAG) which consists of cartilage-specific extracellular matrices (ECMs) [10]. We have also reported the *in vivo* functions of a silk fibroin scaffold for cartilage repair in a rabbit model [11]. Subsequently, Yamamoto et al. [12] focused on the initial cell adhesion to the fibroin scaffold and investigated the time-dependent adhesive states between a chondrocyte and a fibroin substrate by evaluating the cell detachment force. They showed that the adhesive force per unit cell spreading area of chondrocytes grown on a fibroin substrate was at a maximum value between 6 and 9 h after seeding; this peak was not observed in chondrocytes grown on a glass substrate, where the cells were reported not to proliferate or synthesize cartilage matrices [13]. The results of these

studies indicate that fibroin-induced cell adhesion is associated with the stability of the chondrogenic phenotype and cartilage ECM synthesis.

An Arg-Gly-Asp (RGD) amino acid sequence is the minimum unit of a cell adhesive activity domain in adherent proteins, such as fibronectin, fibrin, and vitronectin, which are all ligands of integrins [14-16]. In addition the sequence is generally used to modulate cell adhesion to artificial materials. In culture, simple addition of RGD peptides or adherent proteins to a scaffold tends to facilitate the dedifferentiation of chondrocytes [5,17]. However, artificially immobilized RGD in/on scaffold components applied with physical or chemical modifications was reported to have some stimulatory effects on the synthesis of GAG [7,8]. Tigli and Gumusderelioglu [7] reported that murine chondrogenic ATDC5 cells cultured in a chitosan scaffold modified with RGD by covalent immobilization produced more GAG than cells grown in a control chitosan scaffold. Jung et al. [8] also reported that chondrocytes cultured in acrylic acid-grafted poly(L-lactic acid) (PLLA) scaffolds on which RGD peptides were chemically immobilized showed higher cellularity and increased accumulation of GAG than control cells.

In the present study, we have investigated the effect of changes in fibroin-induced cell adhesion on cartilage tissue formation using RGDS-transgenic fibroin, particularly focusing on the initial chondrocyte–material adhesion. Fibroin protein consists of a heavy chain (H-chain; molecular weight, 360 kDa) and a light chain (L-chain; molecular weight, 27 kDa), which are linked by a disulfide bond to form a heterodimer [18]. There have been several studies of genetic modification of the H-chain [19] or the L-chain [20-23]. As the L-chain protein can be cloned and modified more easily than the H-chain [19], a tandem repeat of Arg-Gly-Asp-Ser ($(RGDS)_2$) was successfully interfused by genetic engineering methods [24] and stably expressed in the fibroin L-chain (L-RGDS×2 fibroin). The initial adhesion of chondrocytes on the substrate was evaluated by measuring adhesive force and spreading area. Cell morphology was also observed by immunofluorescence staining of F-actin and vinculin, and relative messenger RNA (mRNA) expression levels were measured. Additionally, the

performance of L-RGDS×2 fibroin sponge as a chondrocyte scaffold was evaluated histologically.

4.2. Materials and Methods

4.2.1. Construction of a vector carrying cDNA encoding L-RGDS×2

The plasmids used for silkworm transgenesis in this study were prepared as follows. pLp-LcDNA-EGFP-L3'UTR and pBac(3×P3-DsRed2afm) constructs were prepared as described by Inoue et al. [21]. An RGDSRGDS-fused fibroin-L-chain construct, pLLL-2×RGDSen, was prepared as follows. Two oligonucleotides (2×RGDS-5: 5'-GAT CGTGGAGACAGCCGTGGAGACAGCTGA-3' and 2×RGDS-3en: 5'-AGCTTCAGC TGTCTCCACGGCTGTCTCCAC-3') were mixed at 100 pmol/μl each in polymerase chain reaction (PCR) buffer (TAKARA BIO Inc., Japan) for 1 min at 95°C, and then incubated overnight at room temperature (RT) to prepare an oligonucleotide cassette. Following this, the cassette was ligated with *Bam*HI- and *Hin*dIII-digested pLp-LcDNA-EGFP-L3'UTR. The resultant plasmid was designated pLLL-2×RGDSen. To obtain a transfer plasmid, the expression cassette in pLLL-2×RGDSen was digested into two pieces with *Hin*dIII and *Eco*RV, and *Hin*dIII and *Bgl*II. Finally, the resulting fragment was cloned between *Bgl*II and the blunt-ended *Asc*I site of pBac(3×P3-DsRed2afm), and then designated pBac(3×P3-DsRed2afm)_LLL-2×RGDSen.

4.2.2. Generation of transgenic silkworms

The genetic modification of the *Bombyx mori* silkworm performed in the present study is being prepared for publication. Briefly, silkworm transgenesis was performed as described by Tamura et al. [24] with minor modifications. The plasmid pBac(3×P3-DsRed2afm)_LLL-2×RGDSen was injected into silkworm eggs along with

a helper plasmid at 3 to 6 h post-oviposition. Hatched larvae (G0) were reared and permitted to mate with each other. The resultant embryos (G1) were screened by using a fluorescent microscope (MZ16 FA; Leica Microsystems, Germany) for transgenic individuals with DsRed2 expression 6 to 7 days after oviposition. The transgenic silkworms were reared together and sib-mated for at least three generations, with sequential screening by the strong excitation of DsRed2 fluorescence in the adult eye. The resulting silkworm strain was designated NK14.

All the recombinant DNA experiments followed the Regulation on Use of Living Modified Organisms at National Institute of Agrobiological Sciences (NIAS), and were approved by the Recombinant DNA Research Committee at NIAS.

4.2.3. SDS-PAGE and Western blotting

Cocoon shells of wild-type or NK14 silkworms were diced into apx. 1 mm^2. They were suspended in an 8 M urea aqueous solution with 5% 2-mercaptoethanol (2ME) and incubated at 80°C for 15 min with some stirrings, followed by washing with distilled water prewormed at 80°C. This urea refinement procedure was repeated twice to roughly remove sericin proteins. The rest silk proteins were dissolved in 9.0 M LiBr aqueous solution by stirring at RT for 1 h. After centrifugation, the supernatant was dialyzed against 8 M urea by using the EasySep (molecular weight cutoff, 14,000; Tomy Seiko Co., Ltd., Japan) in accordance with the manufactures instructions. Then the protein concentration was determined by the absorbance at 280-nm ultraviolet light and adjusted to 20 mg/ml with 8 M urea. The fibroin solution was mixed with the equal volume of the Laemmli Sample Buffer (Bio-Rad Laboratories Inc., USA) containing 5% 2ME and incubated at 60°C for 20 min. 5 μl of the resultant solutions were applied to sodium dodecyl sulfate-polyacrylamide gel electrophoresis (SDS-PAGE) for for Coomassie brilliant blue (CBB) staining or for immunoblotting, respectively. SDS-PAGE and Western blotting were performed as described in Item 2.2.3. Rabbit anti-$(RGDS)_2$ polyclonal antiserum (9936-2; Operon Biotechnologies Inc., USA) and

horseradish peroxidase (HRP)-conjugated goat anti-rabbit IgG polyclonal antibody (ab6721; Abcam plc., UK) were reacted used as the primary and the secondary antibodies, respectively.

4.2.4. Preparation of plate substrates

Protein substrates were prepared using wild-type fibroin (WTF), L-RGDS×2 fibroin (LRF) and ProNectin® F (PN; Sanyo Chemical Industries Ltd., Japan), and non-coated glass was used as a control substrate (CON). Proteins were coated on the following glass plates (Matsunami Glass Ind., Ltd., Japan): ultra-thin glass plates (45 × 1.5 mm; thickness, 30 μm; Young's modulus, 71.4 GPa) for evaluating cell adhesive force; cover glass plates (18 × 18 mm; thickness, 0.15 mm) for evaluating cell spreading area and for real-time PCR analysis; cover glass plates (diameter, 15 mm; thickness, 0.15 mm) for measuring contact angles and for immunofluorescence staining of actin and vinculin; and cover glass plates (24 × 60 mm; thickness, 0.15 mm) for measuring ζ potential. All plates were made of borosilicate glass of the same quality.

WTF aqueous solution was prepared from degummed silk fibers of *Bombyx mori* silkworm cocoons [10-12]. The LRF protein contained modified fibroin L-chains fused with the $(RGDS)_2$ sequences at the carboxyl-terminus. The LRF was produced by the NK14 transgenic silkworms generated as described in Item 4.2.2. The LRF aqueous solution was prepared using the same technique as for the preparation of the WTF aqueous solution. The amount of the LRF proteins contained in total fibroin proteins was adjusted as follows. Fibroin proteins from the NK14 silkworm cocoons were applied to native PAGE, and band intensities were compared with the fibroin L-chain of a standard fibroin solution in a Western blot assay with anti-fibroin L-chain antibody (Operon Biotechnologies Inc.). The concentration of LRF molecules was adjusted to 0.6, 1.5, and 3.0 mol% by mixing the LRF solution with the WTF solution. In the experiments other than those to investigate the dose-dependent effects of LRF molecules, the 3.0 mol% LRF was used as the LRF group.

The concentration of the fibroin solutions was determined by a bicinchoninic acid assay and adjusted to 1.0% (wt/vol) for all coating treatments, as described previously [12]. Fibroin-coated glass plates were extensively washed with phosphate-buffered saline (PBS; Nacalai Tesque Inc., Japan) before use. PN substrates were prepared with ProNectin® F according to the manufacturer's instructions. Briefly, a stock solution was diluted to 10 μg/ml in PBS, and glass plates were soaked in the diluted solution for 5 min at RT. After removing the coating solution, the glass plates were washed twice with PBS.

4.2.5. Preparation of fibroin sponges

WTF sponges were prepared as described previously [25]. Briefly, dimethyl sulfoxide (DMSO) was added gradually, with stirring, to a WTF aqueous solution at the determined volume depending on the final concentration of the WTF (4.0% (wt/vol)) and DMSO (1.0%). The mixed solution was incubated at –20°C for 17 h to form a sponge-like material by phase separation. LRF sponges were prepared from the NK14 transgenic silkworm cocoons using the same protocol for preparing WTF sponges. The sponges had a porous structure with a mean pore diameter of about 80 μm. They were sterilized in an autoclave before use.

4.2.6. Measurement of surface properties of substrates

The surface properties of the substrates as represented by contact angle and ζ potential were evaluated immediately after the samples were extensively washed with ultrapure water and dried in a clean bench. Static water contact angles on the substrates were determined by the sessile drop method using CA-Z2 (Kyowa Interface Science Co., Ltd., Japan) at RT. A droplet (4 μl) of ultrapure water was placed on the surface of a sample and the contact angle was measured. This procedure was repeated three times at different areas on the same surface, and the contact angle of the sample was determined

as the mean value of the three measurements. Three different samples in each group were used to determine the contact angle of the group.

The ζ potential of each substrate was measured using an ELS-7000AS instrument with the cell unit for flat plate samples (Otsuka Electronics Co., Ltd., Japan) in 10 mM NaCl at 25°C. The pH of the streaming solution was adjusted to 7.4 with HCl and NaOH aqueous solutions. Three different samples in each group were used to determine the ζ potential of the group (n = 3).

4.2.7. Scanning electron microscopy (SEM)

Scanning electron microscopy (SEM) was used to observe the effect of the genetic modification on the topology of fibroin films and fibroin sponges. In preparation of the fibroin-coated glass plates, the plates were washed extensively with ultrapure water and dried in a clean bench. Immediately following this, they were sputter-coated with gold-palladium using an E-1010 instrument (Hitachi Ltd., Japan) and imaged by a scanning electron microscope (S-2380N; Hitachi Ltd.). Three different specimens of each fibroin film were used for the observation.

In preparation of the fibroin sponges, the sponges were washed twice with PBS for 10 min and dehydrated in a graded ethanol series (70%, 80%, 90%, 95%, and 100% ethanol for 5, 5, 10, 10, and 10 min, respectively). The remaining ethanol was replaced by incubating twice in tert-butyl alcohol for 10 min. Specimens were then frozen on dry ice and dried using an ES-2030 instrument (Hitachi Ltd.). Following this, the freeze-dried fibroin sponges were sputter-coated with gold-palladium and imaged as described above. Three different samples of each fibroin sponge were used for the observation.

4.2.8. Chondrocytes and cell seeding

Chondrocytes were prepared as described in Item 2.2.7. After expansion in culture,

chondrocytes were removed from the flask by mixing with 0.25% trypsin-EDTA (Nacalai Tesque Inc.) and washed twice with PBS. In the culture on the plate substrates, the cells were seeded at 2.0×10^4 cells/cm^2 and incubated with Dulbecco's modified Eagle's Medium (DMEM) (Nacalai Tesque Inc.) containing 10% fetal bovine serum (FBS; Nacalai Tesque Inc.) and 1% antibiotic mixture (10,000 units/ml penicillin, 10,000 μg/ml streptomycin, and 25 μg/ml amphotericin B; Nacalai Tesque Inc.) at 37°C in a humidified atmosphere of 95% air and 5% CO_2. In the culture in/on the fibroin sponges, on the other hand, the chondrocytes were seeded onto the fibroin scaffold (diameter, 8 mm; thickness, 1 mm) at a concentration of 5.0×10^5 cells/scaffold and cultured with DMEM containing 10% FBS, 1% antibiotic mixture, and 0.2 mM ascorbic acid (A8960; Sigma-Aldrich Co., USA) at 37°C in a humidified atmosphere of 95% air and 5% CO_2. The medium was changed every 2 days.

All the animal experiments followed the Regulation on Animal Experimentation at Kyoto University, and were approved by the Animal Research Committee at Kyoto University.

4.2.9. Chondrocyte attachment to substrates and competitive inhibition with soluble RGD peptides

The influence of different substrates on the attachment of chondrocytes was observed using a phase-contrast microscope (IX-71; Olympus Corp., Japan). At 24 h after seeding, the cells on each substrate were washed twice with PBS and fixed with 4% paraformaldehyde (PFA) solution for 15 min at RT. After removing the solution, a 1 ml of PBS was added and then the attaching cells were photographed. Chondrocytes were incubated on LRF substrates with serum-free medium containing different concentrations (0, 0.1, 1, and 10 μg/ml) of Gly-Arg-Gly-Asp-Ser-Pro (GRGDSP) peptides (SP001; TAKARA BIO Inc.). After incubation for 24 h, the cells were photographed, as described above. Experiments were repeated at least three times, and similar results were noted each time.

4.2.10. Apparatus and procedure for measuring adhesive force

After incubation for 3, 6, 9, 12, or 24 h, cell adhesive force was measured as described in Item 3.2.6. The maximum deflection of the leaf spring was determined by counting the pixels using ImageJ (http://imagej.nih.gov/ij/; National Institute of Health, USA) from the photographs taken during the detaching process. The number of measurements of adhesive force in each group at 3, 6, 9, 12, and 24 h after seeding was as follows: WTF group, n = 17, 10, 13, 24, and 19; LRF group, n = 9, 10, 8, 9, and 8 for 0.6 mol%, n = 10, 10, 10, 9, and 9 for 1.5 mol%, and n = 13, 13, 7, 9, and 16 for 3.0 mol%; CON group, n = 26, 31, 39, 40, and 27; and PN group, n = 24, 27, 31, 38, and 36, respectively.

4.2.11. Determination of cell spreading area

Chondrocytes were seeded onto the different substrates as described above. After incubation for 3, 6, 9, 12, and 24 h, cells were washed twice with PBS and fixed with 4% PFA solution for 15 min at 37°C. They were then stained with a 1% (wt/vol) CBB solution for 2 min and washed twice with PBS. Digital images of the cells were acquired by microscopy. The cell spreading area was measured by analyzing the binarized images using ImageJ. The CBB solution was prepared by dissolving Coomassie® Brilliant Blue R250 (Sigma-Aldrich Co.) powder in a solution containing 50% of methanol and 1% of acetic acid. The number of measurements of spreading area in each group at 3, 6, 9, 12, and 24 h after seeding was as follows: WTF group, n = 24, 29, 33, 23, and 28; LRF group, n = 29, 30, 44, 45 and 33 for 0.6 mol%, n = 31, 35, 39, 41 and 38 for 1.5 mol%, and n = 35, 30, 27, 27, and 27 for 3.0 mol%; CON group, n = 29, 34, 44, 38, and 49; and PN group, n = 44, 44, 37, 58, and 43, respectively.

4.2.12. Immunofluorescence staining of F-actin and vinculin

After incubation for 6, 12, or 24 h, F-actin, vinculin, and the nucleus of chondrocytes

grown on the substrates were stained as described previously [12]. Briefly, after fixing with 4% PFA solution, the cells were permeabilized and incubated in fresh blocking solution prepared with 1% (wt/vol) bovine serum albumin (Serological Corp., USA). Rhodamine phalloidin (R415; Molecular Probes, USA) was used to stain F-actin, while anti-vinculin (MAB3574; Chemicon International Inc., USA) was used as the primary antibody and fluorescein isothiocyanate-conjugated goat anti-mouse IgG was used as the secondary antibody (AP124F; Chemicon International Inc.) to stain vinculin. Additionally, 4',6-diamidino-2-phenylindole (S7113, Chemicon International Inc.) was used to stain the nucleus. Stained chondrocytes were observed with an inverted fluorescence microscope (IX-71 and BH2-RFL-T3; Olympus Corp.).

4.2.13. Real-time PCR analysis

After incubation for 6, 12, or 24 h, real-time PCR analysis were performed as described in Item 3.2.4. Primers (Sigma-Aldrich Co.) were designed for rabbit glyceraldehyde-3-phosphate dehydrogenase (GAPDH) as the house-keeping gene, integrins α5 and β1, aggrecan, and collagen type II αI chain. Primer sequences are shown in Table 4.1. In each group at each time point, n = 4 for mRNA expression levels, except for the levels of aggrecan in the WTF and LRF groups at 6 h after seeding (n = 3).

4.2.14. Evaluation of the number of cells attaching to fibroin sponges

After incubation for 9 or 24 h after seeding, cell number in WTF or LRF sponges was quantified by a lactate dehydrogenase (LDH) assay [29]. The samples were washed three times with PBS and put into 0.5% Triton X-100 (9690T; Research Organics Inc., USA) in PBS solution and incubated at 4°C for 24 h to dissolve the cells in the sponge. The LDH activity of the dissolved solution was measured using the kinetics of NADH-consuming reactions at 340 nm absorbance. The cell number was calculated using the LDH activity with calibration. The number of measurements of cell number in

each group at 9 and 24 h was as follows: WTF group, n = 5 and 5; LRF group, n = 5 and 4, respectively.

Table 4.1. Primer sequences for real-time PCR analysis.

Gene target	Primer sequence (5' - 3')	GenBank ID	Reference #
GAPDH	Sense: TCACCATCTTCCAGGAGCGA Antisense: CACAATGCCGAAGTGGTCGT	L23961	[26]
Integrin α5	Sense: GGCAGCTATGGCGTCCCACTGTGG Antisense: GGCATCAGAGGTGGCTGGAGGCTT	S77513	[27]
Integrin β1	Sense: GTGGTTGCTGGAATTGTTCTTATT Antisense: TTTTCCCTCATACTTCGGATTGAC	S77516	[27]
Aggrecan	Sense: CTACGACGCCATCTGCTACA Antisense: CCTCTTCAGTCCCGTTCT	L38480	[28]
Collagen type II αI chain	Sense: GCACCCATGGACATTGGAGGG Antisense: GACACGGAGTAGCACCATCG	S83370	[28]

4.2.15. Histological evaluation of regenerated cartilage

After culturing for 3 or 7 days, regenerated cartilage organized in/on WTF or LRF sponges was fixed with 20% neutral buffered formalin and incubated for more than 24 h at 4°C. Samples were embedded in paraffin and cut into 7-μm-thick sections. Specimens were sectioned parallel to the length of the scaffold, and stained for safranin O and immunostained for collagen type I (F-56; DAIICHI FINE CHEMICAL Co., Ltd., Japan) and type II (F-57; DAIICHI FINE CHEMICAL Co., Ltd.). Photographs of stained samples were taken under a microscope. From each group, three samples were prepared for the staining, and for repeatability, culture experiments were performed in triplicate.

4.2.16. Statistical analysis

Effects of the dose of the LRF protein on chondrocyte initial adhesion were analyzed using one-way ANOVA followed by the Tukey or Tukey-Kramer test for post hoc comparisons. By contrast, quantitative data were analyzed between WTF and LRF groups and between CON and PN groups using two-sided Student's t-test. A value of $p < 0.05$ was considered significant. In the Figs 4.4, 4.5, and 4.7, asterisks indicate statistical significance between WTF and LRF groups, and sharp symbols indicate differences between CON and PN groups.

4.3. Results

4.3.1. SDS-PAGE and Western blotting

Proteins were extracted from silk fibers of wild-type and NK14 silkworms with 8 M urea with 5% 2ME, separated by SDS-PAGE, and immunoblotted with anti-$(RGDS)_2$ antibodies (Fig. 4.1). On CBB-stained gels (A), it seems difficult to distinguish the band

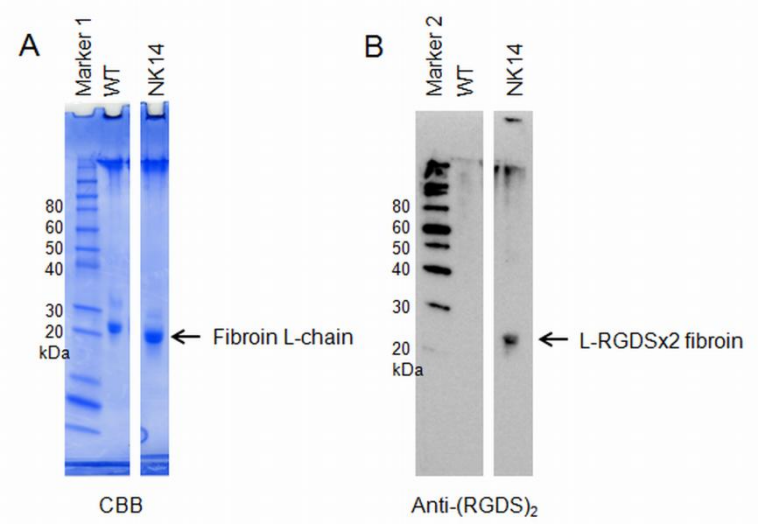

Fig. 4.1. SDS-PAGE (A) and Western blotting (B) of proteins extracted from the wild-type (WT) and NK14 transgenic silk fibers. Separated proteins on a gel were stained with CBB (A). Proteins on another gel were transferred onto a PVDF membrane and then reacted with anti-$(RGDS)_2$ antibodies (B). Novex® Sharp Protein Standard (Invitrogen Corp., USA) was used as the Marker 1, while MagicMark™ XP Western Protein Standard (Invitrogen Corp.) was used as the Marker 2. Arabic numerals at the left side of the photographs are molecular weight in kDa.

of the L-chain protein of the LRF from that of the native fibroin L-chain because the molecular weight of an $(RGDS)_2$ peptide is apx. 0.8 kDa, which is too small to be separated by SDS-PAGE. Another possibility is that the amount of the LRF protein might be so small that the band of the protein did not detected by the CBB staining. However, such a band was clearly observed on Western blot (B) for the silk fibers of the NK14 silkworms but not for silk fibers of the wild-type silkworms.

4.3.2. Surface properties of substrates

Surface properties such as contact angle and ζ potential of each substrate are shown

Table 4.2. Surface properties of each substrate as represented by contact angle and ζ potential.

Substrate	Contact angle [deg]	ζ potential [mV]
WTF	67.2 ± 0.8	-34.89 ± 2.27
LRF	65.7 ± 0.7 n.s.	-36.79 ± 6.19 n.s.
CON	60.9 ± 1.0	-59.84 ± 10.27
PN	59.8 ± 0.9 n.s.	-58.01 ± 10.13 n.s.

Data is shown in the form: mean ± SD. Three different samples in each group were used to determine the contact angle and ζ potential of the each group.
n.s.: No significant differences were detected between the WTF and LRF substrates, and between the CON and PN substrates by the two-sided Student's t-test.

in Table 4.2. There were no significant differences in either contact angle or ζ potential between the WTF and LRF groups or between the CON and PN groups.

4.3.3. Observations of fibroin films by SEM and chondrocyte attachment

The representative scanning electron micrographs of the WTF and LRF films are shown in Fig. 4.2A. Both surfaces were almost smooth to the extent of SEM observations, and no marked differences between the WTF and LRF substrates were displayed.

Chondrocytes cultured on each substrate for 24 h are shown in Fig. 4.2B–D. More chondrocytes were found to adhere to the substrate with the increase in LRF concentrations as shown in Fig. 4.2B. The number of cells that attached to the PN and LRF substrates appeared to be higher than the number of cells that attached to the CON and WTF substrates, however, chondrocyte adhesion to an LRF substrate was inhibited dose-dependently by GRGDSP peptide in the medium.

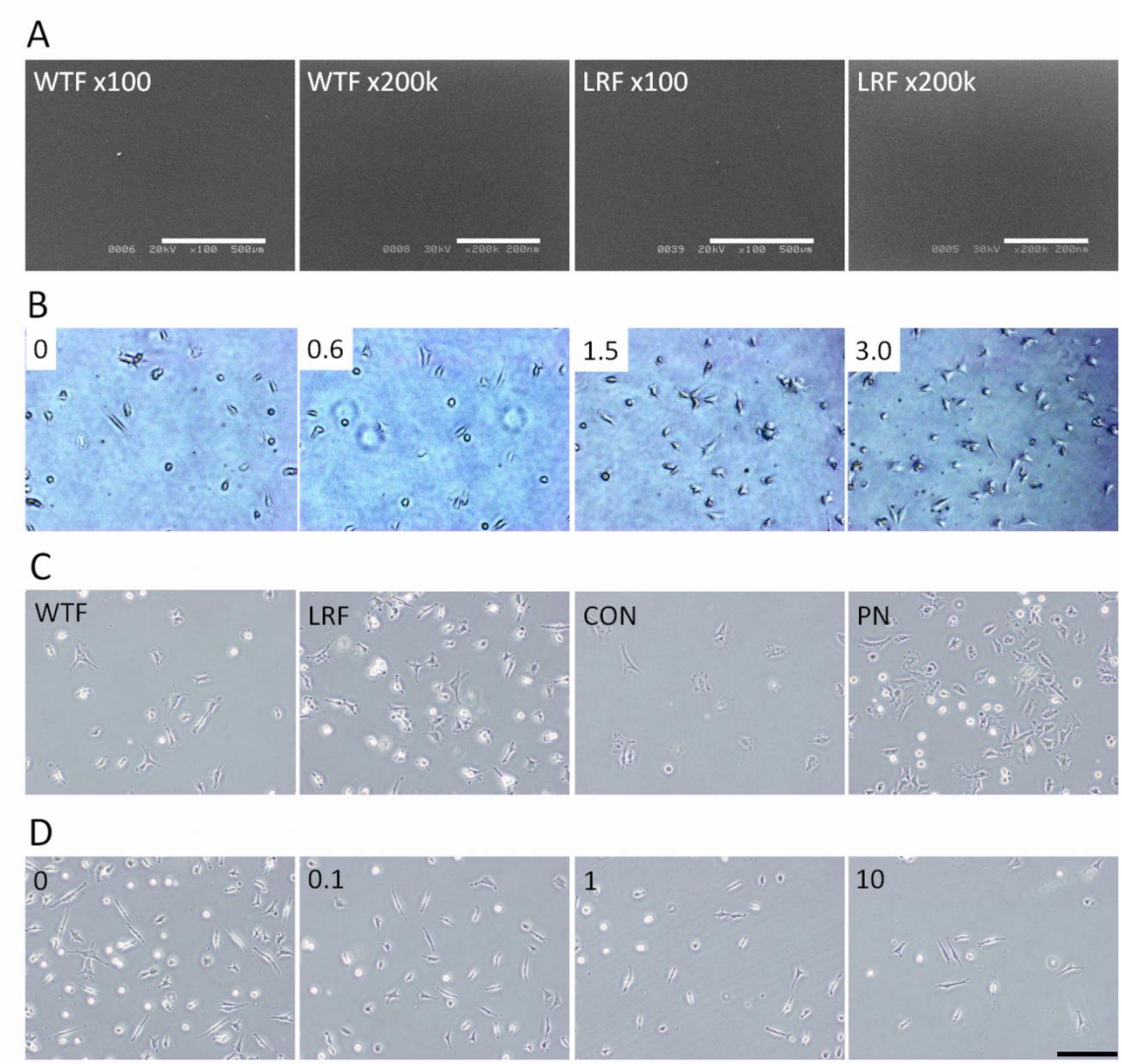

Fig. 4.2. Scanning electron micrographs of WTF and LRF films (A). Scale bar = 500 μm for 100-fold magnification and 200 nm for 200,000-fold magnification. Photographs of chondrocytes grown on LRF substrates with different concentrations (0, 0.6, 1.5, and 3.0 mol%) of LRF molecules (B), the cells grown on WTF, LRF, CON, and PN substrates at 24 h after seeding (C), and photographs of the cells grown on LRF substrate with soluble GRGDSP peptides in the serum-free medium at concentrations of 0, 0.1, 1, and 10 μg/ml (D). Scale bar = 200 μm for B–D.

4.3.4. Effects of L-RGDS×2 fibroin dose on chondrocyte adhesive force and spreading area

The time-dependent changes in the adhesive force of chondrocytes grown on substrates with different percentages (0, 0.6, 1.5, and 3.0 mol%) of LRF molecules are shown in Fig. 4.3A. The 3.0 mol% group exhibited a higher adhesive force than the other groups during 12 h after seeding, while, at 24 h, the 0 mol% group showed a significantly higher force than the 1.5 and 3.0 mol% groups.

The cell spreading area as a function of culture time is shown in Fig. 4.3B. No significant differences among the groups were observed at 3 h after seeding. The 0.6 mol% group showed a significantly smaller area than the 1.5 and 3.0 mol% groups at 6 h after seeding. Meanwhile, at 12 h, the spreading are of the 0.6 mol% group was significantly larger than the other groups. The spreading area of the 1.5 mol% group was significantly larger than that of the 0 mol% group at 24 h.

4.3.5. Cell adhesive force

The time-dependent changes in adhesive force of chondrocytes grown on each substrate are shown in Fig. 4.4. The LRF and PN groups tended to show higher adhesive force than the WTF and CON groups, respectively. However, at 12 h after seeding, the LRF group demonstrated more force than the WTF group, and the PN group showed more force than the CON group. The adhesive force of the LRF group was significantly higher than that of the WTF group at 3, 9, and 12 h after seeding, but significantly lower at 24 h. The PN group showed significantly higher adhesive force than the CON group only at 12 h after seeding. In the WTF and LRF groups, the adhesive force did not change monotonically as in the CON and PN groups, but instead reached a maximum value within 12 h after seeding.

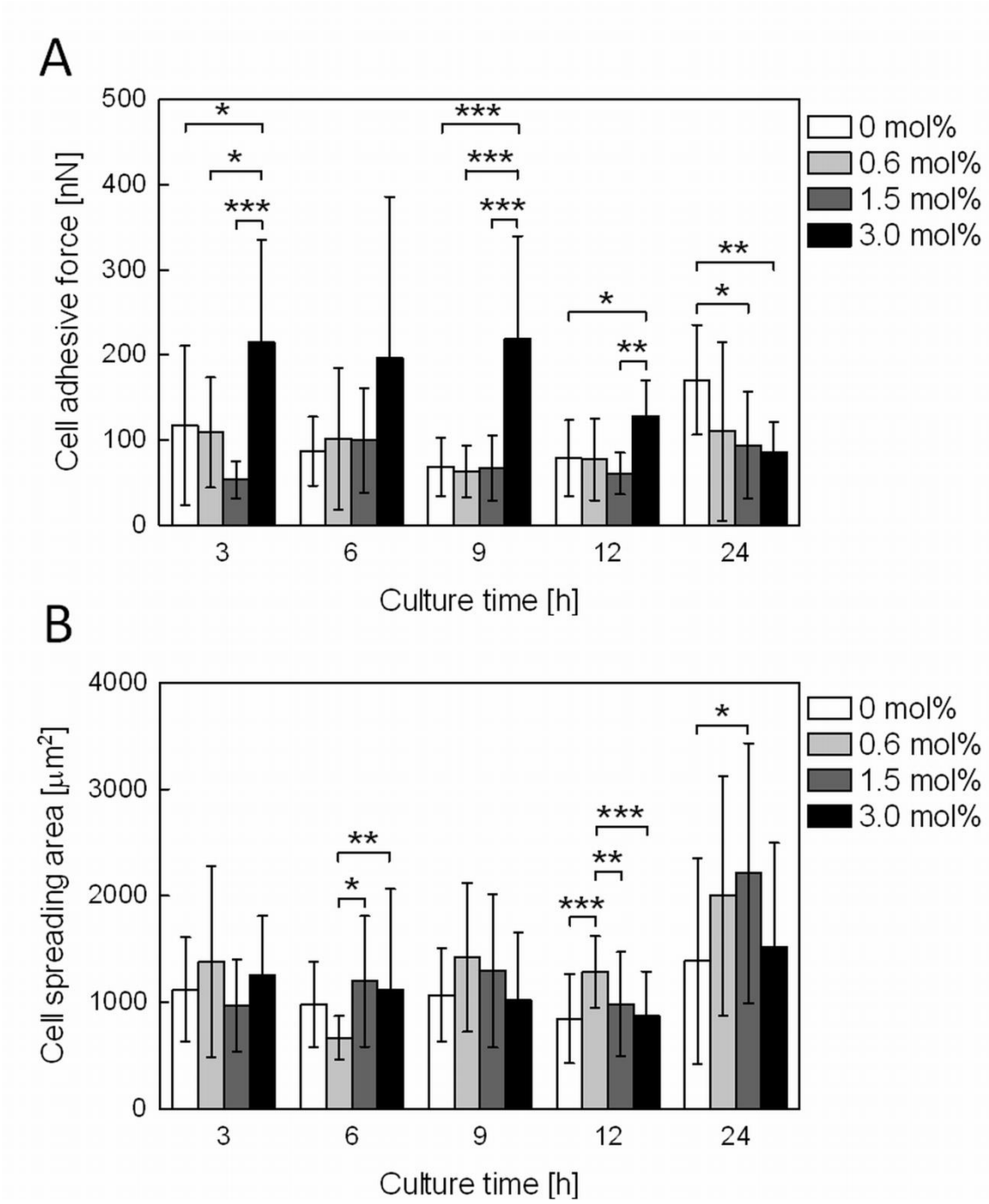

Fig. 4.3. Adhesive force (A) and spreading area (B) of chondrocytes grown on the LRF substrates with 0, 0.6, 1.5, and 3.0 mol% of LRF molecules at 3, 6, 9, 12, and 24 h after seeding. Data is shown in the form: mean ± SD. Asterisks indicate statistical significance (*: $p < 0.05$, **: $p < 0.01$, ***: $p < 0.001$; post hoc comparisons following to one-way ANOVA).

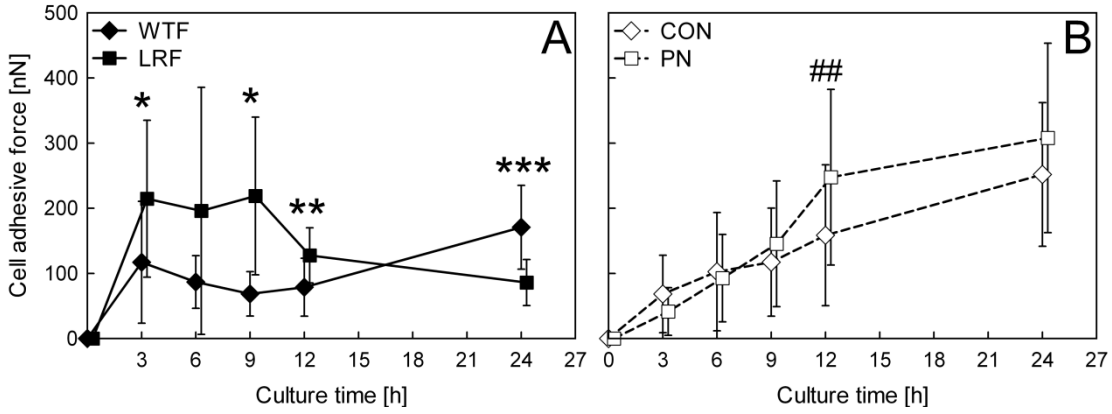

Fig. 4.4. Time-dependent changes in adhesive force to detach single chondrocytes on WTF and LRF substrates (A), and CON and PN substrates (B). Data is shown in the form: mean ± SD. Asterisks indicate significant differences between the WTF and LRF groups, and sharps indicate significant differences between the CON and PN groups (*: $p < 0.05$, **, ##: $p < 0.01$, ***: $p < 0.001$; two-sided Student's t-test).

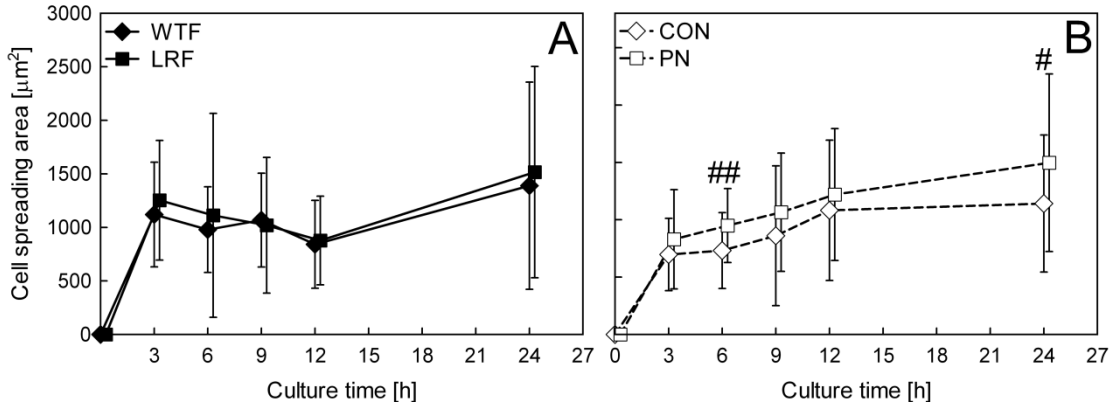

Fig. 4.5. Time-dependent changes in spreading area of single chondrocytes grown on WTF and LRF substrates (A), and CON and PN substrates (B). Data is shown in the form: mean ± SD. Sharps indicate significant differences between the CON and PN groups (#: $p < 0.05$, ##: $p < 0.01$; two-sided Student's t-test).

4.3.6. Cell spreading area

The cell spreading area as a function of culture time is shown in Fig. 4.5. No significant differences were found between the WTF and LRF groups; both groups tended to show similar time-course changes in spreading area. On the other hand, chondrocytes grown on the PN substrate tended spread to a larger area than those grown on the CON substrate, and these effects were significant at 6 and 24 h after seeding.

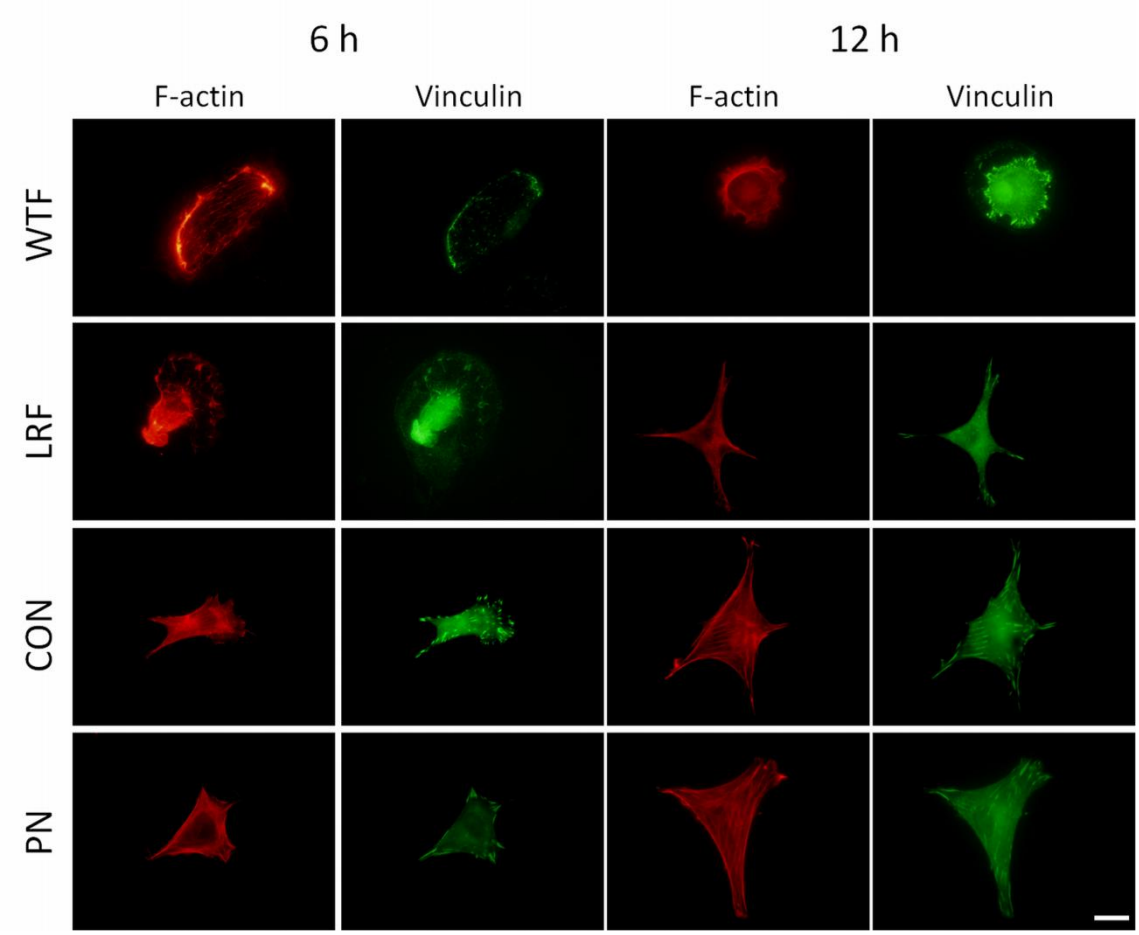

Fig. 4.6. Immunofluorescence staining of F-actin and vinculin in a chondrocyte grown on WTF, LRF, CON, and PN substrates at 6 and 12 h after seeding. Scale bar = 20 μm.

4.3.7. Cell morphology

The representative photographs of F-actin and vinculin staining for each substrate at 6 and 12 h after seeding are shown in Fig. 4.6. At 6 h after seeding, immature actin fibers and dot-like vinculin were sporadically present in chondrocytes grown on both the WTF and LRF substrates. At 12 h, this cell morphology was not observed but polymerized actin fibers were formed, and dash-like vinculin was observed at the cell processes in the LRF group. Finally, at 24 h after seeding, the latter F-actin structure and vinculin distributions were observed in both the WTF and LRF groups (data not shown). As described above, time-dependent morphological changes were shown in chondrocytes cultured on the two fibroin substrates. In contrast, polymerized actin fibers and dash-like vinculin were constantly observed in the CON and PN groups.

4.3.8. mRNA expression levels

Figure 4.7 shows the changes in the mRNA expression levels of integrins $\alpha 5$ and $\beta 1$, aggrecan, and collagen type II at 6, 12, and 24 h after seeding, and the data were normalized with respect to the expression level at 0 h after seeding. The aggrecan expression in the WTF and LRF groups showed a peak within 24 h after seeding, whereas the aggrecan expression in the CON and PN groups only changed slightly with time. The LRF group exhibited higher expression of aggrecan and integrins $\alpha 5$ and $\beta 1$ at 12 h, whereas there were no significant differences in the mRNA expression levels between the CON and PN groups.

4.3.9. SEM observation of fibroin sponges and initial cell number

Figure 4.8A shows the representative scanning electron micrographs for the WTF and LRF sponges. Both sponges appeared to be similar in their morphology, possessing similar pore size, pore structure, and pore size distribution.

The time-course changes in the number of chondrocytes in/on the WTF and LRF

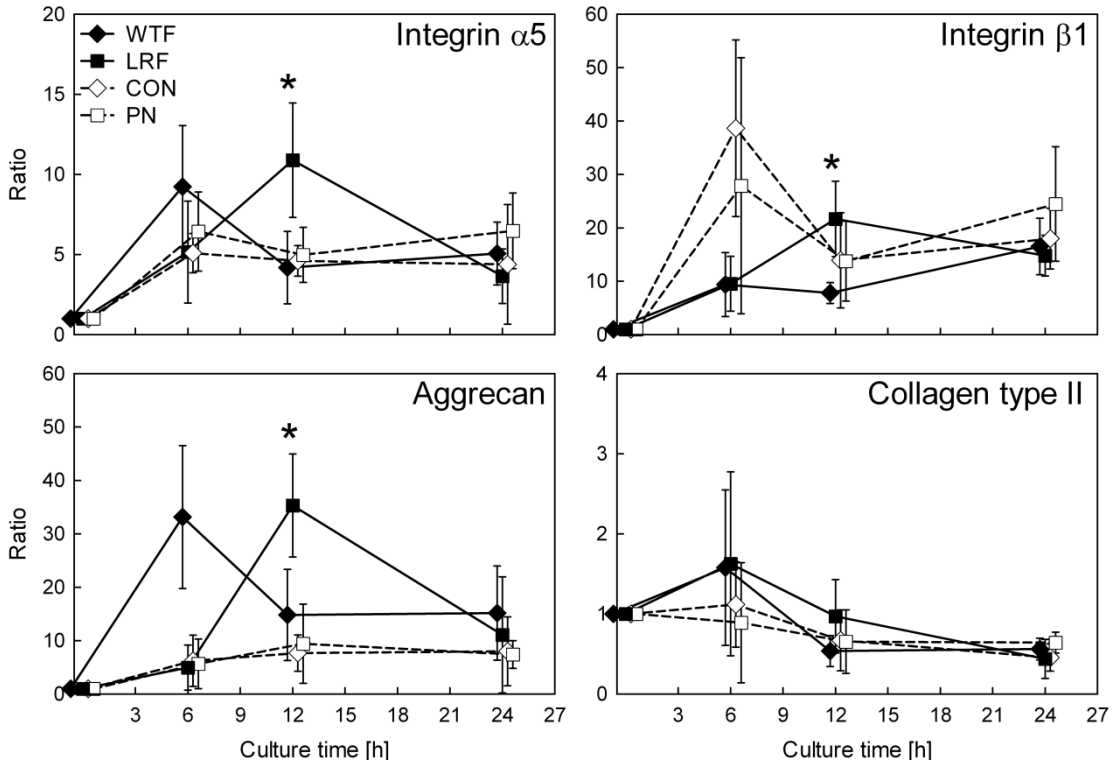

Fig. 4.7. Time-course changes in relative mRNA expression levels of integrins α5 and β1, aggrecan, and collagen type II in chondrocytes grown on WTF, LRF, CON, and PN substrates. The data were normalized to the expression level at 0 h after seeding. Data is shown in the form: mean ± SD. Asterisks indicate significant differences between the WTF and LRF groups (*: $p < 0.05$; two-sided Student's by t-test).

sponges are shown in Fig. 4.8B. Both groups exhibited time-dependent increase in the cell number. At 9 h after seeding, the LRF group showed significantly higher cell number than the WTF group. As 5.0×10^5 cells were seeded onto each scaffold, chondrocytes in/on the LRF sponge could proliferate within 9 h after seeding. However, there were no significant differences between the groups at 24 h although the LRF group showed a slightly larger number of cells.

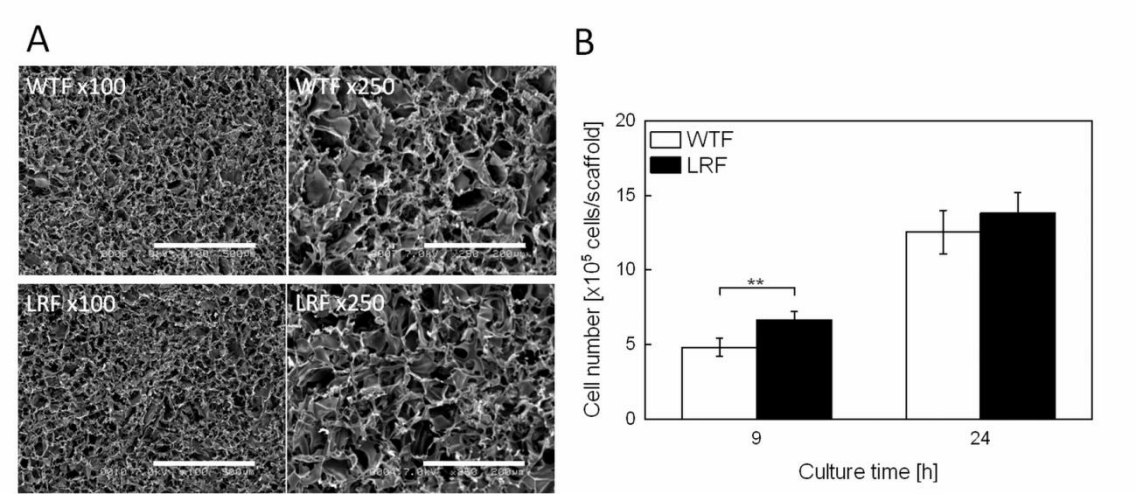

Fig. 4.8. Scanning electron micrographs of WTF and LRF sponges (A). Scale bar = 500 and 200 μm for 100- and 250-fold magnifications, respectively. The number of chondrocytes in/on WTF and LRF sponges at 9 and 24 h after seeding (B). Data is shown in the form: mean ± SD. Asterisks indicate significant differences between the groups (**: $p < 0.01$; two-sided Student's by t-test).

4.3.10. Histology findings

Histological observation of the regenerated cartilage synthesized on the WTF and LRF scaffolds are shown in Fig. 4.9. More cartilage-like tissues were formed in the LRF group than in the WTF group after 3 days in culture. Furthermore, after culturing for 7 days, two- to three-fold thicker tissues were formed at the surface of the LRF scaffold compared to the WTF scaffold. The expression of collagen type I was not detected in both groups.

4.4. Discussion

The transgenic silkworms named NK14 were able to transcript the transgene, translate its product, and secrete the LRF, which was confirmed by Western blotting

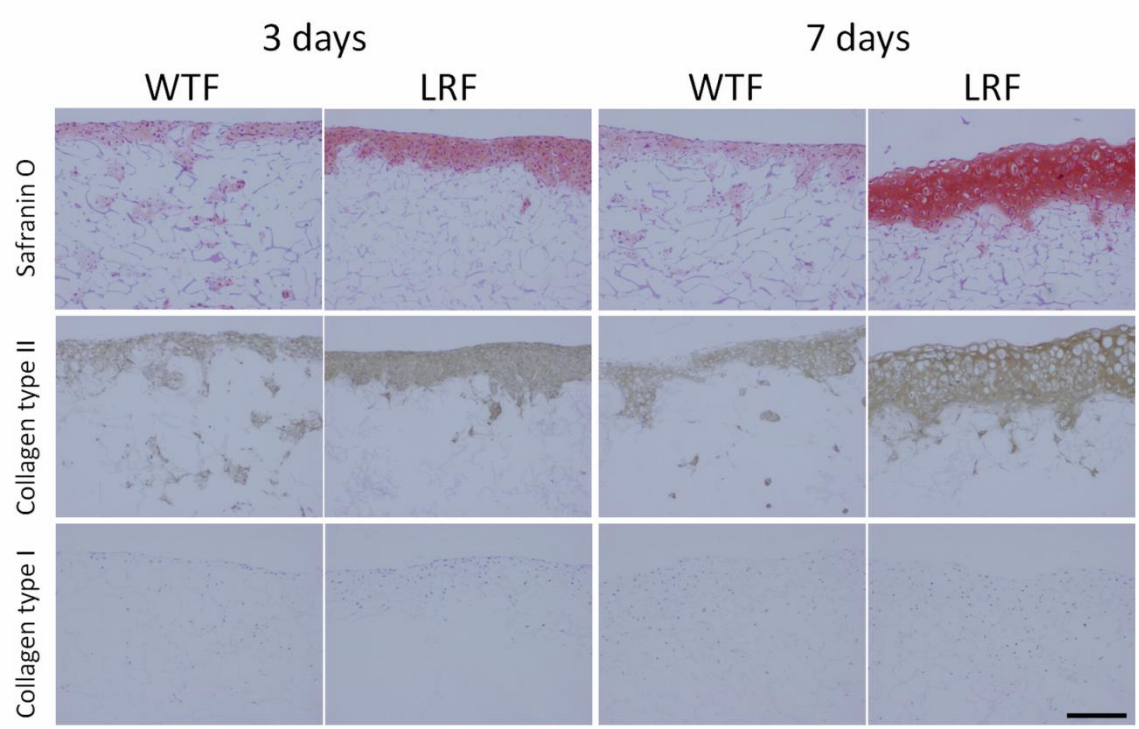

Fig. 4.9. Photographs of regenerated cartilage tissues using WTF and LRF sponges at 3 and 7 days in culture. The tissues were stained for safranin-O and immunostained for collagen type I and II. Scale bar = 200 μm.

with anti-$(RGDS)_2$ antibodies as shown in Fig. 4.1. Then, we evaluated the LRF as a scaffold for chondrocytes.

It is generally thought that introduction of RGD peptides into a substrate facilitates integrin-mediated cell attachment. In the present study, this explanation was confirmed by the fact that the PN and LRF substrates had a higher cell-adhesive activity than the CON and WTF substrates, respectively, as shown in Fig. 4.2C. Besides, as the attachment of chondrocytes to fibroin substrates increased with the dose of LRF molecules, $(RGDS)_2$ amino acids fused with the fibroin L-chain certainly affect cell adhesion. However, it is widely accepted that in addition to integrin-mediated biologic adhesion, surface properties of a material (e.g., wettability and charge) greatly affect cell–substrate adhesion [30-35]. In the present study, there were no significant

differences in contact angle or ζ potential between the WTF and LRF substrates or between the CON and PN substrates. Additionally, no marked differences were observable on the surfaces of the WTF and LRF films in SEM analysis as shown in Fig. 4.2A. These results suggest that the physicochemical properties of the substrates have little effect on levels of chondrocyte adhesion.

Integrins appear to be the major cell surface receptors by which a cell can adhere mechanically to ECMs, and chondrocytes have been shown to express several members of the integrin family [36]. As shown in Fig. 4.2D, competitive inhibition of chondrocyte attachment to an LRF substrate with soluble GRGDSP peptides indicated that integrin receptors on a suspending chondrocyte were blocked by the peptides and could not bind to ligands on the surface of a substrate. These results suggest that differences in cell-adhesive activity between the WTF and LRF substrates were caused by RGDS sequences in the LRF proteins, which did not exist on the WTF substrate. Therefore, RGDS in the L-chain works on cell adhesion, suggesting that biologic interactions between cell and material rather than physicochemical ones were predominant in the present experiments. Thus, the relationship between chondrogenesis and chondrocyte–material adhesion induced by RGDS sequences in the fibroin L-chain is discussed below.

Generally, by using fibronectin- and RGD-induced substrates, chondrcoyte–material adhesion is enhanced, which leads phenotypic and mechanical changes of chondrocytes: the cells tend to lose their chondrogenic phenotype [5,6,17] and the mechanical properties of the cells such as adhesive force are strengthened [37]. The latter effect was seen with both RGDS expressed in the fibroin L-chain and ProNectin® F coated on a glass substrate as shown in Fig. 4.4, although there was no dose-dependent effects on cell adhesive force from 0 to 1.5 mol% LRF. The mRNA expression of aggrecan, which encodes cartilage-specific proteoglycan, peaked at a similar level in the WTF and LRF groups, although its expression was delayed in the latter. In addition, chondrocytes grown on LRF sponges could synthesize thicker cartilage tissues than those cultured on WTF sponges during the early culture period. These results shown in Figs. 4.7 and 4.9

suggest that RGDS amino acids fused with the L-chain can facilitate cell adhesive strength, without down-regulating the chondrocyte-specific phenotype.

Chondrocytes grown on the WTF and LRF substrates exhibited a maximum adhesive force within 12 h after seeding, but both the CON and PN groups showed only a monotonic increase. Others have also shown monotonous enhancement of adhesive force in cells cultured on glass, fibronectin, or a culture dish, although the detaching process and direction of force measurement were different [37-39]. These results could indicate that the specific time-dependent changes in adhesive force of the WTF and LRF groups were predominantly affected by the characteristic of fibroin, and that the RGDS sequences in the L-chain had an influence on the expression period and the peak value. However, the RGDS in the L-chain appeared to have no effect on cell spreading, unlike the enhancement effect of PN coated on a glass substrate and RGD peptides fixed on a substrate as seen in both the present and previous studies [1,2].

Considering that proteoglycan has been reported to inhibit and regulate integrin-mediated cell–material adhesion [40,41], the specific gene expression of integrins $\alpha 5$ and $\beta 1$, which recognize an RGD sequence in ECMs [14-16,36], and aggrecan in the LRF group could be related to the adhesive force. Furthermore, higher gene expression of integrins in the LRF group might affect the earlier changes in actin polymerizations and distributions of focal adhesion points. This is supported by reports that integrins bind to the cytoskeleton (to a polymerized actin called F-actin), mediated by anchor molecules such as vinculin, talin, and α-actinin, and clusters to construct focal adhesions [42-44]. Although the development of F-actin and the expression of focal adhesion points are important factors for adhesive force [12,37-39], there appears to be no relations between them in chondrocytes grown on the two fibroin substrates.

The results of the present study suggest that RGDS amino acids fused with the L-chain protein of the silk fibroin facilitate cartilage tissue formation as shown in Fig. 4.9 but, in contrast to PN, do not induce spreading and dedifferentiation of chondrocytes. Hsu et al. [5] suspected that the effect of RGD could be substrate (scaffold)-dependent, showing that an RGD-containing protein introduced into chitosan-alginate-hyaluronate

composite or PLLA-poly(D,L-lactide-coglycolide) blended scaffolds demonstrated different effects on chondrogenesis [5,45]. Jung et al. [8] suggested that an optimal concentration of RGD might vary in different cell or substrate types and help to form cartilaginous tissues, but very strong adhesion is likely to suppress matrix production. The results of adhesion of single chondrocytes grown on an LRF substrate (Figs. 4.4–4.6) suggest that adhesion between a chondrocyte and an LRF substrate was not excessively strong as well as chondrocyte adhesion to PN; instead, moderate adhesion was sufficient to maintain the chondrogenic phenotype. In particular, the specific enhancement effect on the peak strength of adhesive force might influence the organization of cartilage tissues because a peak was not observed in the force of chondrocytes cultured on glass or PN substrates, on which chondrocytes cannot synthesize hyaline-like cartilage tissues [13,17]. Although it is difficult to explain precisely the mechanisms involved in the specific behavior of initial adhesion and chondrogenesis from the results of the present study, we infer that changes in adhesive force are crucial via the deformation of cell membranes, the distribution pattern of focal contacts, and the effect of substances synthesized by chondrocytes, as described previously by Yamamoto et al. [12]. These adhesion structures can affect the signal cascade of phenotypic expression and/or production of ECMs [46,47]. Hence, considering that there were not remarkable differences in the initial number of chondrocytes on/in WTF or LRF scaffolds at 24 h after seeding as shown in Fig. 4.8B, early integrin-mediated signal changes induced by the adhesion to LRF within 24 h (i.e., the increase and/or delay of integrin mRNA expressions as shown in Fig. 4.7) might stimulate cartilage tissue formation. Another possibility for the facilitation of chondrogenesis is that the adhesive force of chondrocytes affected their migration and aggregation. This suggestion is supported by the findings that cell adhesive strength is related to cell motility [48,49] and that chondrocyte movement and distribution in a fibroin sponge play a central role in the production of cartilage-specific matrices [50].

A fibroin H-chain protein is reported to be composed of a crystalline region linked with an amorphous region [51], whereas it is assumed that there are no crystal structures

in an L-chain [52,53] (where the RGDS sequences are fused in the present study). On the other hand, ProNectin® F is reported to be composed of the crystallized sequence containing (Gly-Ala-Gly-Ala-Gly-Ser)$_9$ ((GAGAGS)$_9$) from fibroin H-chain, which forms a β-sheet structure where a 10 amino acid sequence from fibronectin containing RGDS is presented in turn [54,55]. Additionally, cell-adhesive activity of an RGD sequence can be affected by its conformation [56,57]. Therefore, the specific effects of RGDS in the fibroin L-chain might be ascribable to the activity of the amino acids and the conformational effects of the sequences. However, further studies are necessary to confirm these discussions and to clarify the mechanisms.

4.5. Conclusions

The results of the present study have demonstrated that chondrocytes grown on the L-RGDSx2 fibroin substrate show similar spreading area but higher mRNA expression levels of integrins α5 and β1 at 12 h after seeding compared to the cells on the wild-type fibroin substrate. Further, the specific enhancement of the peak adhesive force has been exhibited within 12 h. These changes were not shown between chondrocytes culture on glass and ProNectin® F substrates. The study also suggests that the sequence in the L-chain can facilitate the synthesis of cartilage tissue.

References

[1] Ohno S, Noshiro M, Makihira S, Kawamoto T, Shen M, Yan, W, et al. RGD-CAP (βig-h3) enhances the spreading of chondrocytes and fibroblasts via integrin $\alpha_1\beta_1$. Biochim Biophys Acta 1999;1451:196-205.

[2] Jeschke B, Meyer J, Jonczyk A, Kessler H, Adamietz P, Meenen NM, et al. RGD-peptides for tissue engineering of articular cartilage. Biomaterials 2002;23:3455-63.

[3] Genes NG, Rowley JA, Mooney DJ, Bonassar LJ. Effect of substrate mechanics on chondrocyte adhesion to modified alginate surfaces. Arch Biochem Biophys 2004;422:161-7.

[4] Meinel L, Hofmann S, Karageorgiou V, Zichner L, Langer R, Kaplan D, et al. Engineering cartilage-like tissue using human mesenchymal stem cells and silk protein scaffolds. Biotechnol Bioeng 2004;88:379-91.

[5] Hsu SH, Chang SH, Yen HJ, Whu SW, Tsai CL, Chen DC. Evaluation of biodegradable polyesters modified by type II collagen and Arg-Gly-Asp as tissue engineering scaffolding materials for cartilage regeneration. Artif Organs 2006;30:42-55.

[6] Connelly JT, Garcia AJ, Levenston ME. Inhibition of in vitro chondrogenesis in RGD-modified three-dimensional alginate gels. Biomaterials 2007;28:1071-83.

[7] Tigli RS, Gumusderelioglu M. Evaluation of RGD- or EGF-immobilized chitosan scaffolds for chondrogenic activity. Int J Biol Macromol 2008;43:121-8.

[8] Jung HJ, Park K, Kim JJ, Lee JH, Han KO, Han DK. Effect of RGD-immobilized dual-pore poly(L-lactic acid) scaffolds on chondrocyte proliferation and extracellular matrix production. Artif Organs 2008;32:981-9.

[9] Meinel AJ, Kubow KE, Klotzsch E, Garcia-Fuentes M, Smith ML, Vogel V, et al. Optimization strategies for electrospun silk fibroin tissue engineering scaffolds. Biomaterials 2009;30:3058-67.

[10] Aoki H, Tomita N, Morita Y, Hattori K, Harada Y, Sonobe M, et al. Culture of

chondrocytes in fibroin-hydrogel sponge. Biomed Mater Eng 2003;13:309-16.

[11] Chueh S, Tomita N, Yamamoto K, Harada Y, Nakajima M, Terao T, et al. Transplantation of allogeneic chondrocytes cultured in fibroin sponge and stirring chamber to promote cartilage regeneration. Tissue Eng 2007;13:483-92.

[12] Yamamoto K, Tomita N, Fukuda Y, Suzuki S, Igarashi N, Suguro T, et al. Time-dependent changes in adhesive force between chondrocytes and silk fibroin substrate. Biomaterials 2007;28:1838-46.

[13] Park GE, Pattison MA, Park K, Webster TJ. Accelerated chondrocyte function on NaOH-treated PLGA scaffolds. Biomaterials 2005;26:3075-82.

[14] Rouslahti E, Pierschbacher MD. Arg-Gly-Asp: a versatile cell recognition signal. Cell 1986;44:517-8.

[15] Rouslahti E, Pierschbacher MD. New perspectives in cell adhesion: RGD and integrins. Science 1987;23:491-7.

[16] Hynes RO. Integrins: versatility, modulation, and signaling in cell adhesion. Cell 1992;69:11-25.

[17] Brodkin KR, Garcia AJ, Levenston ME. Chondrocyte phenotypes on different extracellular matrix monolayers. Biomaterials 2004;25:5929-38.

[18] Tanaka K, Kajiyama N, Ishikura K, Waga S, Kikuchi A, Ohtomo K, et al. Determination of the site of disulfide linkage between heavy and light chains of silk fibroin produced by *Bombyx mori*. Biochim Biophys Acta 1999;1432:92-103.

[19] Kojima K, Kuwana Y, Sezutsu H, Kobayashi I, Uchino K, Tamura T, et al. A new method for the modification of fibroin heavy chain protein in the transgenic silkworm. Biosci Biotechnol Biochem 2007;71:2943-51.

[20] Tomita M, Munetsuna H, Sato T, Adachi T, Hino R, Hayashi M, et al. Transgenic silkworms produced recombinant human type III procollagen in cocoons. Nat Biotechnol 2003;21:52-6.

[21] Inoue S, Kanda T, Imamura M, Quan GX, Kojima K, Tanaka H, et al. A fibroin secretion-deficient silkworm mutant, *Nd-s*^{D}, provides an efficient system for producing recombinant proteins. Insect Biochem Mol Biol 2005;35:51-9.

[22] Adachi T, Tomita M, Shimizu K, Ogawa S, Yoshizato K. Generation of hybrid transgenic silkworms that express *Bombyx mori* prolyl-hydroxylase α-subunits and human collagens in posterior silk glands: production of cocoons that contained collagens with hydroxylated proline residues. J Biotechnol 2006;126:205-19.

[23] Yanagisawa S, Zhu Z, Kobayashi I, Uchino K, Tamada Y, Tamura T, et al. Improving cell-adhesive properties of recombinant *Bombyx mori* silk by incorporation of collagen of fibronectin derived peptides produced by transgenic silkworms. Biomacromolecules 2007;8:3487-92.

[24] Tamura T, Thibert C, Royer C, Kanda T, Abraham E, Kamba M, et al. Germline transformation of the silkworm *Bombyx mori* L. using a *piggyBac* transposon-derived vector. Nat Biotechnol 2000;18:81-4.

[25] Tamada Y. New process to form a silk fibroin porous 3-D structure. Biomacromolecules 2005;5:217-28.

[26] Majima T, Marchuk LL, Shrive NG, Frank CB, Hart DA. In-vitro cyclic loading of an immobilized and mobilized ligament autograft selectively inhibits mRNA levels for collagenase (MMP-1). J Orthop Sci 2000;5:503-10.

[27] Ohashi H, Maeda T, Mishima H, Otori T, Nishida T, Sekiguchi K. Up-regulation of integrin α5β1 expression by interleukin-6 in rabbit corneal epithelial cells. Exp Cell Res 1995;218:418-23.

[28] Huang CY, Hangar KL, Frost LE, Sun Y, Cheung HS. Effects of cyclic compressive loading on chondrogenesis of rabbit bone-marrow derived mesenchymal stem cells. Stem Cells 2004;22:313-23.

[29] Tamada Y, Kulik EA, Ikeda Y. Simple method for platelet counting. Biomaterials 1995;16: 259-61.

[30] Van Wachem PB, Hogt AH, Beugeling T, Feijen J, Bantjes A, Detmers JP, et al. Adhesion of cultured human endothelial cells onto methacrylate polymers with varying surface wettability and charge. Biomaterials 1987;8:323-8.

[31] Kishida A, Iwata H, Tamada Y, Ikada Y. Cell behaviour on polymer surfaces grafted with non-ionic and ionic monomers. Biomaterials 1991;12:786-92.

[32] Tamada Y, Ikada Y. Cell adhesion to plasma-treated polymer surfaces. Polymer 1993;34:2208-12.

[33] Lee JH, Lee JW, Khang G, Lee HB. Interaction of cells on chargeable functional group gradient surfaces. Biomaterials 1997;18:351-8.

[34] Arima Y, Iwata H. Effect of wettability and surface functional groups on protein adsorption and cell adhesion using well-defined mixed self-assembled monolayers. Biomaterials 2007;28:3074-82.

[35] Arima Y, Iwata H. Effects of surface functional groups on protein adsorption and subsequent cell adhesion using self-assembled monolayers. J Mater Chem 2007;17:4079-87.

[36] Loeser RF. Chondrocyte integrin expression and function. Biorheology 2000;37:109-16.

[37] Athanasiou KA, Thoma BS, Lanctot DR, Shin D, Agrawal CM, LeBaron RG. Development of the cytodetachment technique to quantify mechanical adhesiveness of the single cell. Biomaterials 1999;20:2405-15.

[38] Hoben G, Huang W, Thoma BS, LeBaron RG, Athanasiou KA. Quantification of varying adhesion levels in chondrocytes using the cytodetacher. Ann Biomed Eng 2002;30:703-12.

[39] Huang W, Anvari B, Torres JH, LeBaron RG, Athanasiou KA. Temporal effects of cell adhesion on mechanical characteristics of the single chondrocyte. J Orthop Res 2003;21:88-95.

[40] Yamagata M, Suzuki S, Akiyama SK, Yamada KM, Kimata K. Regulation of cell-substrate adhesion by proteoglycans immobilized on extracellular substrates. J Biol Chem 1989;264:8012-8.

[41] Imoto E, Kakuta S, Hori M, Yagami K, Nagumo M. Adhesion of a chondrocytic cell line (USAC) to fibronectin and its regulation by proteoglycan. J Oral Pathol Med 2002;31:35-44.

[42] Greenwood JA, Murphy-Ullrich JE. Signaling of de-adhesion in cellular regulation and motility. Microsc Res Tech 1998;43:420-32.

[43] Giancotti FG, Ruoslahti E. Integrin signaling. Science 1999;285:1028-32.

[44] Martin KH, Slack JK, Boerner SA, Martin CC, Parsons JT. Integrin connections map: to infinity and beyond. Science 2002;296:1652-3.

[45] Hsu S, Whu SW, Hsieh S, Tsai C, Chen DC, Tan T. Evaluation of chitosan-alginate-hyaluronate complexes modified by an RGD-containing protein as tissue engineering scaffolds for cartilage regeneration. Artif Organs 2004;28:693-703.

[46] Enomoto M, Leboy PS, Menko AS, Boettiger D. β1 integrins mediate chondrocyte interaction with type I collagen, type II collagen, and fibronectin. Exp Cell Res 1993;205:276-85.

[47] Takagi M, Kitabayashi T, Koizumi S, Hirose H, Kondo S, Fujikawa M, et al. Correlation between cell morphology and aggrecan gene expression level during differentiation from mesenchymal stem cell to chondroytes. Biotechnol Lett 2008;30:1189-95.

[48] DiMilla PA, Barbee K, Lauffenburger DA. Mathematical model for the effects of adhesion and mechanics on cell migration speed. Biophys J 1991;60:15-37.

[49] DiMilla PA, Stone JA, Quinn JA, Albelda SM, Lauffenburger DA. Maximal migration of human smooth muscle cells on fibronectin and type IV collagen occurs at an intermediate attachment strength. J Cell Biol 1993;122:729-37.

[50] Kawakami M, Tomita N, Shimada Y, Yamamoto K, Tamada Y, Kachi ND, et al. Chondrocyte distribution and cartilage regeneration in silk fibroin sponge. Biomed Mater Eng 2011;21:53-61.

[51] Mita K, Ichimura S, James TC. Highly repetitive structure and its organization of the silk fibroin gene. J Mol Evol 1994;38:583-92.

[52] Tanaka K, Kajiyama N, Ishimura K, Waga S, Kikuchi A, Ohtomo K, et al. Determination of the site of disulfide linkage between heavy and light chains of silk fibroin produced by *Bombyx mori*. Biochim Biophys Acta 1999;1432:92-103.

[53] Yamaguchi K, Kikuchi Y, Takagi T, Kikuchi A, Oyama F, Shimura K, et al. Primary structure of the silk fibroin light chain determined by cDNA sequencing and peptide

analysis. J Mol Biol 1989;210:127-39.

[54] Cappello J, Crissman JW. The design and production of bioactive protein polymers for biomedical applications. Polymer Prepr 1990;31:193-4.

[55] Anderson JP, Cappello J, Martin DC. Morphology and primary crystal structure of a silk-like protein polymer synthesized by genetically engineered *E. Coli* bacteria. Biopolymers 1994;34:1049-57.

[56] Maeda T, Oyama R, Ichihara-Tanaka K, Kimizuka F, Kato I, Titani K, et al. A novel cell adhesive protein engineered by insertion of the Arg-Gly-Asp-Ser tetrapeptide. J Biol Chem 1989;264:15165-8.

[57] Hersel U, Dahmen C, Kessler H. RGD modified polymers: biomaterials for stimulated cell adhesion and beyond. Biomaterials 2003;24:4385-415.

Chapter 5
Summary and Conclusions

5.1. Summary

Chapter 2

A large number of cellular scaffolds modified to have functional substitutes have been developed by using chemical modification or post-conjugation techniques, but the processes are elaborate and costly. Here, we have developed basic fibroblast growth factor (bFGF)-fused fibroin by the use of transgenic silkworm technology, aiming at creating a scaffold with cell-growth function. Our molecular design has enabled the bFGF to be released from the fibroin molecule by collagenase. However, a process to fabricate a spongy scaffold of the bFGF-fused fibroin inactivated cell-proliferative effects of the growth factor. Thus the solution and sponge of the bFGF-fused fibroin were subjected to a refolding treatment with the glutathione redox system to restore its biological activity. The bFGF-fused fibroin degummed in a boiling 0.02 M Na_2CO_3 and dissolved in 9.0 M LiBr reactivated by the refolding process, showing growth-promoting effects on NIH3T3 fibroblasts. Meanwhile, the bFGF in the fibroin sponge refolded after autoclaving showed slight effects on the proliferation of NIH3T3 cells and on the matrix production of chondrocytes. Further studies are required for a practical use of the genetically-modified fibroin fused with a bioactive macromolecule.

Chapter 3

Cellular mechanical properties are implicated in numerous cell behaviors, but their

involvement in cell differentiation process has remained unclear. Since mechanical interactions between chondrogenic cells and their surrounding environment heavily affect the maintenance of their differentiation phenotype, here, using a chondrogenic cell strain ATDC5, we evaluated cell mechanical properties (e.g., adhesive force and stiffness) and gene expression levels in differentiation culture. The adhesive force appeared to be affected by both cellular cytoskeletal and adhesive constructions. Treatment with Y27632, which accordingly inhibits actin polymerization, decreased the adhesive force while increased chondrogenic gene expressions, suggesting the both of them are interrelated via the mediation of actin cytoskeleton. However, the mechanical property did not represent chondrogenic differentiative stages as obviously as the biochemical characteristics did. Meanwhile, interestingly, changes in cell distribution maps of the force in the differentiation process indicated that the cells have different levels of mechanical properties in the undifferentiated state, whereas they tend to converge when the differentiative stage is in a lull. These results reaffirm the cellular diversity during differentiation from a mechanical perspective and provide important information to the fields of generation and scaffold-based tissue regeneration, where cell–substrate adhesion plays a role.

Chapter 4

Initial chondrocyte–silk fibroin interactions are implicated in chondrogenesis when using fibroin as a scaffold for chondrocytes. Here, we focused on integrin-mediated cell–scaffold adhesion and prepared cell adhesive fibroin in which a tandem repeat of the Arg-Gly-Asp-Ser (RGDS) sequence was genetically interfused in the fibroin light chain (L-chain) (L-RGDSx2 fibroin). We investigated the effects of the sequence on chondrocyte adhesion and cartilage synthesis, in comparison to the effects of ProNectin® F. As the physicochemical surface properties (e.g., wettability and ζ potential) of the fibroin substrate were not affected by the modification, specific cell adhesion to the RGDS predominately changed the chondrocyte adhesive state. This was also supported by the competitive inhibition of chondrocyte attachment to the

L-RGDSx2 fibroin substrate with soluble RGD peptides in the medium. Unlike ProNectin® F, the expression of RGDS in the fibroin L-chain had no effect on chondrocyte spreading area but enhanced mRNA expression levels of integrins α5 and β1, and aggrecan at 12 h after seeding. Although both the sequence and ProNectin® F increased cell adhesive force, chondrocytes grown on the fibroin substrate exhibited a peak in the force with time in culture. These results suggested that moderate chondrocyte adhesion to fibroin induced by the RGDS sequence was able to maintain the chondrogenic phenotype and, from the histology findings, the sequence could facilitate chondrogenesis.

5.2. Conclusions

This study aimed at the development of useful, practical scaffolds which enable effective cartilage regeneration, where transgenic silkworm technology was used to design silk fibroin molecules for the sake of appending new functions to fibroin scaffold. Three purposes were targeted to accomplish the final goal of this study: to append promoting effects on cell proliferation to silk fibroin scaffold; to seek the index of scaffold designing alternative to bioactive macromolecules; and to add stimulatory effects on chondrogenesis by modulating the cell-adhesive function of silk fibroin scaffold. Conclusions to the three purposes are described as follows:

1) bFGF was genetically fused with the fibroin L-chain molecule, which intended to make silk fibroin scaffold have enhancement effects on cell proliferation. Although recombinant silk fibroin ‘molecule’ which stimulates cell proliferation was developed successfully, we have not yet accomplished to create fibroin ‘scaffold’ with such function. This is because the bFGF fused with the L-chain was inactivated in the process to form the 3-D porous structure of fibroin. Bioactive macromolecules fused with fibroin molecule were shown to be difficult to function

after fabricated into scaffold.

2) Measurement of cell adhesive force at several phases of chondrogenic differentiation showed a possibility that mechanical cell–material interactions reflect chondrogenic phenotype. This finding suggests that changes in the cell-adhesive function of silk fibroin which affect cell mechanical properties can result in the efficiency of chondrogenesis in/on fibroin scaffold.
3) RGDS peptides genetically fused with the fibroin L-chain affected chondrocyte adhesion, including the adhesive force, and facilitated chondrogenesis in/on fibroin spongy scaffold. The RGDS strengthened the adhesive force of chondrocytes as shown in the effect of ProNectin® F, however, chondrocytes grown on the RGDS-fused fibroin substrate maintained the specific behavior of the adhesive force stemmed from the cell–fibroin interaction. These findings suggest the RGDS and the fibroin act synergistically on chondrocytes, which can be induced by the fact that the RGDS peptides were designed to be fused with the L-chain.

Transgenic silkworm technology makes it possible to create chimeric silk fibroin molecule in accordance with our design: we can design which peptides or proteins to be introduced and where they are fused. For the sole purpose of creating silk fibroin protein fused with biologically-active macromolecule, all we have to do is to design the modified fibroin molecule, construct the vector, and generate the silkworm strain. Then the silkworms produce the modified fibroin proteins in their posterior silkglands, and the proteins relatively well-maintain the activity of the macromolecule as shown in the case of bFGF-fused fibroin. However, in order to develop silk fibroin scaffold with the function stemmed from the recombinant macromolecule, it is essential to design the whole process, including the fabrication, preservation, and usage of the scaffold. In contrast, it is clarified that silk fibroin fused with recombinant peptide composed of several amino-acid residues stably shows functions induced by the recombinant peptide even after fabricated into scaffold. The results of this study has also suggested the effect of recombinant peptides or proteins on chondrocytes is dependent on their location in

the fibroin molecule, which means the function of recombinant molecules is not simply added to but can be exerted synergistically with the function of silk fibroin. We infer that a peptide or protein fused with the H-chain is immobilized more rigidly that fused with the L-chain. To design and develop functional scaffolds for tissue engineering, it is necessary to feedback the results in evaluation of tissue regeneration *in vitro* and *in vivo* to the design of scaffold at the molecular level, but there are lots of indexes to be reflected to the designing and their integration is complicating. Cell mechanical properties induced by the adhesion to the scaffold can represent the information on cell differentiation and scaffold materials. Therefore, the mechanical evaluation of cells grown in/on scaffold can simplify the scaffold designing to achieve its practical application.

5.3. Perspectives

Tissue engineering is an interdisciplinary field that applies the principles and methods of engineering and the life science toward the development of biological substitutes that restore, maintain, or improve tissue function, and to achieve the ultimate goal of functional neoorganogenesis for human use, the close, interdisciplinary collaboration of surgeons, engineers, chemists, and biologists is required. However, there are few opportunities for such collaboration and interdisciplinary educational systems have not been established especially in Japan. To accomplish this study, I have used a variety of techniques including the development of scaffold materials using transgenic techniques and evaluations with biochemical and biomechanical methods. The results of this study are multidisciplinary findings and can be important for the clinical application of scaffold materials for tissue engineering. Particularly, biomechanical viewpoints, evaluations, and analysis are essential to clarify the mechanisms for the regeneration of 3-D structures and functions of living tissues in a scaffold. They are also important to achieve bioenvironmental designing for effective tissue regeneration. In the current

situation, however, biomechanical studies including this study lack validity in biological phenomena *in vivo*, which is caused by the limitation of the techniques in the biomechanical field. In order to resolve this issue and to make biomechanical studies useful for the practical use of tissue engineering, new technologies need to be created by fusing multidisciplinary methods. Fortunately, I had opportunities to discuss and study with researchers from various academic fields, including clinical medicine, biomaterial, molecular biology, and microengineering. Using these interdisciplinary connections and experimental techniques, I would like to create new biotechnologies and biomaterials that can help promote the clinical application of regenerative medicine from biomechanical viewpoints. I am sure to keep problem-oriented studying by fusing multidiscipline.

5.4. Research achievements

5.4.1. Original Research Papers

Chapter 2

1. Kambe Y, Kojima K, Tomita N, and Tamada Y. Development of bFGF-fused silk fibroin, evaluation of its activity, and application as a scaffold for cartilage regeneration. Biomaterials, *in preparation*.

Chapter 3

2. Kambe Y, Hayashi N, and Tomita N. Adhesive force behavior of single ATDC5 cells in chondrogenic culture. Biochemical and Biophysical Research Communications 2012; 420: 241-6.

Chapter 4

3. Kambe Y, Yamamoto K, Kojima K, Tamada Y, and Tomita N. Adhesion of a single

chondrocyte on RGDS-transgenic fibroin substrate and tissue formation (in Japanese). Japanese Journal of Clinical Biomechanics 2009; 30: 71-6.

4. Kambe Y, Takeda Y, Yamamoto K, Kojima K, Tamada Y, and Tomita N. Effect of RGDS-expressing-fibroin dose on initial adhesive force of a single chondrocyte. Bio-Medical Materials and Engineering 2010; 20: 309-16.

5. Kambe Y, Yamamoto K, Kojima K, Tamada Y, and Tomita N. Effects of RGDS sequence genetically interfused in the silk fibroin light chain protein on chondrocyte adhesion and cartilage synthesis. Biomaterials 2010; 31: 7503-11.

5.4.2. Presentation at international conferences

1. Kambe Y, Yamamoto K, Kojima K, Tamada Y, and Tomita N. Adhesive force of a single chondrocyte on RGDS-transgenic fibroin substrate, 55th Annual Meeting of the Orthopaedic Research Society 2009; 1294: Las Vegas, USA.

2. Kambe Y, Yamamoto K, Kojima K, Tamada Y, and Tomita N. RGDS sequences genetically induced in the fibroin light-chain protein operate positively for cartilage tissue synthesis. 56th Annual Meeting of the Orthopaedic Research Society 2010; 1328: New Orleans, USA.

3. Kambe Y, Yamamoto K, Kojima K, Tamada Y, and Tomita N. Effects of RGDS genetically interfused into fibroin light chain protein on chondrocytes adhesive force. 4th World Congress on Adhesion and Related Phenomena 2010; O-17.1: Arcachon, France.

4. Kambe Y, Kojima K, Tomita N, and Tamada Y. Development of bFGF-fused silk and its mitogenic activity. 9th World Biomaterials Congress 2012; 2285: Chengdu, China.

The others

5. Hirakata E, Tomita N, Tamada Y, Suguro T, Nakajima M, Kambe Y, Yamada K, Yamamoto K, Kawakami M, Shenzhi X, Otaka A, Okumura H, and Suzuki S. Cartilage repair of patella using fibroin based cell-delivery system. 18th European Conference on Orthopaedics 2010; P107: Davos, Switzerland.

6. Hayashi N, Kambe Y, Yamamoto K, Kojima K, Tamada Y, and Tomita N. Effect of RGDS sequences introduced in silk fibroin substrate on the adhesive force of chndrocyte. 6th World Congress on Biomechanics 2010; D4-D-T4.4-03: Singapore, Singapore.

7. Takahashi K, Kambe Y, Hayashi N, Yamada Y, Yamamoto K, Kojima K, Tamada Y, and Tomita N. Effects of low-intensity pulsed ultrasound stimulation on chondrocytes cultured on RGD-induced fibroin substrate. International Society for Technology in Arthoplasty, 24th Annual Congress 2011; 517: Bruges, Belgium.

5.4.3. Awards and other remarks

1. Alumnus of the Nano-Medinine Merger Education Unit at Kyoto University, 2009.

2. Best Poster Award at the report meeting of problem solution training in the Nano-Medinine Merger Education Unit at Kyoto University, 2009.

3. Biomaterials 2010–The Year in Images, 2010.

4. Best Presentation Award at the 21st JSME Conference on Frontiers in Bioengineering, 2011.

5. Alumnus of the Education Program for Global Leaders in Advanced Engineering

and Pharmaceutical Sciences at Kyoto University, 2011.

6. Best Poster Award at the Tsukuba Biomedical Forum 2012, 2012.

7. Research Fellow of the Japan Society for the Promotion of Science (DC2), 2012

8. Young Scientist Award at the 9th World Biomaterials Congress, 2012.

9. Alumnus of the Institutional Program for Young Researcher Oversea Visits, Subject R34 at Department of Mechanical Engineering and Science, Kyoto University, 2012.

Acknowledgements

This doctoral dissertation would never have been possible without the guidance, the help, and the support from several individuals who in one way or another contributed and extended their valuable assistance in the preparation and completion of this study.

First and foremost, I would like to express my deepest gratitude to my supervisor, Dr. Naohide Tomita, Professor of the Graduate School of Engineering, Kyoto University. In addition to his excellent suggestions from both mechanical and medical viewpoints, his belief to conduct problem-oriented research always inspired me. He let me experience a lot of things, such as participation in multidiscipline conferences, temporary transfers to a company and national institutes in Japan and overseas.

I owe my sincere gratitude to Dr. Yasushi Tamada, Leader of the Silk Materials Research Unit, National Institute of Agrobiological Sciences. He offered me precious opportunities to study in his research unit for two years, while he supported me with continuous advice and encouragement from the standpoint of biomaterials. He also provided the fibroin films and sponges used in this study.

I would like to express my special gratitude to Dr. Koji Yamamoto, Assistant Professor of the Graduate School of Medicine, Kyoto University. I learned a lot from his sincere attitude toward study. He always cared me even while I was in difficulties, and I cannot appreciate him too much.

I would like to show my great thanks to Dr. Katsura Kojima, Senior Researcher of the Silk Materials Research Unit, National Institute of Agrobiological Sciences, for his sincere support in teaching me molecular-biological knowledge and techniques, creating transgenic silkworms, and providing cocoons of the silkworms.

My special thanks go to Dr. Taiji Adachi, Professor of the Institute for Frontier Medical Sciences, Kyoto University, and Dr. Ari Ide-Ektessabi, Professor of the Graduate School of Engineering, Kyoto University, who reviewed this thesis and offered valuable suggestions and insights.

I am grateful to Dr. Masaya Yamamoto, Associate Professor of the Institute for Frontier Medical Sciences, Kyoto University, for his advice and assistance in measuring the ζ potential of protein-coated substrates.

I would like to express my thanks to Mr. Takahisa Matsushita and Ms. Kumiko Kogishi for helping with histological staining of regenerated cartilage.

I am indebted to all of my colleagues in the Tomita Laboratory, including Yuji Takeda, Nobumasa Hayashi, and Kazuya Takahashi, who helped collect experimental data; Turner Alex, who carefully corrected my poor English; and Akihisa Otaka, who gave me helpful suggestions.

I am also thankful to my colleagues in the Silk Materials Research Unit, including Hiroko Saitoh, who prepared the fibroin-coated glass plates; and Hitomi Takayanagi and Hiroko Saitoh, who bred silkworms.

I appreciate Kyoto University-Venture Business Laboratory for the use of their experimental laboratory.

This study was supported in part by Integrated Research Project for Plant, Insect and Animal Using Genome Technology (Ministry of Agriculture, Forestry and Fisheries of Japan), Grant-in-Aid for Creative Scientific Research (Japan Science and Technology Agency), and Agri-Health Translational Research Project (Ministry of Agriculture, Forestry and Fisheries of Japan).

Finally, I would like to express my gratitude to my family: especially to my parents for their understanding, love, and continuous support – both mentally and financially; and to my wife for her smile and cheers.

March 2013

Yusuke KAMBE

DOCTORAL THESIS

Molecular Design of Silk Fibroin for Functional Scaffolds

Department of Mechanical Engineering and Science

Graduate School of Engineering

Kyoto University

March 2013

Yusuke KAMBE
